Integrating Network and Intrinsic Changes in GnRH Neuron Control of Ovulation

by

Caroline E. Adams

A dissertation submitted in partial fulfillment
of the requirements for the degree of
Doctorate of Philosophy
Molecular and Integrative Physiology
in the University of Michigan
2018

Doctoral Committee:

Professor Sue Moenter, Co-Chair
Professor Santiago D. Schnell, Co-Chair
Associate Professor Victoria Booth
Associate Professor Carol Elias
Professor Daniel B. Forger
Professor Geoff G. Murphy

Caroline E. Adams

adamsce@med.umich.edu

ORCID iD: 0000-0001-6028-0196

© Caroline E. Adams 2018

Acknowledgements

First and foremost, I would like to thank my co-mentors Drs. Sue Moenter and Santiago Schnell. None of this would have been possible without their support. Sue and Santiago are fantastic scientists and, even more importantly, dedicated teachers. It is due to their patience, guidance, and humor that I have been able to learn the essential scientific concepts and techniques and the many intangible skills that were necessary for completing this dissertation work.

I would also like to thank the many very skilled and generous members of both Sue's and Santiago's labs for making my time more enjoyable here. Jeff, for helping me make every one-person job a fun two-person job. Tova, for sharing the journey to becoming a physician-scientist with me. Luhong, for her wise (and wisecracking!) advice.

I am particularly grateful to Marina ("tigger"), Eden, Charlotte, Rudi, Xi, and Allison for their friendship and for our many coffee breaks together, to Kasia, Kristin, Michelle, and Marcio for my earliest training in the Moenter and Schnell laboratories, and to Beth and Laura for their technical (and emotional) assistance and support.

I am also grateful to Tony for teaching me electrophysiology concepts and techniques in extraordinary detail and for sharing the rig with me, as well as to Mark, Dan, Justin, and Wylie for sharing their expertise in mathematical modeling.

I thank my thesis committee, Drs. Victoria Booth, Carol Elias, Daniel Forger, and Geoff Murphy. Their mentorship and advice have made this dissertation possible.

I would like to acknowledge Dr. Ken Belanger, my advisor while obtaining my Bachelor's degree in Molecular Biology at Colgate University. He was a committed and patient teacher and fostered my own enthusiasm for research. My research experience in his laboratory shaped my decision to pursue a doctorate degree.

I am lucky to have many amazing friends. In particular, I am thankful to Scott and Anat for a decade plus of support and friendship. Scott and Anat have joined me on many vacations during my time as a graduate student and our time together was always a welcome reprieve from my studies. I thank Stephanie for the many hours we spend online together. I would also like to thank the friends I've made in Michigan: my classmates Amanda and Talha for trying out almost every restaurant in Ann Arbor with me, Andrew and Alex, upperclassmen who helped to pave the way before me, and Judy who trusted me to be her mentor.

I am deeply thankful to my family for their unconditional love and encouragement. I would not be who I am today without them. Most especially, I thank my parents Stuart and Jacky Adams, who never doubted me, and my sisters Emily and Juliet, who recommended books to me and kept in contact with me despite the distance through Skype. I am also deeply grateful to have a wonderful "other" mother, role-model as a future physician, and namesake in my Aunt Caroline.

I could not have made it to this point without my partner Ehsan. I thank him for his boundless support. His intellectual curiosity and devotion to his research inspires me to persist in my own studies when it got tough. Most importantly, I thank him for all the Persian food.

Finally, I thank my cats, Phineas and Persephone, for their love and companionship.

Table of Contents

List of Tables

List of Figures

List of Abbreviations

ACSF	artificial cerebrospinal fluid
ADP	afterdepolarization
AGRP	agouti-related peptide
AHP	afterhyperpolarization
AMPA	α-amino-3-hydroxy-5-methyl-4-isoxazolepropionic acid
AMPAR	α-amino-3-hydroxy-5-methyl-4-isoxazolepropionic acid receptor
AP	action potential
APV	D-2-amino-5-phosphonovaleric acid
ATP	adenosine triphosphate
AVPV	anteroventral periventricular nucleus
cAMP	cyclic adenosine monophosphate
Cm	cell capacitance
CNQX	6-cyano-7-nitroquinoxaline
DPN	diarylpropionitrile
EPSCs	excitatory post-synaptic currents
ERα	estrogen receptor alpha
ERβ	estrogen receptor beta
FSCV	fast-scan cyclic voltammetry
FSH	follicle-stimulating hormone
FWHM	full width at half maximum

GABA	gamma-aminobutyric acid
$GABA_A$	A-type gamma-aminobutyric acid receptor
GnRH	gonadotropin-releasing hormone
GPR54	kisspeptin g protein-coupled receptor (also known as KISS1R)
GT1	immortalized GnRH-secreting cells
HVA	high-voltage-activated calcium current
I_A	A-type potassium current
I_{ADP}	afterdepolarization current
I_{AHP}	afterhyperpolarization current
I_{app}	applied current
I_{Ca}	calcium current
I_h	hyperpolarization-activated nonspecific cation current
Ihold	holding current
I_{HVA}	high-voltage-activated calcium current
I_K	delayed rectifier potassium current
I_{KCa}	calcium-activated potassium current
I_L	leak current
I_{LVA}	low-voltage-activated calcium current
I_{Na}	sodium current
I_{NaF}	fast transient sodium current
I_{NaP}	persistent sodium current
IPR	inositol-trisphosphate receptors
I_S	slow inward calcium current
I_T	T-type calcium current

KISS1R	kisspeptin g protein-coupled receptor (also known as GPR54)
KW	kruskal-wallis
LH	luteinizing hormone
LHβ	luteinizing hormone subunit beta
LVA	low-voltage-activated calcium current
MCMC	Markov Chain Monte Carlo
MUA	multi-unit activity
NMDA	N-methyl-D-aspartate
NMDAR	N-methyl-D-aspartate receptor
OCVm	on-cell measurements of membrane potential
OVX	ovariectomized mice
OVX+E	ovariectomized mice treated with estradiol implant
OVX+E+E	ovariectomized mice treated with estradiol implant and estradiol injection
PeN	preoptic periventricular nucleus
POA	preoptic area
POMC	pro-opiomelanocortin
PSC	postsynaptic current
PSg	postsynaptic conductance
PVH	paraventricular nucleus
Rin	input resistance
Rs	series resistance
sADP	slow afterdepolarization potential
SCN	suprachiasmatic nucleus
SK	calcium-activated potassium current

TRPC	transient receptor potential cation channel
TTX	tetrodotoxin
$V_{1/2act}$	membrane potential at which ½ of current is activated
$V_{1/2inact}$	membrane potential at which ½ of current is inactivated

Abstract

Infertility affects 15-20% of couples; failure to ovulate is a common cause. Ovulation is triggered when estradiol switches from negative feedback action on the pituitary and hypothalamus to positive feedback, initiating a surge of gonadotropin-releasing hormone (GnRH) secretion that causes a surge of luteinizing hormone (LH) release, which triggers ovulation. Our understanding of the neurobiological changes underlying the switch from negative to positive feedback is incomplete. High levels of estradiol are essential, and in rodents, the LH surge tends to occur at a specific time-of-day. GnRH neurons, however, do not express the estrogen receptor required for feedback, thus estradiol-sensitive afferents likely convey estradiol information to GnRH neurons. We hypothesized that GnRH neurons switch from negative to positive feedback by integrating multiple changes to their synaptic inputs and intrinsic properties.

To investigate the neurobiological mechanisms that underlie surge generation, daily GnRH/LH surges can be induced by ovariectomy and estradiol replacement (OVX+E) in rodents. GnRH neuron activity and release are increased in the afternoon (positive feedback) and decreased in the morning (negative feedback). No time-of-day changes are observed in OVX mice that do not receive an estradiol implant. Previous studies using the daily surge model have elucidated multiple GnRH neuron intrinsic and fast-synaptic changes during the switch from negative to positive feedback. It is unclear which if any of these changes are necessary for increasing GnRH firing rate during positive feedback. We hypothesized that changes to GnRH neuron intrinsic properties culminate in an increase in excitability to current steps during positive feedback and a decrease in excitability during negative feedback. To our surprise, changes to GnRH neuron ionic conductances rendered GnRH neurons more excitable during positive feedback relative to all other groups, but changes to ionic conductances between OVX and negative feedback animals had no net effect on GnRH neuron excitability. A mathematical model using a novel application of a rigorous parameter estimation

method predicted that multiple, redundant combinations of changes to GnRH intrinsic conductances can produce the firing response in positive feedback. Changes to two interdependent parameters that determine the kinetics of voltage-gated potassium channels accounted for the similar neural responses during negative feedback and in OVX mice.

Although enhancing GnRH neuron excitability is expected to increase firing rate during positive feedback, it is unclear if this change is necessary or if the concomitant increase is fast-synaptic transmission is sufficient for increasing GnRH neural activity during positive feedback. To test this, we used dynamic clamp to inject positive feedback, negative feedback, and OVX postsynaptic conductance trains into cells from positive feedback, negative feedback, and OVX mice. Positive feedback conductance trains were more effective in initiating spiking in cells from all three animal models relative to negative feedback and OVX trains. However, the positive feedback train elicited twice the number of action potentials from positive feedback mice relative to those from all other groups.

Lastly, we extended our previous work to measure changes to GnRH neuron excitability and GABAergic inputs during the estrous cycle. We demonstrated that GABA postsynaptic current frequency and GnRH neuron excitability are both increased during positive feedback (proestrus) relative to negative feedback (diestrus) and strikingly similar to changes observed in the daily surge model. Collectively, these studies demonstrate that GnRH neurons act to integrate and amplify multiple signals to increase firing rate during the preovulatory surge.

Chapter 1: Introduction

The hypothalamic-pituitary-ovarian axis regulates reproduction

Precise central neural control is required for ovulation in vertebrates. In mammals, at the end of the follicular phase of the reproductive cycle, one or more mature ovarian follicles are signaled to rupture and each release an egg for fertilization. In some species, including rabbits, ovulation is induced by copulation; this association made it possible for scientists to study the neural link to reproduction as early as the 18th century. In 1797, Jon Haighton recounted to the Royal Society his observation that, in rabbits, sex made "by sympathy the ovarian vesicles enlarge, project, and burst" (Haighton and Garthshore, 1797). Haighton rejected the hypothesis that semen directly stimulated the ovary to release an egg because he had severed the Fallopian tubes. He conjectured sympathy, or crosstalk, between the vagina and ovaries through the nervous system occurred to induce ovulation.

The study of the brain's role in reproduction accelerated in the early 20th century. In 1936, Marshall and Verney induced ovulation when they passed electrical current through a rabbit's brain (Marshall and Verney, 1936). A year later, Harris refined their work when he induced ovulation by electrically stimulating a specific region of the brain, the hypothalamus (Harris, 1937). Scientists speculated that a neural signal was also necessary for ovulation in animals that do not require copulation to ovulate. Humans, non-human primates, sheep, rodents, and many other mammals ovulate spontaneously at the end of the follicular phase (proestrus in rodents) of the reproductive cycle. Studying spontaneous ovulation became tractable as techniques, such as the vaginal smear, were developed to follow cycle stage in live rats and mice. In 1950, Everett and Sawyer delayed spontaneous ovulation by anesthetizing rats with phenobarbital on the afternoon of proestrus. In their control animals, ovulation occurred between 1 and 2 am on the morning of estrus (lights off at 7 pm), but anesthesia delayed ovulation by 24 hours if administered during a critical period (3 – 5 pm before lights off) earlier that day

(Everett and Sawyer, 1950). Everett and Sawyer hypothesized that a neural signal initiated spontaneous ovulation during this period. Eight years later, Critchlow stimulated the hypothalamus directly to trigger “spontaneous” ovulation (Critchlow, 1958). The hypothalamus also controls reproductive function in humans. In the 1950s, hypothalamic pathologies were first associated with hypogonadism and precocious puberty in humans (Bauer, 1954).

The study of the brain and reproduction did not occur in isolation. At the same time, scientists began to elucidate a role for the pituitary in reproduction. In 1921 and 1922, Evans and Long noted that injecting pituitary extract into a rat’s peritoneal cavity enlarged its ovaries and disrupted its estrous cycles (Evans and Long, 1921b, a; Evans and Long, 1922). Similarly, surgical removal of the pituitary caused ovarian atrophy, and pituitary transplants beneath the hypothalamus (site of the *sella turcica,* home of the pituitary) restored estrous cycles and spontaneous ovulation (Smith, 1926; Greep, 1936). However, when the pituitary was transplanted to sites outside of the *sella turcica,* reproductive function was not restored (Harris and Jacobsohn, 1952). These studies supported two early hypotheses: first, that the pituitary may be important for reproduction in spontaneously ovulating species, and second, that the hypothalamus is necessary for pituitary control of reproduction.

Support for the hypothalamo-pituitary control of ovulation and reproduction continued to expand through the 20th century. A releasing factor in the hypothalamus was hypothesized to initiate pituitary hormone release to control reproduction. By 1971, Schally had isolated and sequenced 11.4 mg of gonadotropin-releasing hormone (GnRH) from the hypothalami of 240,000 (Oscar Mayer) pigs (Schally et al., 1971a).

We know now that gonadotropin-releasing hormone neurons are the final common pathway for central neural control of reproduction. There are approximately 800 and 1300 GnRH neurons in the adult female mouse and rat, respectively, and the majority is found in the preoptic area and anterior hypothalamus (Hoffman and Finch, 1986; Wray and Hoffman, 1986; Wray et al., 1989; Wu et al., 1997). Many of these neurons project to and secrete GnRH into the median eminence (Pelletier et al., 1974; Bennett et al., 1975). GnRH is a decapeptide hormone that is carried from the capillary beds of median

eminence down long portal vessels into the capillary beds of the anterior pituitary (Popa and Fielding, 1930; Wislocki and King, 1936; Green and Harris, 1949; Matsuo et al., 1971). There, GnRH binds to receptors on pituitary gonadotropes to trigger the release of two hormones, follicle stimulating hormone (FSH) and luteinizing hormone (Schally et al., 1971b). The release of these hormones stimulates follicular maturation and the production of sex steroids in the ovaries. Ovarian steroids provide feedback on the pituitary and hypothalamus to regulate hormone release. Collectively, hypothalamus, pituitary, and ovaries control complex hormonal interactions to precisely coordinate the reproductive cycle.

GnRH release initiates pituitary LH release

For the majority of the reproductive cycle, GnRH is released in pulsatile manner and drives the release of FSH and pulses of LH. In rodents, sheep, and other mammalian models, a switch from pulsatile GnRH to a surge of continuous GnRH release initiates the LH surge, which triggers ovulation at the end of the follicular phase and formation of corpora lutea from emptied follicles (Sarkar et al., 1976; Moenter et al., 1991).

To study patterns of hormone release during the menstrual cycle, radioimmunoassays were developed to detect human LH in 1966 and rhesus macaque LH in 1970 (Midgley, 1966; Monroe et al., 1970b). When measured daily, LH levels in the macaque did not appear to vary for the majority of the menstrual cycle, with the exception of the LH surge (Monroe et al., 1970a). However, when they measured LH levels in gonadectomized macaques at 60-minute intervals, LH levels were highly variable with abrupt peaks occurring throughout the 24-hour period (Atkinson et al., 1970). By sampling more frequently, Knobil and colleagues were the first to observe that these seemingly random peaks in LH concentrations were in fact organized pulses of LH release, occurring every ~60 minutes in ovariectomized (OVX) females (Dierschke et al., 1970). Each LH pulse was characterized by an abrupt rise from baseline that peaked within a 10-minute interval, followed by exponential decay toward baseline.

From these studies, Knobil hypothesized that each LH pulse was the consequence of a pulse of GnRH release into the median eminence of the hypothalamus. His hypothesis was first backed by indirect evidence: lesions to the hypothalamus abolished LH release

and hourly exogenous GnRH pulses restored it (Adams et al., 1981). Administering GnRH continuously did not re-establish pulsatile LH release, but triggered a transient release of FSH and LH before down-regulating both hormones (Belchetz et al., 1978). Knobil's hypothesis was supported when endogenous GnRH pulses were first measured by sampling pituitary portal blood in sheep and each LH pulse coincided with a pulse of GnRH (Clarke and Cummins, 1982). GnRH likely induces LH release directly, because cultured rat pituitary cells express GnRH receptors and release LH in response to GnRH (Naor et al., 1980). Furthermore, administration of anti-GnRH and GnRH antagonists obliterates LH pulses (Lincoln and Fraser, 1979; Ellis et al., 1983). GnRH pulses have now been measured by sampling pituitary portal blood or by push-pull perfusion in the hypothalamus in intact female rats, rabbits, mares, and rhesus monkeys (Neill et al., 1977; Levine et al., 1982; Moenter et al., 1991; Irvine and Alexander, 1994).

GnRH release throughout the menstrual cycle is regulated by steroid feedback

GnRH/LH pulse frequency and amplitude are modulated by sex steroids. GnRH pulse frequency, in turn, modulates the ratio of FSH to LH synthesis by and release from the pituitary (Wildt et al., 1981). For much of the cycle, estradiol and progesterone have negative feedback actions at the level of the hypothalamus and pituitary. In macaques, administration of low frequency GnRH pulses favors FSH release and high frequency favors LH release (Wildt et al., 1981). As a consequence of their feedback actions, estradiol and progesterone levels help determine GnRH/LH pulse frequency and gonadotropin release during the follicular and luteal phases of the cycle.

Negative Feedback

At the start of the follicular phase of the human cycle, estradiol levels are low and GnRH/LH pulses occur approximately every 1 or 2 hours (Backstrom et al., 1982; Filicori et al., 1986; Rossmanith et al., 1990). As maturing follicles develop, they produce rising levels of estradiol. These rising levels of estradiol reduce GnRH pulse amplitude and increase pulse frequency, and mean GnRH and LH release are decreased at this time (Backstrom et al., 1982; Filicori et al., 1986; Rossmanith et al., 1990; Moenter et al., 1991; Evans et al., 1994). In addition to suppressing GnRH

release, estradiol also acts directly at the pituitary to decrease gonadotrope responsiveness to GnRH, by suppressing gonadotropin gene transcription, to further reduce LH release (Clarke and Cummins, 1984; Shupnik et al., 1988; Clarke et al., 1989).

Sex steroids also have negative feedback effects after ovulation occurs. During the luteal phase of the cycle, circulating levels of progesterone are high relative to the early follicular phase. Progesterone reduces GnRH pulse frequency (Goodman and Karsch, 1980; Goodman et al., 1981; Skinner et al., 1998). As progesterone levels rise, LH pulses decrease in frequency, occurring every 3 to 4 hours in women (Backstrom et al., 1982; Filicori et al., 1986; Rossmanith et al., 1990). At the level of the pituitary, progesterone alone does not appear to alter LH pulse amplitude or baseline levels; however, if coupled with estradiol, progesterone enhances the pituitary effects of estradiol negative feedback (Clarke and Cummins, 1984). Estradiol is also required for progesterone to suppress GnRH pulse frequency (Goodman et al., 1981; Skinner et al., 1998). Estradiol is likely necessary because estradiol induces progesterone receptor expression in the pituitary and brain (Blaustein and Wade, 1978; MacLusky and McEwen, 1978). Thus, estradiol and progesterone act together to suppress GnRH/LH release in the luteal phase.

Positive Feedback

At the end of the follicular phase, a dominant follicle produces rising levels of estradiol. High levels of estradiol first suppress GnRH release (negative feedback) and then induce the release of a continuous surge of GnRH (positive feedback)(Moenter et al., 1990). The action of estradiol also switches from negative to positive feedback at the pituitary and pituitary gonadotropes are more responsive to GnRH in part due to increases in gonadotropin gene transcription (e.g., LHβ) and GnRH receptor density at this time (Adams et al., 1981; Clarke and Cummins, 1984; Clarke et al., 1988; Moenter et al., 1990; Shupnik and Rosenzweig, 1991). As a consequence, the GnRH surge initiates a robust surge of LH, which triggers ovulation.

Although the negative feedback effects of estradiol were well characterized as early as the 1930s, our understanding of positive feedback by estradiol and its initiation of the

GnRH/LH surges emerged more gradually (Everett, 2006). In 1934, Hohlweg injected prepubertal rats with estradiol to induce ovulation, which they confirmed by observing corpora lutea formation the following day (Hohlweg and Chamorro, 1937). Hohlweg's data demonstrated that estradiol could induce ovulation rather than inhibit it. In 1965, Docke and Dörner prevented estradiol-induced ovulation by lesioning the medial preoptic area and/or suprachiasmatic nucleus of the hypothalamus in rats (Docke and Dorner, 1965). Their findings suggested that estradiol induces ovulation at the level of the hypothalamus, likely through changes to GnRH release. Starting in the 1980s, GnRH response to estradiol was measured directly. In both sheep and primates, exogenous estradiol first suppresses GnRH/LH release before a switch in action occurs after several hours and a surge of GnRH/LH is initiated (Levine et al., 1985; Moenter et al., 1990). During the natural cycle, pre-ovulatory GnRH surges have been demonstrated in rats, sheep, monkeys, and horses (Sarkar et al., 1976; Moenter et al., 1991; Pau et al., 1993; Irvine and Alexander, 1994). In mice, GnRH release is increased in brain slices during positive feedback (Glanowska et al., 2012).

In primate models, a surge in GnRH release is not an absolute requirement for the LH surge. Exogenous pulsatile GnRH infusion is sufficient for restoring menstrual cycles and ovulation in rhesus macaques and women with GnRH deficiency (Knobil et al., 1980; Martin et al., 1990). Estradiol positive feedback may not alter GnRH release in primates during the natural cycle, but this is unlikely. Direct measurements of GnRH release in rhesus macaques demonstrate that estradiol-induced and physiologic pre-ovulatory GnRH surges do occur (Xia et al., 1992; Pau et al., 1993). Instead, it is more likely that direct estradiol feedback onto pituitary gonadotropes is sufficient for initiating a surge of LH release in the face on unchanging GnRH input, through enhanced responsiveness to GnRH at this time (Adams et al., 1981).

In addition to an estradiol signal, a time-of-day dependent signal is necessary for initiating GnRH/LH surges in some species including rats and mice. GnRH/LH surges occur on the afternoon of proestrus in nocturnal rodents, and in the morning for the diurnal (i.e., most active in daytime hours) rodent Arvicanthis niloticus (Sarkar et al., 1976; Mahoney et al., 2004). In ovariectomized nocturnal mice, rats, and hamsters implanted with estradiol capsules (OVX+E), LH levels are suppressed in the morning by

estradiol negative feedback and elevated in the afternoon by estradiol positive feedback (Norman et al., 1973; Legan and Karsch, 1975; Christian et al., 2005). This shift in response to estradiol occurs on a daily basis (thus named the “daily surge model”).

The time-of-day signal was first demonstrated by Everett and Sawyer in 1950 when phenobarbital, an anesthetic, blocked ovulation only when administered during a “critical period” on the afternoon of proestrus (Everett and Sawyer, 1950). The signal likely arises from the suprachiasmatic nucleus (SCN), home of the central clock. SCN fibers synapse onto GnRH neurons and GnRH afferents, and lesions to the SCN prevent spontaneous ovulation (Brown-Grant and Raisman, 1977; Watson et al., 1995; Van der Beek et al., 1997; Vida et al., 2010).

The necessity of a time-of-day signal for initiating ovulation is less clear in large mammals. Women primarily have LH surges during late sleep/early waking hours and perturbing circadian clock (e.g., via shift work) can cause menstrual cycle irregularities and increased wait times to pregnancy (Bisanti et al., 1996; Cahill et al., 1998; Kerdelhue et al., 2002; Labyak et al., 2002; Boden and Kennaway, 2006). However, administering estradiol in OVX sheep or primates does not initiate GnRH/LH surges at a consistent time-of-day, rather, estradiol initiates GnRH/LH surges with a specific time delay (~16 hours after estradiol administration in sheep)(Levine et al., 1985; Moenter et al., 1990). Exogenous estradiol may override a daily signal in these models, but it remains an open question whether a time-of-day signal is necessary for initiating pre-ovulatory (“natural”) GnRH/LH surges in sheep and primates.

GnRH neuron activity is regulated by estradiol feedback

The switch from negative to positive feedback and initiation of the GnRH surge could reflect changes to GnRH neuron activity or firing-independent mechanisms. Initially, it was not feasible to make electrophysiological recordings from GnRH neurons to measure their firing activity or GnRH release (Wakerley and Lincoln, 1973). In mice, about 800 GnRH neurons are widely dispersed across the preoptic area and anterior hypothalamus, both of which have highly heterogeneous neuron populations, and GnRH neurons cannot be identified by morphology or location alone. To circumvent this problem, tungsten electrodes were placed into the hypothalamus of rhesus macaques

to measure the electrical activity of many neighboring neurons (multi-unit activity, or MUA). MUA activity was monitored while also sampling circulating LH (Wilson et al., 1984). Each LH pulse coincided with peaks in electrical activity in the hypothalamus. Their data indicated that coordinated neuron activity (required for MUA peaks) in the hypothalamus is correlated with LH release. Unfortunately, MUA studies do not reveal the identities of active neurons, but neurons active during LH release may initiate the release GnRH.

In 1999, new genetic manipulations made it possible to express green fluorescent protein (GFP) under the control of the GnRH promoter in mice, permitting electrophysiological recordings to be made of fluorescent-identified GnRH neurons in brain slices (Spergel et al., 1999; Suter et al., 2000; Han et al., 2004). Researchers could now address whether GnRH neuron firing is correlated with GnRH release. In the brain slices prepared from the daily surge model, GnRH firing was increased during positive feedback, when LH levels are high, and suppressed during negative feedback, when LH levels are low, relative to OVX controls (Christian et al., 2005). During the natural cycle, GnRH neuron firing rate is increased on the afternoon of proestrus compared to rates on the afternoon of diestrus (Silveira et al., 2016). The data from both studies suggest that estradiol feedback modulates GnRH activity to drive changes in GnRH (and LH) release. Hormone (e.g., vasopressin and oxytocin) release reflects firing activity in other hypothalamic neuron types, but GnRH neuron release could conceivably occur independently of spikes (Wakerley and Lincoln, 1973; Dutton and Dyball, 1979; Bicknell and Leng, 1981). Recently, fast-scan cyclic voltammetry using carbon fiber electrodes has made it possible to measure real-time GnRH release in the median eminence of brain slices. Pulses of GnRH release were increased in frequency during positive feedback in daily surge mice (OVX+E PM) relative to negative feedback (OVX+E AM)(Glanowska et al., 2012). These results further demonstrate that GnRH neuron firing is correlated with GnRH release, making GnRH neuron activity one target for regulation by estradiol feedback and an important area of study. However, action potentials are not required for GnRH secretion in all cases and may be region (POA or median eminence) dependent (Glanowska and Moenter, 2015).

Because GnRH activity may initiate GnRH release, many electrophysiological studies have aimed to elucidate how estradiol and time-of-day signals modify GnRH neuron activity. GnRH neurons do not express ERα, the estrogen receptor necessary for estradiol feedback, thus estrogen-sensitive afferents likely convey these signals through synaptic release of GABA, glutamate, and neuromodulators (Skynner et al., 1999; Hrabovszky et al., 2000; Herbison et al., 2001; Hrabovszky et al., 2001; Couse et al., 2003; Wintermantel et al., 2006; Christian et al., 2008). To modulate GnRH activity, estradiol and time-of-day signals may change the frequency and amplitude of fast-synaptic inputs (e.g., GABA/glutamate) and/or alter GnRH neuron intrinsic properties (e.g., voltage-gated channels).

Voltage-gated currents in GnRH neurons are by modulated estradiol feedback

GnRH neurons express voltage-gated ion channels, including sodium, potassium, and calcium channels. The net current through these channels sets spontaneous firing rates and determines if spiking occurs in response to fast-synaptic input (excitability). Estradiol feedback modulates many of these ion channels (DeFazio and Moenter, 2002; Chu and Moenter, 2006; Christian and Moenter, 2007, 2008; Christian et al., 2009; Sun et al., 2010; Wang et al., 2010; Pielecka-Fortuna et al., 2011; Gaskins and Moenter, 2012; Glanowska and Moenter, 2015). Modifying ion channel expression and activity may be one way in which estradiol and time-of-day signals regulate GnRH neuron activity.

Voltage-gated sodium channels carry inward current (I_{Na}) under physiological conditions that, if unopposed, depolarizes the cell membrane and initiates firing. Their voltage-dependence sets the threshold for initiating the all-or-none response of an action potential, and the rapid activation of these channels shapes the upward stroke of the action potential. Sodium currents have been measured in dissociated GnRH neurons from OVX and OVX+E animals 5 – 7 days after surgery instead of 2 – 4 days in the daily surge model (Wang et al., 2010). In these neurons, *in vivo* estradiol reduced persistent sodium (I_{NaP}) currents active at subthreshold potentials and transient sodium currents (I_{NaF}) that drive action potentials. Both changes are expected to reduce firing in OVX+E neurons. However, dissociated neurons were removed from the brain up to 24

hours before recording and it is not clear if these data reflect changes that happen during negative and/or positive feedback *in vivo*.

In neurons from the daily surge model, estradiol increased a sodium current underlying the afterdepolarization (ADP) that follows an action potential (I_{ADP}) independent of time-of-day (Chu and Moenter, 2006). As a consequence, both OVX+E AM and PM neurons were more likely to fire a second spike after a first was initiated by current injection. This is likely to have little effect in OVX+E AM neurons, because a first spike is rarely initiated at this time. However, I_{ADP} may contribute to the increase in repetitive spiking observed in OVX+E PM relative to OVX controls (Gaskins and Moenter, 2012). Repetitive spikes are important because bursts of action potentials have been correlated with hormone release in other neuroendocrine systems (Dutton and Dyball, 1979; Cazalis et al., 1985).

Sodium channels are not the only targets of estradiol feedback in GnRH neurons. Estradiol also modifies certain types of voltage-gated calcium channels. Voltage-gated calcium channels are divided into two types: low-voltage-activated (LVA) T-type channels activated at low or subthreshold potentials and high-voltage-activated or HVA opened at more depolarized potentials (Hille, 2001). Because T-type channels are activated near resting potential, they can initiate single spikes and spikes that occur after a period of hyperpolarization (rebound spikes)(Simms and Zamponi, 2014). Two different feedback paradigms have been used to study T-type currents. In the daily surge model, LVA-mediated currents are only a few picoamperes in amplitude, but they are capable of initiating rebound spikes and may contribute to burst firing (Sun et al., 2010). However, T-type currents do not appear to be modulated by estradiol feedback in the daily surge model. In a second feedback paradigm, mice were ovariectomized and implanted with estradiol or sesame oil (Zhang et al., 2009). Six days later, estradiol was administered by subcutaneous injection to initiate an LH surge (positive feedback) the following afternoon. Mice were sacrificed on the next day. In this paradigm, T-type channel mRNA levels and T-type current density were elevated during positive feedback compared to OVX controls. These data appear to contradict data from the daily surge model, but the conflict may be accounted for by differing levels of estradiol in the two paradigms. Indeed, T-type currents were greatly reduced in mice from the

second paradigm that received an estradiol implant but did not receive an additional bolus of estradiol. Collectively, T-type currents may initiate and maintain spiking in GnRH neurons, but their roll role in the switch from negative to positive feedback remains unclear.

Time-of-day and estradiol signals do regulate HVA-mediated calcium currents in the daily surge model (Sun et al., 2010). Both L-type and N-type HVA currents are up-regulated during positive feedback (OVX+E PM) and suppressed during negative feedback (OVX+E AM). HVA channels are typically activated during an action potential and net calcium flows into the cell under physiological conditions. Calcium influx depolarizes the membrane and can activate calcium-dependent processes inside the cell (Simms and Zamponi, 2014). L-type channels are expressed on the cell body and contribute to calcium-dependent gene transcription (Gomez-Ospina et al., 2006). N-type channels are typically expressed in the soma, dendrites, and nerve terminals and can mediate neurotransmitter release (Westenbroek et al., 1992; Reid et al., 2003).

Voltage-gated potassium channels carry outward current, under most physiological conditions, to help set resting membrane potential and oppose action potential initiation, and repolarize the membrane during a spike. GnRH neurons have both transient, rapidly inactivating A-type currents (I_A) and sustained, slowly inactivating delayed rectifier currents (I_K)(Abe and Oka, 1999; DeFazio and Moenter, 2002; Pielecka-Fortuna et al., 2011). Both types are modulated by estradiol feedback. A-type currents are of particular interest because they can be active at subthreshold potentials and can counter action potential initiation by opposing inward sodium and calcium currents. In the daily surge model, A-type peak current densities are suppressed during positive feedback (OVX+E PM) compared to OVX PM animals (DeFazio and Moenter, 2002; Pielecka-Fortuna et al., 2011). Estradiol also shifted I_A activation and inactivation to more depolarized potentials in OVX+E PM neurons, and these three changes are expected to opposing effects. Contending effects make it difficult to predict the net effect of I_A on GnRH firing. Similarly, A-type peak current densities are up-regulated during negative feedback (relative to OVX AM and +FB neurons), but this is opposed to a hyperpolarized shift in inactivation at this time. Most likely, subthreshold I_A is suppressed to increase firing rates during positive feedback and/or up-regulated to

decrease spiking during negative feedback. Estradiol feedback also modulates I_K: negative feedback increases delayed rectifier current densities, while positive feedback increases them. I_K is typically activated during repolarization that follows an action potential and decreasing I_K may increase repetitive firing during positive feedback and increasing I_K may reduce spiking during negative feedback.

Estradiol and time-of-day signals alter sodium, potassium, and sodium channel properties including current density, channel expression, and voltage-dependence. For some of these currents, the net effect on excitability is easy to predict—for example, increasing I_{Ca} during positive feedback is likely to increase spiking, and suppressing it during negative feedback decreases firing. I_{Na} and I_A are more challenging because estradiol feedback has conflicting effects on their properties. These two currents are most critical for determining excitability because they are activated at subthreshold potentials. We propose to build a mathematical model of a GnRH neuron to predict how changes to I_{Ca}, I_{Na}, and I_K/I_A alter GnRH neuron excitability during positive and negative feedback. We postulate that the alterations to ion channels during positive feedback increase both spontaneous firing and responsiveness to fast-synaptic inputs (discussed below). However, it is unclear if these changes to intrinsic properties are necessary for the switch from negative to positive feedback, or if increasing fast-synaptic inputs alone is sufficient. Thus, we will also use our model to test if these changes are necessary for the switch from negative to positive feedback.

Fast-synaptic inputs are altered by estradiol feedback

GABA and glutamate account for the majority of fast-synaptic input to GnRH neurons (Spergel et al., 1999; DeFazio et al., 2002; Han et al., 2002). Blockade of ionotropic GABA and glutamate receptors increases GnRH neuron firing rates during negative feedback (OVX+E AM) and decreases them during positive feedback (OVX+E PM), reversing effects the time-of-day and estradiol on firing rate (Christian and Moenter, 2008). These data indicate that GABAergic and glutamatergic inputs are critical for sculpting GnRH activity for both positive and negative feedback.

GABA

Ionotropic $GABA_A$ receptors are GABA-gated ion channels permeable to chloride and to a lesser extent, bicarbonate (Kaila and Voipio, 1987; Kaila, 1994). GnRH neurons maintain high levels of chloride and when $GABA_A$ receptors are activated, chloride influx generates a post-synaptic current (PSC) that can depolarize the cell membrane and induce spiking (DeFazio et al., 2002). In the daily surge model, GABA input is modulated by estradiol and time-of-day. GABA PSC frequency is suppressed in the morning (OVX+E AM) by negative feedback and elevated in the afternoon (OVX+E PM) by positive feedback relative to OVX controls (Christian and Moenter, 2007). Because these experiments were performed in acutely prepared brain slices, some connections between GnRH and their afferents were severed depending on the slice orientation. To elucidate GABA inputs arising from caudal/rostral and medial/lateral directions, both coronal and sagittal slice orientations were utilized. In sagittal slices, the estradiol-induced increase in PSC frequency was activity (action potential) dependent. Furthermore, physical cuts to disrupt connections between GnRH neurons and SCN (and other caudal populations) dramatically decreased PSC frequency. SCN neurons make and release GABA and synapse onto GnRH neurons (Moore and Speh, 1993; De La Iglesia et al., 1999; Vida et al., 2008). These data suggest that GABA inputs from the SCN relay an activity-dependent time-of-day signal directly to GnRH neurons. In coronal slices, the estradiol-induced increase in PSC frequency was activity independent, suggesting that estradiol alters vesicle release probability or synaptic plasticity in connections preserved in this configuration. PSC frequency during positive feedback was also cell location dependent. GnRH soma located in the midventral POA had the greatest frequencies, and may represent a sub-population of GnRH neurons that are responsible for the surge (Boukhliq et al., 1999; Sim et al., 2001).

Estradiol also modulates PSC amplitude in a time-of-day dependent manner. Both activity-dependent and activity-independent (“miniature”) GABA PSCs are increased in amplitude during the positive feedback compared to OVX and negative feedback controls. There is no difference in amplitude between OVX and negative feedback PSCs. Postsynaptic changes to receptor density and expression, or receptor activation/deactivation may alter PSC amplitude and frequency. GnRH neurons express

ERβ and both acutely applied estradiol and DPN (an ERβ agonist) enhance PSC amplitudes in OVX mice (Skynner et al., 1999; Herbison et al., 2001; Hrabovszky et al., 2001; Chu et al., 2009). Thus, changes to $GABA_A$ receptors may be modulated directly at the level of the GnRH neuron through estrogen receptor β (ERβ) signaling. However, ERβ is not necessary for estradiol feedback and if enhancing GABA PSC amplitude is essential for positive feedback, additional changes to $GABA_A$ receptors or intracellular chloride levels are likely signaled by estrogen-sensitive afferents.

Glutamatergic blockers were used in these studies to isolate GABA PSCs. This has at least one drawback in that blocking glutamate likely alters neuron firing and GABA release throughout the slice. Thus, it is also important to determine if $GABA_A$ inputs are necessary for initiating the LH surge in other animal models. In mice, ERα knock-out in GABA neurons blocks positive feedback and the LH surge in mice (Cheong et al., 2015). Although these data suggest GABA plays a critical role in surge induction, ERα positive GABA neurons can also express glutamate and kisspeptin, confounding the conclusions of this study. In a second animal model, when $GABA_A$ receptor expression was suppressed in GnRH neurons, GABA PSC frequency and amplitudes were reduced by ~70% but estradiol-induced LH surges were not significantly impacted (Lee et al., 2010b). One drawback to this study is that the impact on PSC frequency and amplitude was not measured or compared between intact, negative, or positive feedback animals. It could be that GABA inputs were not significantly reduced during positive feedback. Alternatively, the reduced number $GABA_A$ receptors may be sufficient for relaying estradiol signals from afferent neurons, or the pituitary may mount an estradiol-induced LH surge in response to reduced GnRH release.

Glutamate

Glutamate is a major excitatory neurotransmitter in the central nervous system. Glutamate activates ionotropic NMDA and AMPA/kainite receptors to generate inward, excitatory post-synaptic currents (EPSCs). In rodents, NMDA and AMPA stimulate LH release in an estrogen-dependent manner: AMPA and NMDA each increased LH levels in OVX+E rats, but had either no effect or an inhibitory effect in OVX rats (Brann and Mahesh, 1992; Arias et al., 1993; Luderer et al., 1993; Ping et al., 1997). A similar

estrogen-dependent effect of NMDA has been observed in female rhesus macaques and ewes (Estienne et al., 1990; Reyes et al., 1991; Urbanski et al., 1997). Endogenous glutamate release in the POA is also increased during estradiol (OVX+E) and progesterone (OVX+E+P) induced surges, and AMPA and NMDA antagonists block LH surges in rats (Lopez et al., 1990; Brann and Mahesh, 1991; Jarry et al., 1992; Luderer et al., 1993; Ping et al., 1994; Jarry et al., 1995; Ping et al., 1997). These data demonstrate that estradiol fine-tunes glutamate-mediated LH release, and supports a role for glutamate in initiating the LH surge, either at the level of the hypothalamus (e.g., GnRH neurons or their afferents) and/or pituitary.

GnRH neurons express functional NMDA and AMPA receptors (NMDAR and AMPAR, respectively) and synaptic terminals containing glutamate contact GnRH neuron soma and dendrites, suggesting a direct role for glutamate in activating GnRH neurons (Eyigor and Jennes, 1996; Spergel et al., 1999; Ottem et al., 2002; Kiss et al., 2003; Pompolo et al., 2003; Ottem et al., 2004; Bailey et al., 2006; Hrabovszky et al., 2012). Both exogenous glutamate and simulated glutamate post-synaptic conductances stimulate action potential firing in GnRH neurons (Kuehl-Kovarik et al., 2002; Suter, 2004). To test the hypothesis that an increase glutamatergic inputs contribute to surge-induction, glutamate EPSCs were isolated and recorded in GnRH neurons prepared from the daily surge model (Christian et al., 2009). AMPAR EPSCs accounted for the majority of glutamate transmission in GnRH neurons and their frequency and amplitude were decreased during negative feedback relative to OVX and positive feedback groups, which did not differ. NMDAR EPSCs were observed in 20-30% of GnRH neurons which supports previous work that observed that while the majority of GnRH soma respond to NMDA, only ~20% respond to AMPA (Spergel et al., 1999). It may be that a decrease in EPSC input during negative feedback drives the decrease in action potential frequency at this time; but the data rejects the hypothesis that an increase in glutamate inputs drives an increase in firing during positive feedback. However, whole-cell recordings in GnRH soma may miss EPSCs initiated in distal processes (Roberts et al., 2006). GnRH neuron processes express active condutances (I_{Na}) and can initiate spiking independent of the soma, and thus, a missed increase in distal inputs during positive feedback could potentially drive the increase in spiking at this time (Roberts et

al., 2008). Alternatively, native EPSC patterns are likely disrupted during brain slice preparation, which severs some synaptic connections, and by applying GABAergic blockers to isolate glutamatergic transmission.

Kisspeptin

In addition to release GABA and glutamate, GnRH neuron afferents also make and release neuromodulators, which can act indirectly to increase or decrease synaptic transmission or directly by altering GnRH neuron intrinsic properties. The neuromodulator kisspeptin is a potent stimulator of GnRH neuron activity and release (Gottsch et al., 2004; Han et al., 2005; Messager et al., 2005; Pielecka-Fortuna et al., 2008). Kisspeptin is encoded by the gene *Kiss1*, named by researchers in Hershey, Pennsylvania, after the Hershey's Chocolate Kiss (Lee et al., 1996). Initially, the gene product (kisspeptin) was named metastin for its role in suppressing metastasis in human melanomas (Ohtaki et al., 2001). Its role in reproduction was first appreciated when two separate research groups simultaneously determined that mutations to the kisspeptin receptor (GPR54 or Kiss1R) prevented progression through puberty, causing hypogonadotropic hypogonadism in both humans and mice (de Roux et al., 2003; Seminara et al., 2003).

In the hypothalami of rats and mice, kisspeptin is expressed by neurons in the anteroventral periventricular nucleus (AVPV), arcuate nucleus, and preoptic periventricular nucleus (PeN)(Gottsch et al., 2004; Clarkson and Herbison, 2006) .Kisspeptin neurons in the AVPV, PeN, and arcuate are hypothesized to relay estradiol signals to GnRH neurons because the majority of these neurons express estrogen receptor α and kisspeptin expression in these cells is regulated by estradiol (Smith et al., 2005; Smith et al., 2006). In the arcuate, ovariectomy increases the number of cells expressing kisspeptin and the amount of kisspeptin expressed per cell, and estradiol (OVX+E) reduces kisspeptin expression. In the AVPV and PeN, estradiol has the opposite effect: ovariectomy suppresses kisspeptin expression and estradiol (OVX+E) restores it. Furthermore, AVPV kisspeptin expression is sexually dimorphic, females have a greater number of kisspeptin neurons relative to males. From these

experiments, the arcuate is postulated to play a role in negative feedback (in males and females) and the AVPV to play a role in positive feedback (in females).

Endogenous kisspeptin release during proestrus is hypothesized to directly and/or indirectly activate GnRH neurons to trigger GnRH release. AVPV kisspeptin expression is increased on the afternoon of proestrus, and AVPV kisspeptin neurons also fire more action potentials at that time (Smith et al., 2006; Wang et al., 2016). Further, GnRH neurons express the kisspeptin receptor and AVPV kisspeptin fibers make contact with GnRH soma (Han et al., 2005; Messager et al., 2005; Pielecka-Fortuna et al., 2008; Yip et al., 2015). Kisspeptin acts directly by modulating multiple GnRH ionic currents, suppressing A-type and calcium-activated potassium currents and activating a non-selective cation current, effects which are expected to enhance GnRH neuron excitability (Zhang et al., 2008; Pielecka-Fortuna et al., 2011; Zhang et al., 2013). Kisspeptin also acts indirectly via (unspecified) afferents to increase GABA PSC frequency and amplitude and glutamate EPSC frequency (Pielecka-Fortuna and Moenter, 2010).

Despite these data, it is unclear if kisspeptin-GPR54 signaling is essential for initiating the GnRH surge. In one study, GPR54 knock-out mice were able to mount an estradiol-induced, GnRH-dependent LH surge (Dungan et al., 2007). In a separate study, neither GPR54 knock-out mice nor Kiss1 knock-out mice were capable of mounting an estradiol-induced LH surge (Clarkson et al., 2008). It is unclear if these differing results are due to differences in mouse strain or surge-induction protocols. However, it could be that in the first study, the estradiol-primed pituitary was able to initiate an LH surge in response to a relatively small amount of GnRH release.

Computational models of GnRH neurons

In addition to performing empirical studies, scientists have also developed computational models of GnRH neurons to address open questions in the field. Mathematical models are powerful tools because they combine data from many experiments to investigate the complex interplay of variables and can predict the most important variables that underlie experimental outcomes. Computational studies have largely focused on two areas: first, the interplay of ionic currents, calcium dynamics, and

hormone release inside the GnRH neuron and second, the integration of ionic and synaptic currents along the length of the GnRH neuron.

The pioneering models by Sherman and his colleagues were developed to study the effect of GnRH on action potential characteristics and calcium dynamics in immortalized GnRH-secreting (GT1) cells (LeBeau et al., 2000; Van Goor et al., 2000). Experimental work had demonstrated GT1 cells spontaneously fire action potentials and that activation of GnRH receptors increased firing frequency, broadened spike width, decreased spike amplitude, and increased calcium entry during each spike. The Sherman model and concurrent experiments indicated that sustained membrane depolarization by GnRH inactivated TTX-sensitive fast-sodium transients to decrease spike amplitude. The decrease in spike amplitude reduced potassium channel activation, slowing repolarization and broadening the spike. Spike broadening increased calcium entry (via L-type calcium channels) to increase hormone (i.e., GnRH) release (Van Goor et al., 2000). In a second study by Arthur Sherman, the mathematical model was enhanced to include separate calcium pools in the endoplasmic reticulum and cytoplasm, and three-additional currents: a store-operated calcium current, a calcium-activated potassium (SK) current, and a third inward current, modulated by cAMP and cytoplasmic calcium levels, predicted to exist to fully recapitulate the experimental results (LeBeau et al., 2000). A number of subsequent studies by other researchers developed models of GT1 cells to predict autocrine (i.e., GnRH) regulation of GnRH pulsatility and concluded that GnRH release and action at its receptor are sufficient for generating GnRH pulses in vitro (Khadra and Li, 2006; Li and Khadra, 2008; Fletcher and Li, 2009; Krupa et al., 2013). However, not all GT1 cells express the GnRH receptor and expression of GnRH receptors remains controversial *in vivo* (Todman et al., 2005; Chen and Moenter, 2009; Wen et al., 2011).

The GT1 model was also extended to GnRH neurons in brain slices to understand how calcium dynamics shape “bursts” of action potential firing, which are thought to stimulate hormone release (Lee et al., 2010a). In this model by Sneyd and colleagues, activation of sodium currents initiated action potential firing, opening voltage-gated L- and T- type calcium channels, and extracellular calcium enters the cell. The influx of calcium triggers calcium-induced calcium entry from the endoplasmic reticulum (via triggers

inositol-trisphosphate receptors, IPRs) into the cytoplasm. High concentrations of cytoplasmic calcium open calcium-activated potassium channels, terminating burst firing and preventing burst initiation until cytoplasmic levels of calcium decrease. The Sneyd model also predicted that calcium dynamics in the soma (e.g., site of IPRs) were able to terminate action potential bursts initiated in a site containing a high density of sodium channels located outside of the cell soma (Chen et al., 2013). The calcium dynamics in this model also have an unexpected effect on post-synaptic currents. PSCs initiated near the soma are less likely to initiate spiking compared to distal PSCs because the influx of calcium in the soma activates calcium-induced calcium entry and hyperpolarizing potassium currents (Chen and Sneyd, 2015).

Although Sneyd's extended model meticulously detailed intracellular calcium dynamics, Sneyd and colleagues largely relied on GT1 cell parameters for modeling ionic currents. This is problematic because properties of GnRH neuron in brain slices differ markedly from the properties of GT1 cells. GnRH neurons have long dendritic processes, larger spike amplitudes (peak amplitude reach +40 mV compared to 0 mV in GT1 cells), greater spike widths, and larger ionic currents during spikes (e.g., sodium currents are approximately ~10 nA in GnRH neurons compared to <1 nA in GT1 cells)(LeBeau et al., 2000; Wang et al., 2010). Indeed, many of their findings differ from those found by other models that chose new equations for fast transient sodium and potassium currents and/or re-estimated the Sherman model parameters to qualitatively reproduce the ionic currents and firing properties of GnRH neurons in brain slices (Roberts et al., 2006; Roberts et al., 2008; Roberts et al., 2009; Csercsik et al., 2010). For example, one such model, developed by Csercsik and colleagues, predicted that voltage-gated potassium currents, rather than calcium-activated potassium currents, were sufficient for terminating burst firing in GnRH neurons (Csercsik et al., 2010). In a model by Suter and colleagues, PSCs near the soma were more likely to initiate somatic spiking compared to PSCs initiated in distal regions (Roberts et al., 2006). In a subsequent model by Suter, PSCs could initiate action potentials along the entire length of the model dendrite rather than at specific sites, leaving the question of synaptic integration unresolved (Roberts et al., 2008).

Surprisingly, few models have addressed the direct or indirect effects of estradiol on GnRH neuron activity/release. In a model developed by Moran and Khadra, the acute actions of estradiol on multiple ionic currents were predicted to promote irregular bursting in GnRH neurons (Moran et al., 2016). No model has predicted the long-term actions of estradiol feedback on GnRH activity to date.

Dissertation Preview

As reviewed above, previous work studying the electrophysiological properties of GnRH neurons has identified a number of changes induced by estradiol feedback. We hypothesize that GnRH neurons integrate changes to their intrinsic properties and fast-synaptic inputs to switch from negative to positive feedback. We have addressed the individual and combinatorial roles of intrinsic and fast-synaptic changes for initiating positive feedback using a combination of whole-cell voltage and current clamp recordings, dynamic clamp, and mathematical modeling.

In chapter two, we test the hypothesis that GnRH neuron responsiveness to extrinsic stimuli is modulated by time-of-day, estradiol, and the neuromodulator kisspeptin. To test this, we used the daily surge paradigm to measure baseline membrane potential and response to current injection of GnRH neurons. To assess the effect of kisspeptin on GnRH neuron excitability, we measured GnRH neuron response to current injection before and during kisspeptin treatment and in the absence of kisspeptin. As reviewed above, multiple conductances are regulated by estradiol and time-of-day but we cannot yet dissect how individual conductances contribute to excitability using empirical methods. Thus, we used a mathematical model to study how changes to intrinsic conductances measured in voltage-clamp experiments regulate excitability during positive and negative feedback and in the open-loop condition using a novel application of the Markov Chain Monte Carlo (MCMC) parameter estimation method. To our knowledge, we are the first to use the MCMC method to estimate parameters using both voltage-clamp and current-clamp data.

In chapter three, we hypothesize that GnRH neuron responsiveness to GABA post-synaptic conductances is modulated by time-of-day and estradiol. We measured GnRH neuron response to GABA post-synaptic conductances in OVX and OVX+E mice in the

AM and PM using dynamic clamp. In chapter four, we expand our work by measuring GnRH neuron excitability and GABAergic drive during negative feedback (diestrus) and positive feedback (proestrus) in the estrous cycle. In chapter five, we integrate our results and conclusions with the existing literature.

Chapter 2: GnRH Neuron Excitability is Regulated by Estradiol Feedback and Kisspeptin[1]

Abstract

GnRH neurons produce the central output controlling fertility and are regulated by steroid feedback. A switch from estradiol negative to positive feedback initiates the GnRH surge, ultimately triggering ovulation. This occurs on a daily basis in ovariectomized, estradiol-treated (OVX+E) mice; GnRH neurons are suppressed in the AM and activated in the PM. To test the hypotheses that estradiol and time-of-day signals alter GnRH neuron responsiveness to stimuli, GFP-identified GnRH neurons in brain slices from OVX+E or OVX female mice were recorded during the AM or PM. No differences were observed in baseline membrane potential. Current-clamp revealed GnRH neurons fired more action potentials in response to current injection during positive feedback relative to all other groups, which were not different from each other despite reports of differing ionic conductances. Kisspeptin increased GnRH neuron response in cells from OVX and OVX+E mice in the AM but not PM. Paradoxically, excitability in kisspeptin knockout mice was similar to the maximum observed in control mice, but was unchanged by time-of-day or estradiol. A mathematical model applying a Markov Chain Monte Carlo method to estimate probability distributions for estradiol and time-of-day dependent parameters was used to predict intrinsic properties underlying excitability changes. A single identifiable distribution of solutions accounted for similar GnRH neuron excitability in all groups other than positive feedback despite different underlying conductance properties; this was attributable to interdependence of voltage-

[1] *The work in this chapter was originally published in 2018 in the Journal of Neuroscience (38:1249-1263).*

gated potassium channel properties. In contrast, redundant solutions may explain positive feedback, perhaps indicative of the importance of this state for species survival.

Significance statement

Infertility affects 15-20% of couples; failure to ovulate is a common cause. Understanding how the brain controls ovulation is critical for new developments in both infertility treatment and contraception. GnRH neurons are the final common pathway for central neural control of ovulation. We studied how estradiol feedback regulates GnRH excitability, a key determinant of neural firing rate using laboratory and computational approaches. GnRH excitability is up-regulated during positive feedback, perhaps driving increased neural firing rate at this time. Kisspeptin increased GnRH excitability and was essential for estradiol regulation of excitability. Modeling predicts multiple combinations of changes to GnRH intrinsic conductances can produce the firing response in positive feedback, suggesting the brain has many ways to induce ovulation.

Introduction

GnRH neurons are the output pathway for central control of fertility. GnRH initiates pituitary secretion of luteinizing hormone (LH) and follicle-stimulating hormone, thus activating gonadal steroidogenesis. Steroid feedback regulates GnRH release. For most of the reproductive cycle, estradiol negative feedback suppresses GnRH release (Filicori et al., 1986; Moenter et al., 1991). At the end of the follicular phase (proestrus in mice), estradiol switches from suppressing release to inducing a sustained surge of release (Sarkar et al., 1976; Moenter et al., 1991). The GnRH surge drives an LH surge, which induces ovulation.

GnRH surges can be induced by exogenous estradiol (Levine et al., 1985; Moenter et al., 1990). In ovariectomized (OVX) mice with estradiol capsules, GnRH neuron firing and release are suppressed in the morning by estradiol negative feedback (OVX+E AM) and elevated in the afternoon (OVX+E PM) by estradiol positive feedback (Christian et al., 2005; Glanowska et al., 2012). No time-of-day dependent shift in GnRH neuron firing rate is observed in OVX mice without estradiol. Both estradiol and time-of-day regulate GnRH neuron conductances in this daily surge, and other estradiol-induced

surge, paradigms (Chu and Moenter, 2006; Zhang et al., 2007; Zhang et al., 2009; Sun et al., 2010; Pielecka-Fortuna et al., 2011). Because those studies were done using voltage-clamp approaches to isolate specific currents, it is not clear if or how the observed changes in conductances alter GnRH membrane potential, specifically excitability (membrane potential response to stimuli) and action potential firing. The changes observed in the conductances studied, and their typical physiologic effects on the membrane potential, led us hypothesize that GnRH neurons are less excitable during negative feedback and more excitable during positive feedback compared OVX mice.

Changes in ionic conductances that may alter membrane excitability are likely mediated by estradiol-sensitive afferents because GnRH neurons do not typically express detectable levels of ERα, which is required for negative and positive feedback (Hrabovszky et al., 2000; Hrabovszky et al., 2001; Couse et al., 2003; Wintermantel et al., 2006; Christian et al., 2008). Anteroventral periventricular (AVPV) kisspeptin neurons, most of which express ERα, may relay estradiol signals to GnRH neurons during positive feedback (Smith et al., 2005; Smith et al., 2006). Kisspeptin directly modulates ionic currents in GnRH neurons and rapidly stimulates GnRH firing (Pielecka-Fortuna et al., 2008; Zhang et al., 2008; Pielecka-Fortuna et al., 2011; Zhang et al., 2013). AVPV kisspeptin neurons exhibit higher firing rates during positive feedback and endogenous kisspeptin release may enhance GnRH excitability at this time (Zhang et al., 2015; Wang et al., 2016).

We hypothesized that time-of-day and estradiol-dependent changes in intrinsic properties render GnRH neurons more excitable during positive feedback and less excitable during negative feedback compared to the open-loop OVX condition. To test this, we used the daily surge paradigm to examine baseline membrane potential and response to current injection of GnRH neurons. To assess if kisspeptin modulates GnRH neuron excitability, the effects of kisspeptin treatment or deletion of the kisspeptin gene were determined. Both kisspeptin and estradiol feedback target multiple conductances that may drive changes in GnRH neuron excitability. We thus adapted a model GnRH neuron (LeBeau et al., 2000; Moran et al., 2016) to test the contribution of individual conductance targets for estradiol and kisspeptin-induced alterations in GnRH

neuron response. This approach employed a Bayesian Markov Chain Monte Carlo (MCMC) method to estimate probability distributions for each parameter and covariances between parameters using data from whole-cell voltage-clamp and current-clamp experiments. MCMC methods are widely used in the physical sciences but have been rarely been applied to integrated biophysical problems, having been used to model single channels or individual whole-cell currents (Rosales et al., 2001; Siekmann et al., 2011; Siekmann et al., 2012; Merel et al., 2016; Mackay et al., 2017), or cardiomyocyte action potentials (Johnstone et al., 2016a; Johnstone et al., 2016b). To our knowledge, this is the first application of MCMC to fit multiple currents from whole-cell experiments.

Materials and methods

All chemicals were purchased from Sigma-Aldrich, unless noted.

Animals

Transgenic mice expressing green fluorescent protein (GFP) under the control of the GnRH promoter (GnRH-GFP) were used (Suter et al., 2000). Kisspeptin knockout mice (Lapatto et al., 2007; Chan et al., 2009) were crossed with GnRH-GFP mice to identify GnRH neurons for electrophysiologic recordings. Mice were housed on a 14-h light:10-h dark cycle with lights off at 6 P.M. (eastern standard time). Teklad 2916 chow (Envigo) and water were available ad libitum. Adult females within the appropriate age range (65-135 days) were randomly selected from our colony. Ovariectomy was performed under isoflurane (VetOne) anesthesia. At the same time as the surgery for OVX, mice were randomized to either receive a Silastic (Dow Corning) capsule containing 0.625 µg 17β-estradiol suspended in sesame oil (OVX+E) or not be treated further (OVX). Bupivacaine (0.25%, APP Pharmaceuticals) was applied to surgical sites to reduce postoperative pain and distress. Electrophysiologic experiments were performed 2-4 days after surgery and estradiol status was confirmed by measurements of uterine mass of control mice for figures 2.1-3 (OVX, n=31, 45.1 ± 1.5 mg; OVX+E, n=39, 167.1 ± 2.6 mg; two-tailed unpaired Student's t-test, $F_{(38,30)}$=4.13, p<0.0001) and of kisspeptin knockout mice for figures 2.4, 2.5 (OVX, n=3, 13.0 ± 2.1; OVX+E, n=6, 37.8 ± 5.8 mg;

two-tailed unpaired Student's t-test, $F_{(5,2)}$=15.5, p=0.02). It is important to point out that this daily surge model does not recapitulate the pattern of estradiol during the cycle. Rather it effectively induces both negative and positive feedback on LH release in vivo and GnRH neuron activity in the brain slice relative to measurements in OVX mice (Christian et al., 2005; Silveira et al., 2016). This separates two variables, time of day and circulating estradiol level, known to contribute to the generation of the LH surge in mice and other rodents and which were the targets of the present investigations.

Brain Slice Preparation

All solutions were bubbled with 95% O_2/5% CO_2 throughout the experiments and for at least 15 min before exposure to tissue. Brain slices were prepared either from 7.5-9.5 h before lights out (AM recordings) or 1-2.5 h before lights out (PM recordings). The brain was rapidly removed and placed in ice-cold sucrose saline solution containing the following (in mM): 250 sucrose, 3.5 KCl, 26 $NaHCO_3$, 10 d-glucose, 1.25 Na_2HPO_4, 1.2 $MgSO_4$, and 3.8 $MgCl_2$, at pH 7.6 and 345 mOsm. Coronal (300 µm) slices were cut with a VT1200S Microtome (Leica Biosystems). Slices were incubated in a 1:1 mixture of sucrose saline and artificial CSF (ACSF) containing (in mM) 135 NaCl, 3.5 KCl, 26 $NaHCO_3$, 10 D-glucose, 1.25 Na_2HPO_4, 1.2 $MgSO_4$, and 2.5 $CaCl_2$, at pH 7.4 and 305 mOsm, for 30 min at room temperature (~21 to 23°C). Slices were then transferred to 100% ACSF at room temperature for 0.5-5 h before recording.

Data Acquisition

During recording, slices containing the preoptic area and anterior hypothalamus, which contain the majority of GnRH neuron somata, were placed into a chamber continuously perfused with ACSF at a rate of 2 ml/min with oxygenated ACSF heated to 28.5-31.5°C with an inline-heating unit (Warner Instruments). In all recordings, ACSF contained 100 µM picrotoxin, 20 µM D-APV, and 20 µM CNQX to block ionotropic GABA and glutamate receptors. GFP-positive cells were visualized with a combination of infrared differential interference contrast and fluorescence microscopy on an Olympus BX51WI microscope. Borosilicate glass capillaries (1.65-mm OD x 1.12-mm ID; World Precision Instruments, Inc.) were pulled by using a Flaming/Brown P-97 unit (Sutter Instrument

Company) to make recording pipettes. Pipettes measured 2-4.5 MΩ when filled with (in mM): 125 K gluconate, 20 KCl, 10 HEPES, 5 EGTA, 0.1 CaCl2, 4 MgATP, and 0.4 NaGTP, 300 mOsm, pH 7.2 with NaOH. Pipettes were wrapped with Parafilm (Bemis) to reduce capacitive transients; remaining transients were electronically cancelled. Pipettes were placed in contact with a GFP-positive neuron using an MP-285 micromanipulator (Sutter Instrument Company). All potentials reported were corrected online for liquid junction potential of −14.2 mV (Barry, 1994). Recordings were made with an EPC-10 dual patch-clamp amplifier (HEKA Elektronik) and a Macintosh computer running Patchmaster software (HEKA Elektronik). Experiments were analyzed offline using custom software (DeFazio and Moenter, 2002; DeFazio et al., 2014) written in IgorPro (Wavemetrics).

Experimental Design

On-Cell Measurement of Membrane Potential (OCVm)

During a recording in the on-cell configuration, the patch of membrane within the pipette is exposed to a potential difference equal to the membrane potential (V_{cell}) minus the pipette command potential ($V_{patch} = V_{cell} - V_{pipette}$). Potassium channels within the pipette can be manipulated by varying the pipette potential and the reversal of current through these channels (E_K) used to estimate the membrane potential (Fricker et al., 1999; Verheugen et al., 1999; DeFazio et al., 2002; DeFazio et al., 2014). This method assumes that the concentration of the potassium in the cell is similar to that in the pipette solution, resulting in a reversal potential for potassium (E_K) near zero. Although the concentration of intracellular potassium in GnRH neurons has not yet been determined, a difference of 15 mM in the typical range of intracellular potassium concentration results in a change in measured membrane potential of only 5 mV using this method. After establishing a >2 GΩ seal, inactivation of potassium channels was reduced by setting $V_{pipette}$ to 100 mV for 60 ms (V_{patch} ~-170 mV, assuming -70 mV V_{cell}). Voltage-dependent channels were then activated by ramping the pipette voltage from 100 mV to -150 mV (V_{patch} ~ -150 to 200 mV) over 30 ms. During the voltage ramp, potassium channels are opened and generate an initial inward current followed by an outward current. Leak correction was applied by subtracting a linear fit of the current

during the ramp before activation of the potassium currents. The ramp potential at which the leak-corrected current is 0 pA reflects the membrane potential of the cell. On-cell measurements were performed in the presence of 1 μM TTX to block action potentials. Membrane currents were sampled at 20 kHz and filtered at 10 kHz. Three to five voltage ramps were averaged for each cell; ramps in which noise prohibited a good linear fit were discarded.

Whole-cell patch-clamp

After achieving a >1 GΩ seal and the whole-cell configuration, membrane potential was held at -60 mV between protocols. Series resistance (Rs), input resistance (Rin), and holding current (Ihold) were measured every 2-3 min using a 5 mV hyperpolarizing step from −60 mV (mean of 20 repeats, 20 ms duration, sampled at 100 kHz). Only recordings with a Rin of >500 MΩ, Ihold of −35 to 30 pA, stable Rs of <20 MΩ, and a stable Cm between 9.5 and 23 pF were used for analysis.

In current-clamp, direct current (<25 pA, 8.6±0.6 pA, n=109) was adjusted to keep cells within 2 mV of -69 mV. Membrane potential was sampled at 20 kHz and filtered at 7.3 kHz. Bridge balance (95%) was used for most cells; for a few cells, bridge balance was not used but results were similar. To determine GnRH neuron excitability, cells were injected with current from 0-30 pA (500 ms, 2 pA steps). This protocol was repeated two to three times per cell and the number of action potentials at each step was averaged. The first spike fired was used to determine the following action potential characteristics: latency from start of the current injection to first spike, firing threshold (first derivative of the voltage trace > 1 mV/s), peak amplitude relative to threshold, full width at half-maximum (FWHM), rate-of-rise, and time and amplitude of after-hyperpolarization potential (AHP, the amplitude and time, relative to action potential initiation, of local minimum after the spike peak). To test the effects of kisspeptin, the above was repeated on another set of cells before and during bath application of 10 nM kisspeptin; to control for time of recording, another set of cells was recorded for a similar amount of time but not treated.

To isolate potassium currents in voltage-clamp in cells from control OVX+E AM mice, we blocked voltage-gated Na^+ and Ca^{2+} channels with 1 μM tetrodotoxin (TTX) and 200

μM $CdCl_2$, respectively. Series resistance was compensated between 55% and 85%. Two distinct voltage-clamp protocols were used to determine inactivation (initial hyperpolarization to -100 mV for 500 ms to remove inactivation, steps from -100 to -10 mV in 10-mV increments for 500 ms, final test pulse of -10 mV for 500 ms), and activation (-100 mV for 500 ms, prepulse of -100 mV or -30 mV, test potentials from -100 mV to 40 mV, 10-mV increments). Inactivation was complete at -30 mV (i.e., no fast transient current was present in current traces after the -30 mV prepulse). I_A was isolated by subtracting the current after the -30 mV from that of more hyperpolarized pulses. Peak current was normalized and divided by the driving force calculated using Ohm's law rather than the Goldman-Hodgkin-Katz to be consistent with the mathematical model. A representative cell was chosen that closely resembled the median activation and inactivation properties of I_A and I_K from our own recordings and from two previous studies (DeFazio and Moenter, 2002; Pielecka-Fortuna et al., 2011).

Statistical Analyses

Data were analyzed using Prism 7 (GraphPad) or SPSS (IBM) and are reported as the mean ± SEM unless otherwise noted. The number of cells per group is indicated by n. No more than two cells were used per animal with at least four animals tested per group. An exception was made for kisspeptin knockout mice, which are infertile and must be bred from compound heterozygotes. For those groups no more than three cells per animal and at least three animals per group were examined. Data requiring one-way analyses were compared using one-way ANOVA with Bonferroni *post hoc* analysis or Kruskal–Wallis test with Dunn's *post hoc* analysis as dictated by data distribution. All data requiring two-way analyses were compared using two-way ANOVA with Bonferroni post hoc analysis; this test is considered sufficiently robust for non-normally as well as normally distributed data (Underwood, 1996). ANOVA analyses did not assume equal subgroup sizes. Percentage values were compared using Chi-square with Yate's correction. Significance was set a $p<0.05$ but all p values <0.1 are specified. All data requiring three-way analyses were compared using a three-way ANOVA with Bonferroni *post hoc* analysis.

Mathematical Modeling

Summary

The mathematical modeling was done in two steps. We started with the model published by Moran et al., 2016. In step 1, values for individual currents were estimated. We used published voltage-clamp data to estimate the parameters that control the size and timing of ionic currents that are changed in the daily surge model (I_A, I_K, I_{HVA}, I_{LVA}). These estimates were loosely constrained by current-clamp data from the present study to make sure action potentials generated by the model looked like those from GnRH neurons. It was also necessary to alter (re-estimate) the values used for the fast sodium current underlying action potential firing to achieve this goal. In step 2, we integrated all the individual currents, along with the current-clamp data (firing at 6 pA steps and action potential shape), to reproduce the firing and action potential characteristics of a GnRH neuron during negative feedback (OVX+E AM). To do this, we allowed four parameters that are dependent on estradiol and time of day to vary (maximum conductance of $I_{A,}$ I_{NaP} and I_{HVA}, and V ½ inactivation of I_A).

We modified a GnRH neuron model developed by Moran and Khadra (Moran et al., 2016) that was itself based upon the original Hodgkin and Huxley GnRH neuron model (LeBeau et al., 2000). In this model, membrane potential is expressed in mV, time is in ms, currents are in pA, and conductances are in nS. The governing equation for membrane potential is described by:

$$C_m \frac{dV}{dt} = -\left(I_{NaF} + I_{NaP} + I_A + I_K + I_{HVA} + I_{LVA} + I_S + I_h + I_{KCa} + I_L\right) + I_{app}, \qquad (1)$$

where C_m= 20 pF is the cell capacitance (Pielecka-Fortuna et al., 2011), V is the cell membrane potential, and t is the time. I_{Na}F and I_{NaP} are fast transient and persistent sodium currents, respectively. I_A is the A-type transient potassium current and I_K is the delayed-rectifier or sustained potassium current. I_{HVA} and I_{LVA} are high-voltage activated and low-voltage activated calcium currents. I_S describes a slow inward calcium current. I_h is the hyperpolarization-activated non-specific cation current. I_{KCa} is a calcium-dependent potassium current, and I_L is the leak current. I_{app} is the applied current, which was set to -6 pA to hold the cell at -70 mV.

Individual ionic currents were modeled using Ohm's law *I=G(V-E)* where *G* is the conductance, *V* is the membrane potential and *E* is the reversal potential for that ion. *(V-E)* describes the driving force across the membrane and *G* is equal to the maximum conductance if all channels are open (*g*) multiplied by the proportion of open channels. For the majority of currents, the proportion of open channels was estimated using the Hodgkin-Huxley formalism:

$$I = gm^p h\left(V - E\right), \tag{2}$$

where *m* and *h* represent activation and inactivation gating variables and *p* is the number of independent activation gates. The Hodgkin-Huxley model was also used for the following currents:

$$I_{NaP} = g_{NaP} m_{NaP} h_{NaP}\left(V - E_{Na}\right), \tag{3}$$

$$I_A = g_A m_A \left(f_A h_{1A} + (1 - f_A) h_{2A}\right)\left(V - E_K\right) \tag{4}$$

$$I_K = g_k m_K^4 \left(V - E_K\right), \tag{5}$$

$$I_{HVA} = g_{HVA} m_{HVA} \left(f_{HVA} h_{1HVA} + \left(1 - f_{HVA}\right) h_{2HVA}\right)\left(V - E_{Ca}\right) \tag{6}$$

$$I_{LVA} = g_{LVA} m_{LVA}^2 h_{LVA}\left(V - E_{Ca}\right), \tag{7}$$

$$I_S = g_S m_S \left(V - E_{Ca}\right), \tag{8}$$

$$I_h = g_h \left(f_h h_{1h} + \left(1 - f_h\right) h_{2h}\right)\left(V - E_h\right) \tag{9}$$

In the case of I_A, I_{HVA}, and I_h, the inactivation variable is the weighted sum of gating variables h_i, which have different voltage-dependent time constants, and represent two different populations of inactivating gates present in the cell membrane:

$$h = \sum_{i=1}^{n} f_i h_i \tag{10}$$

where f_A=0.8, f_{HVA} = 0.2, f_h = 0.384 for h_{1A}, h_{1HVA}, and h_{1h}, respectively.

The activation and inactivation gating variables are governed by:

$$\frac{dm}{dt} = \frac{m_\infty(V) - m}{\tau_m(V)}, \tag{11}$$

$$\frac{dh_i}{dt} = \frac{h_\infty(V) - h_i}{\tau_{h_i}(V)}, \tag{12}$$

where m_∞ and h_∞ are steady-state activation and inactivation functions and τ is the time constant (which can be voltage-dependent or independent) in ms. Steady-state activation and inactivation functions are of the form:

$$x_\infty(V) = \frac{1}{1+\exp\left(\frac{V - V_h}{k}\right)}, x = m, h, \tag{13}$$

V is the membrane potential, V_h is voltage at half activation or inactivation and k is the steepness of the steady-state function. In the case of m_k, the steady-state function was raised to the power of 1/4 to increase slope steepness to be consistent with the experimentally-derived steady-state activation for I_K (Moran et al., 2016). Our previous work in the daily surge model indicated slopes of the empirical steady-state activation curves for I_K and I_A were ~1.7 pA/mV and ~2.1 pA/mV respectively (Pielecka-Fortuna et al., 2011); re-examination of those data suggest the A-type current may not have been completely inactivated in some cells. We thus made new estimates from individual cells from new voltage-clamp experiments in the daily surge model and from OVX PM and OVX+E PM female mice (DeFazio and Moenter, 2002); these studies indicate the empirical slopes for I_K and I_A are ~10 pA/mV and ~15 pA/mV, respectively (estimated using Ohm's law). As a consequence, we did not to raise the steady-state function of m_K to the power of 1/4 to increase slope as in the Moran et al. model (Moran et al., 2016).

Voltage-dependent time constants were estimated from one of two functions:

$$\tau_i = \frac{e_i}{\exp\left(\frac{a_i + V}{b_i}\right) + \exp\left(\frac{c_i + V}{d_i}\right)} + f_i, i = h_{NaP}, m_A, m_K, m_{HVA}, m_{LVA}, \tag{14}$$

$$\tau_i = c_i \cdot \exp\left(-\left(\frac{V - a_i}{b_i}\right)^2\right), \; i = h_{h,1}, h_{h,2}, \tag{15}$$

where V is the membrane potential and a, b, c, d, e, and f are constants. Parameter estimates for f were close to zero or zero for m_A, m_K, and m_{LVA}. In the model developed by Moran et al., the rate of activation (time constant $\tau_{m,HVA}$) for HVA current was voltage-dependent; however, voltage-clamp data from Sun et al. indicate that the speed of activation is voltage-independent. The initial parameter estimates for the HVA activation speed using equation 14 resulted in $\tau_{m,HVA}$ <0.005 ms from -100 to 100 mV (10 mV steps). Thus, $\tau_{m,HVA}$ for the HVA current activation variable is voltage independent in our adaptation of the model.

Fast transient sodium current is described using a Markov model with each of three subunits having three states, open (O), closed (C), and inactivated (I):

$$I_{NaF} = g_{NaF} O^3 \left(V - E_{Na}\right), \tag{16}$$

$$\frac{dC}{dt} = r_3\left(V\right) I + \beta\left(V\right) O - \left(\alpha\left(V\right) + r_4\right) C, \tag{17}$$

$$\frac{dO}{dt} = r_2 I + \alpha\left(V\right) C - \left(\beta\left(V\right) + r_1\right) O, \tag{18}$$

$$I = 1 - C - O, \tag{19}$$

V is the membrane potential, r_1, r_2, r_4 are voltage-independent constants and r_3, α, and β are voltage-dependent constants described by:

$$i = \frac{a_i}{1 + \exp\left(\dfrac{V + b_i}{c_i}\right)}, i = \alpha, \beta, r_3, \tag{20}$$

where a, b, and c are constants.

Calcium-activated potassium currents were estimated with the current equation:

$$I_{KCa} = g_{KCa} \frac{Ca^2}{K^2 + Ca^2}\left(V - E_K\right). \tag{21}$$

Here, K = 1.0 μM, and Ca is the calcium concentration (μM) in the cytosol. Cytosolic calcium increased when calcium entered the cell through voltage-gated channels (I_{Ca})

and decreased when it was pumped out of the cytosol through calcium-ATPases. Calcium is governed by the following equations:

$$\frac{dCa}{dt} = f\left(-\alpha I_{Ca} - k_p \frac{Ca^2}{K_p{}^2 + Ca^2}\right), \tag{22}$$

$$I_{Ca} = I_{LVA} + I_{HVA} + I_S, \tag{23}$$

where f=0.0025 is the fraction of unbound calcium in the cytosol, I_{Ca} is the total calcium current, k_p=0.265 μM/ms is the maximum pump rate, K_p = 1.2 μM is the concentration of calcium at which half of the pumps are occupied, α=0.00185 μM/(pA·ms) is a current to flux conversion factor.

Leak current was estimated with the following function:

$$I_L = g_L\left(V - E_L\right). \tag{24}$$

Parameter Estimation

Parameter estimation was performed using Goodman and Weare's Affine Invariant Markov Chain Monte Carlo Ensemble sampler, implemented using the emcee package (http://dfm.io/emcee/current/) (Goodman and Weare, 2010; Foreman-Mackey et al., 2013). MCMC methods generated a Markov chain of parameter sets (θ_1, θ_2,…,θ_n), containing m parameters. For each parameter set, a posterior probability (likelihood of set θ_i given the data) is calculated from Bayes' theorem:

$$p\left(\theta \mid data\right) \propto p\left(data \mid \theta\right) p\left(\theta\right) \tag{25}$$

where $p(\theta)$ is the prior probability for the parameters before observing any data. Since we possessed little prior information regarding parameter values, we chose uniform distributions bounded within physiologic ranges (e.g., -200 mV to 200 mV for $V_{1/2}$ inactivation or activation) as priors for each parameter. $p(data|\theta)$ is the likelihood of observing the data if the true parameters were equal to θ. Log probabilities were used to increase computation speed and accuracy. The log likelihood was determined by:

$$\log p\left(data \mid \theta\right) = -\left(\sum_{i=1}^{N} \frac{\left(model_i - data_i\right)^2}{2\sigma^2} + \log\left(2\pi\sigma^2\right) \right) \quad (26)$$

where N is the total number of sampled points, i refers to the i_{th} point, $data_i$ to the i_{th} point in the data (e.g., the membrane potential or current at i), $model_i$ refers to the to the i_{th} point in the model having parameter set θ. σ was equal to 0.5.

MCMC methods preferentially sample states with greater likelihoods, generating a posterior probability distribution for each parameter. For each simulation, 100 individual Markov chains, aka 'random walks', were generated. To increase mixing between samples and avoid individual random walkers from becoming stuck in local minima, a parallel tempering algorithm was used. For MCMC simulations using voltage-clamp data, five 'temperatures' were used with each set according to an exponential temperature ladder in which each level increases by a factor of $\sqrt{2}$. For MCMC simulations using current-clamp data, three 'temperatures' were used to make computation time manageable.

Previous voltage-clamp experiments have isolated I_A, I_K, I_{HVA}, and I_{LVA} in the daily surge model (Sun et al., 2010; Pielecka-Fortuna et al., 2011). Activation and inactivation curves for I_{LVA} from another estradiol feedback model were used. We used these experiments and experiments measuring I_{LVA} from another model of estradiol feedback (Zhang et al., 2009) to estimate parameters for I_A, I_K, I_{HVA}, and I_{LVA} during negative feedback. For I_{HVA} and I_{LVA}, the models were simultaneously fit to activation and inactivation curves as well as time-course data from an activation protocol in voltage-clamp. Specific voltage-clamp protocols can be found in Figure 2.6. Because potassium currents play a large role in determining action potential shape, parameters for I_A and I_K were estimated from both current-clamp and voltage-clamp experiments. For I_A, the model was simultaneously fit to activation and inactivation curves, time-course data from an activation protocol in voltage-clamp, and to an average action potential and current vs number of action potentials response curve in current-clamp. For I_K, the model was simultaneously fit to an activation curve, time-course data from an activation protocol in voltage-clamp, and to an average action potential and current vs number of action potentials response curve in current-clamp. For I_A, I_{HVA}, and I_K, parameters were

estimated using experiments from a single representative cell. The current vs number of action potentials response curve from a single representative trace was used to provide a discrete number of action potentials at each step. Modeling of current injections was from 0 – 30 pA with 10 pA steps to reduce computation time. Differences in liquid junction potentials across experiments were corrected. To accurately reproduce the upswing of an action potential, it was also necessary to estimate parameters controlling the switch from the closed to open state for I_{NaF}. These parameters were estimated from current-clamp data alone.

After parameters I_A, I_K, I_{HVA}, and I_{LVA} had been individually estimated, we used these new parameters and re-estimated time-of-day and estradiol-dependent parameters to reproduce average action potential shape during negative feedback and the slope of the current vs number of action potential curves. For this, 6 pA steps from 0 - 30 pA were used as a compromise between computational intensity and not wanting to miss changes occurring between 10 pA steps.

Parameter values are otherwise unchanged from Moran et al., (Moran et al., 2016). Maximum conductance values and reversal potentials from voltage-clamp experiments and for negative feedback can be found Table 2.1, as well as $V_{1/2}$ inactivation for I_A. Parameter values for the activation and inactivation variables can be found in Table 2.2. Parameter values for I_{NaF} can be found in Table 2.3.

Table 2.1. Parameter values for ionic currents appearing in equations 2-9.
E is the reversal potential. In step 1, the maximum conductance, g_{vc} , was estimated from fit (Figure 2.6) of voltage-clamp experiments (Zhang et al., 2009; Sun et al., 2010; Pielecka-Fortuna et al., 2011) constrained by current-clamp data (Figure 2.2). In step 2, the maximum conductance, $g_{neg\ FB}$, was estimated that reproduces the current-clamp data during negative feedback. Parameters that were allowed to vary in Figure 2.7 and 2.8 are shown marked with *.

		Step 1	***Step 2***
	***E* (mV)**	**g_{vc} (nS)**	**$g_{neg\ FB}$ (nS)**
I_{NaF}	54	-	758
I_{NaP}	54	-	0.39*
I_A	-101	70.2	313*
I_K	-101	57	57
I_{LVA}	82.5	0.0679	0.0679
I_{HVA}	82.5	7.31	5.16*
I_S	82.5	-	0.18
I_h	-40	-	1
I_{KCa}	-101	-	1.18
I_L	-65	-	1
		(mV)	**(mV)**
I_A $V_{1/2}$ *inactivation*	-	-60	-69.8*

Table 2.2. Parameter values for the activation and inactivation variables appearing in equations 13-15.
V_h and *k* are the voltage at half activation or inactivation and the steepness of the steady-state function. τ is the time constant which is voltage independent for m_{Nap}, h_{1A}, h_{2A}, h_{LVA}, m_{HVA}, h_{1HVA}, h_{2HVA} and m_s. For h_{NaP}, m_A, m_K, m_{LVA}, h_{1}h and h_{2h}, τ is voltage-dependent and governed by equation 14 (*a*, *b*, *c*, and *d* are in mV, *e* and *f* are in ms) or equation 15 (*a* and *b* are in mV, and *c* is in ms). Parameters that were re-estimated from Moran et al., 2016 are shown in bold.

	I_{NaP}		I_A			I_K	I_{LVA}		I_{HVA}			I_S	I_h	
	m	*h*	***m***	**h1**	**h2**	***m***	***m***	***h***	***m***	***h_1***	***h_2***	*m*	h_1	h_2
V_h (mV)	-41.5	-47.4	**-29.4**	**-60**	**-60**	**-19.7**	**-51.4**	**-80.1**	**-11**	**-36.6**	**-36.6**	-45	-77.4	-77.4
k (mV)	-3.0	8.2	**-6.64**	**4.26**	**4.26**	**-12.3**	**-4.07**	**5.5**	**-7**	**14.6**	**14.6**	-12	9.2	9.2
τ (ms)	0.4	Eq 14	Eq 14	**7.67**	**100**	Eq 14	Eq 14	**250**	**0.816**	**53.4**	**728**	1500	Eq 15	Eq 15
a	-	67.3	**-2.91**	-	-	**23.8**	**31.3**	-	-	-	-	-	-89.8	-82.6
b	-	-27.5	**25.6**	-	-	**18**	**10.1**	-	-	-	-	-	11.6	25.7
c	-	67.3	**65.3**	-	-	**23.8**	**31.3**	-	-	-	-	-	35.8	370.9
d	-	27.5	**-10.6**	-	-	**-18**	**-10.1**	-	-	-	-	-	7.6	54.1
e	-	574.5	1	-	-	**10.6**	**109**	-	-	-	-	-	-	-
f	-	62.6	**0.0527**	-	-	0	**0.0391**	-	-	-	-	-	-	-

Table 2.3. Parameters values for the Markov model of I_{NaF} (equations 16-19).
α(V) and β(V) describe the transition rates (ms^{-1}) between the closed and open states, r_1 and r_2 describe the transition rates between the open and inactivated states, and r_3(V) and r_4 describe the transition rates between the inactivated and closed states. α(V), β(V), and r_3(V) are voltage-dependent while r_1, r_2, and r_4 are voltage-independent. Parameters that were allowed to vary during modeling are shown in bold. Maximum conductance was re-estimated to be 758 nS.

	α(V)	***β(V)***	***r_1***	***r_2***	***r_3(V)***	***r_4***
rate (ms^{-1})	Eq. 20	Eq. 20	1.0	0.2	Eq. 20	0.05
a (ms^{-1})	55	60	-	-	30	-
b (mV)	**6.4**	32	-	-	77.5	-
c (mV)	**-15.9**	10	-	-	12	-

Results

GnRH neuron baseline membrane potential is not modulated by time-of-day or estradiol

GnRH neuron firing rate is decreased during negative feedback (OVX+E AM) and increased during positive feedback (OVX+E PM) relative to OVX controls, which have an intermediate firing level (Christian et al., 2005). Baseline membrane potential can influence firing rate. Estimates of baseline membrane potential were obtained from GFP-identified GnRH neurons in brain slices using an on-cell approach that maintains the native intracellular milieu. Figure 2.1A shows the voltage protocol used (top) and the membrane current response (bottom) before leak subtraction; Figure 2.1B shows representative leak-subtracted responses (see Materials and Methods for details). No time-of-day or estradiol-dependent change in baseline membrane potential was observed among groups (Figure 2.1C, n=8 each OVX AM and PM, n=9 each OVX+E AM and PM, two-way ANOVA/Bonferroni, $p>0.3$, estradiol $F_{(1,41)}=0.2$, time-of-day $F_{(1,41)}=2.8$, interaction $F_{(1,41)}=3.2$).

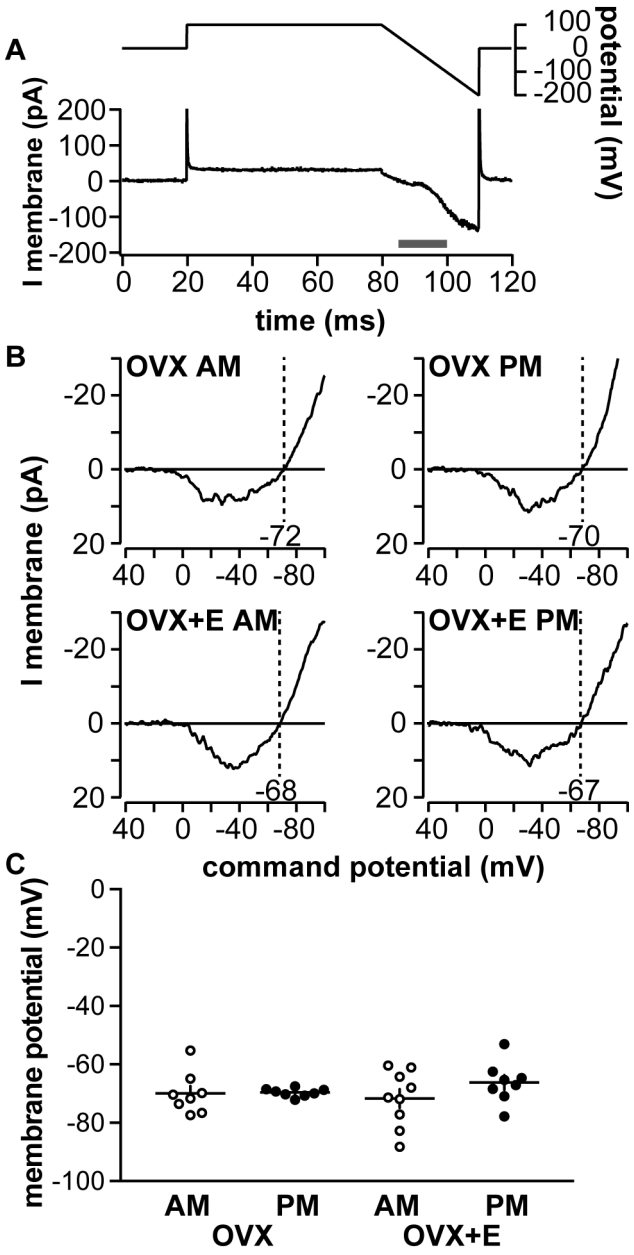

Figure 2.1. Baseline membrane potential of GnRH neurons is not modulated by time-of-day or estradiol.
A. OCVm recording methodology. Top, Voltage protocol. Bottom, resulting membrane current. **B.** Representative leak-subtracted OCVm traces from OVX AM, OVX PM, OVX+E AM, and OVX+E PM neurons. **C.** No difference in baseline membrane potential (individual values and mean ± SEM, two-way ANOVA/Bonferroni) was observed among experimental groups.

GnRH neuron excitability is increased during positive feedback

All whole-cell recording parameters are shown in Table 2.4.

In the daily surge model, estradiol and time-of-day interact to modify calcium and potassium currents. These changes are predicted to make GnRH neurons less excitable during negative feedback and more excitable during positive feedback relative to open-loop (OVX) groups. To investigate directly if time-of-day and estradiol modulated GnRH neuron excitability, we measured GnRH neuron response to depolarizing steady-state current injections (0-30 pA, 2 pA steps, 500ms). Input resistance was not different among groups (Table 2.4). Current injections were initiated from a mean membrane potential of -69 ± 2 mV, near the value determined in the above experiments. Figure 2.2A shows representative responses to +12 and +24 pA injections. Once firing was initiated, GnRH neurons from OVX+E PM mice fired more spikes at each current step from 18-30 pA compared to all other groups (Figure 2.2B, OVX AM n = 10, OVX PM n = 9, three-way repeated-measures ANOVA/Bonferroni, $p<0.05$). No difference was observed among cells from OVX AM, OVX PM, and OVX+E AM groups ($p>0.15$). GnRH neuron excitability, measured as action potential firing response to current injection, is thus increased during positive feedback, consistent with our hypothesis, but not reduced during negative feedback, contrary to our hypothesis.

Despite the marked increase in action potential firing during positive feedback, effects on action potential properties were modest. Estradiol reduced spike amplitude in cells recorded in the AM (Figure 2.2E, OVX AM vs OVX+E AM, two-way ANOVA/Bonferroni, $p=0.008$, Table 2.5). Estradiol and/or time-of-day dependent effects on spike latency (Figure 2.2C, two-way ANOVA/Bonferroni, $p=0.1$, Table 2.5), firing threshold (Figure 2.2D, two-way ANOVA, interaction $p=0.08$, Table 2.5) and AHP amplitude (Figure 2.2H, two-way ANOVA/Bonferroni, $p=0.07$, Table 2.5) approached but did not achieve the level set for significance. No time-of-day or estradiol-dependent changes were observed in FWHM (Figure 2.2F), rate-of-rise (Figure 2.2G), or AHP time (Figure 2.2I, two-way ANOVA/Bonferroni, Table 2.5).

Table 2.4. Whole-cell recording properties for Figures 2.2-4.

Mean±SEM of GnRH whole-cell passive properties from Figure 2.2				
	OVX AM	*OVX PM*	*OVX+E AM*	*OVX+E PM*
Input resistance (MΩ)	1019±133	897.8±39	955.6±81	992.6±82
Capacitance (pF)	15.5±0.6	17.8±0.8	16.9±0.6	16.3±1.0
Series resistance(MΩ)	11.8±0.9	10.7±0.5	11.4±0.8	12.0±1.0
Holding current (pA)	-0.1±2	-6.4±5	3.3±3	0.3±4
Two-way ANOVA parameters for comparison of GnRH passive properties among groups: cells from OVX AM, OVX PM, OVX+E AM, OVX+E PM (Figure 2.2)				
	estradiol	*time-of-day*	*interaction*	
Input resistance (MΩ)	$F_{(1,41)}$=0.03	$F_{(1,41)}$=0.2	$F_{(1,41)}$=0.7	
Capacitance (pF)	$F_{(1,41)}$=0.001	$F_{(1,41)}$=1.1	$F_{(1,41)}$=3.6 (p=0.07)	
Series resistance(MΩ)	$F_{(1,41)}$=0.3	$F_{(1,41)}$=0.09	$F_{(1,41)}$=1.0	
Holding current (pA)	$F_{(1,41)}$=2.0	$F_{(1,41)}$=1.7	$F_{(1,41)}$=0.2	
Mean±SEM of GnRH whole-cell passive properties from Figure 2.3				
	OVX AM	*OVX PM*	*OVX+E AM*	*OVX+E PM*
Input resistance (MΩ) before kisspeptin during kisspeptin	 1003±111 2061±253	 970.8±59 1378±216	 1097±93 1711±314	 1283±193 2302±471
Capacitance (pF) before kisspeptin during kisspeptin	 17.3±0.9 18.0±1.0	 16.4±0.9 16.9±0.9	 16.0±0.7 16.9±0.6	 14.4±1.2 14.8±1.3
Series resistance(MΩ) before kisspeptin during kisspeptin	 10.0±0.5 10.4±0.8	 10.5±0.6 10.5±0.8	 10.8±0.7 12.5±1.3	 10.5±0.4 10.8±0.3
Holding current (pA) before kisspeptin during kisspeptin	 7.1±3 -39±6	 0.8±3 -39±5	 4.3±3 -25±5	 2.3±2 -18±3

Three-way ANOVA $F_{(1,32)}$ values for comparison of GnRH passive properties among groups: cells from OVX PM, OVX+E AM, OVX+E PM (Figure 2.3)							
	E2	*AM/ PM*	*kiss*	*E2 x kiss*	*AM/PM x kiss*	*E2 x AM/PM*	*E2 x kiss x AM/PM*
Input resistance (MΩ)	1.1	0.03	39***	0.3	0.4	3.4 (p=0.07)	3.6 (p=0.07)
Capacitance (pF)	3.1 (p=0.09)	2.4	43***	0.03	2.5	0.2	0.3
Series resistance(MΩ)	1.3	0.2	3.3 (p=0.08)	1.5	2.1	1.0	0.8
Holding current (pA)	5.2*	0.01	283***	21***	3.4 (p=0.08)	0.7	0.2

Mean±SEM of GnRH whole-cell passive properties from Figure 2.4			
	OVX PM	*OVX+E AM*	*OVX+E PM*
Input resistance (MΩ)	1194±181	1314±208	1531±218
Capacitance (pF)	13.1±1	14.0±1	14.1±0.8
Series resistance(MΩ)	11.9±0.8	11.6±0.9	11.1±0.9
Holding current (pA)	-3.3±3	-3.2±4	-10±3.6
One-way ANOVA parameters for comparison of GnRH passive properties among groups: cells from OVX PM, OVX+E AM, OVX+E PM (Figure 2.4)			
Input resistance (MΩ)	KW statistic = 0.6		
Capacitance (pF)	$F_{(2,22)}$=0.4		
Series resistance(MΩ)	KW statistic = 0.6		
Holding current (pA)	$F_{(2,22)}$=1.3		

*p<0.05; **p<0.01; ***p<0.001.

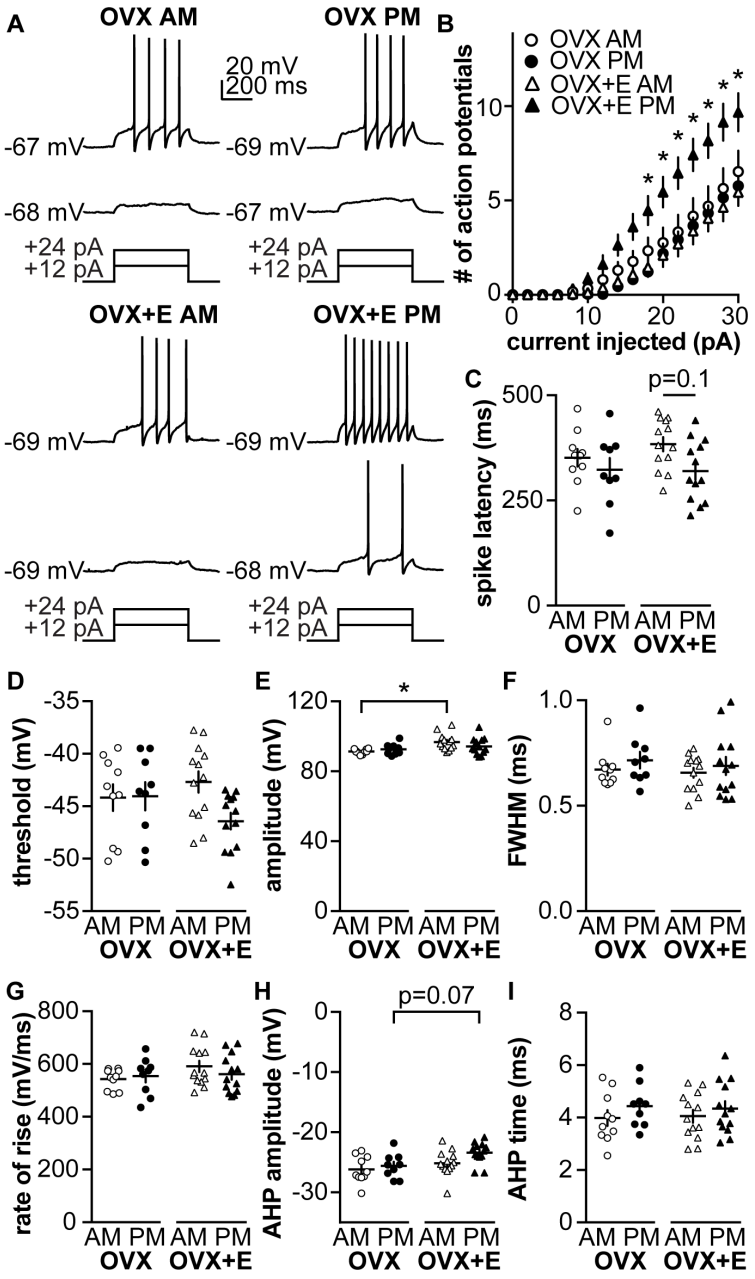

Figure 2.2. GnRH neuron excitability is increased during positive feedback.
A. Representative traces from neurons in each group during 500 ms current injections of 12 and 24 pA (injection protocol below). **B.** Mean ± SEM spikes elicited for each current injection step. **C-I** Individual values and mean ± SEM for: **C,** latency to first spike, **D,** action potential threshold, **E,** action potential amplitude, **F**, full-width at half-maximum, **G**, action potential rate of rise, **H**, afterhyperpolarization potential (AHP) amplitude, and **I**, AHP time. *p<0.05 vs OVX+E PM three-way repeated-measures ANOVA/Bonferroni test in B (estradiol: $F_{(1,41)}$=3.5, p=0.07; time-of-day: $F_{(1,41)}$=3.7, p=0.06; current: $F_{(15,615)}$=154, p<0.001; current x estradiol: $F_{(15,615)}$=2.7, p=0.1; current x time-of-day: $F_{(15,615)}$=4.2 p<0.05, estradiol x time-of-day: $F_{(1,41)}$=8.9 p<0.01, current x estradiol x time-of-day: $F_{(15,615)}$=6.7 p<0.1) or two-way ANOVA/Bonferroni in C-I.

Table 2.2.5. Two-way ANOVA parameters for comparison of action potential characteristics among groups: cells from OVX AM, OVX PM, OVX+E AM and OVX+E PM.

parameter (figure)	estradiol	time-of-day	interaction
spike latency (fig. 2.2C)	$F_{(1,41)}$=0.5	$F_{(1,41)}$=4.7*	$F_{(1,41)}$=0.7
threshold (fig. 2.2D)	$F_{(1,41)}$=0.2	$F_{(1,41)}$=2.8 (p=0.1)	$F_{(1,41)}$=3.2 (p=0.08)
AP amplitude (fig. 2.2E)	$F_{(1,41)}$=9.1**	$F_{(1,41)}$=0.2	$F_{(1,41)}$=2.5
FWHM (fig. 2.2F)	$F_{(1,41)}$=0.4	$F_{(1,41)}$=1.2	$F_{(1,41)}$=0.03
rate of rise (fig. 2.2G)	$F_{(1,41)}$=1.9	$F_{(1,41)}$=0.2	$F_{(1,41)}$=1.0
AHP amplitude (fig. 2.2H)	$F_{(1,41)}$=6.9*	$F_{(1,41)}$=3.5 (p=0.07)	$F_{(1,41)}$=0.9
AHP time (fig. 2.2I)	$F_{(1,41)}$=0.001	$F_{(1,41)}$=1.8	$F_{(1,41)}$=0.08

*p<0.05; **p<0.01; ***p<0.001.

Kisspeptin increases GnRH excitability in a time-of-day dependent manner

Kisspeptin is a neuromodulator that increases GnRH neuron firing activity and release (Han et al., 2005; Pielecka-Fortuna et al., 2008; Glanowska and Moenter, 2015). To investigate if kisspeptin increases excitability, we repeated the above experiments before and during bath application of 10 nM kisspeptin. To compare response to kisspeptin among groups (n=9 each: OVX AM, OVX PM, OVX+E AM, and OVX+E PM), area under the curve (AUC), calculated using the trapezoid rule (Abramowitz and Stegun, 1964), and number of spikes per step was calculated before (Figure 2.3A, dotted area) and during kisspeptin treatment (Figure 2.3A, dotted plus solid areas). Kisspeptin increased AUC in cells recorded in the AM from both OVX and OVX+E mice (Figure 2.3B, three-way repeated-measures ANOVA/Bonferroni, p=0.003 OVX AM and p=0.009 OVX+E AM, Table 2.6), but had no effect on cells recorded in the PM in either steroid condition (p>0.1). During kisspeptin treatment, some cells in all groups initiated action potential firing after termination of the current step, whereas no cells studied under control conditions fired at this time (Figure 2.3C, Chi-square with Yate's correction, p<0.0001). To test if any of these results could be attributed to a spontaneous shift in excitability over the course of recording of this duration, excitability was compared before and during "mock" treatment (n=2 cells OVX AM, n=4 OVX PM, and n=4 OVX+E AM which were combined, and n=5 OVX+E PM). No difference was observed over time (two-way repeated-measures ANOVA/Bonferroni), and no cells fired following termination of the current step, indicating the above observed shifts in firing were kisspeptin-dependent. Kisspeptin increased input resistance and decreased

holding current in all groups except OVX PM (Table 2.4); this may in part account for increased firing in response to the same current injection, but the difference in response between AM and PM, and the occurrence of spikes after termination of current injection indicated some of the changes are attributable to kisspeptin action.

Kisspeptin modulated some action potential characteristics, reducing action potential FWHM (Figure 2.3G) independent of time-of-day or estradiol (three-way, repeated-measures ANOVA/Bonferroni, all $p \leq 0.01$, Table 2.6). Kisspeptin also delayed the peak of the AHP (AHP time) in cells from all groups except OVX+E mice recorded in the PM (positive feedback, three-way, repeated-measures ANOVA/Bonferroni, all $p \leq 0.01$). In cells from OVX+E mice studied in the AM (negative feedback), kisspeptin decreased action potential amplitude (Figure 2.3F, three-way, repeated-measures ANOVA/Bonferroni, $p=0.02$) and rate-of-rise (Figure 2.3H, three-way, repeated-measures ANOVA/Bonferroni, $p=0.02$). Kisspeptin did not shift spike latency (Figure 2.3D), firing threshold (Figure 2.3E) or AHP amplitude (Figure 2.3I, three-way, repeated-measures ANOVA/Bonferroni). In cells that received “mock” treatment, action potential properties did not shift with the exception of rate-of-rise, which was decreased (three-way, repeated-measures ANOVA/Bonferroni, $p<0.02$).

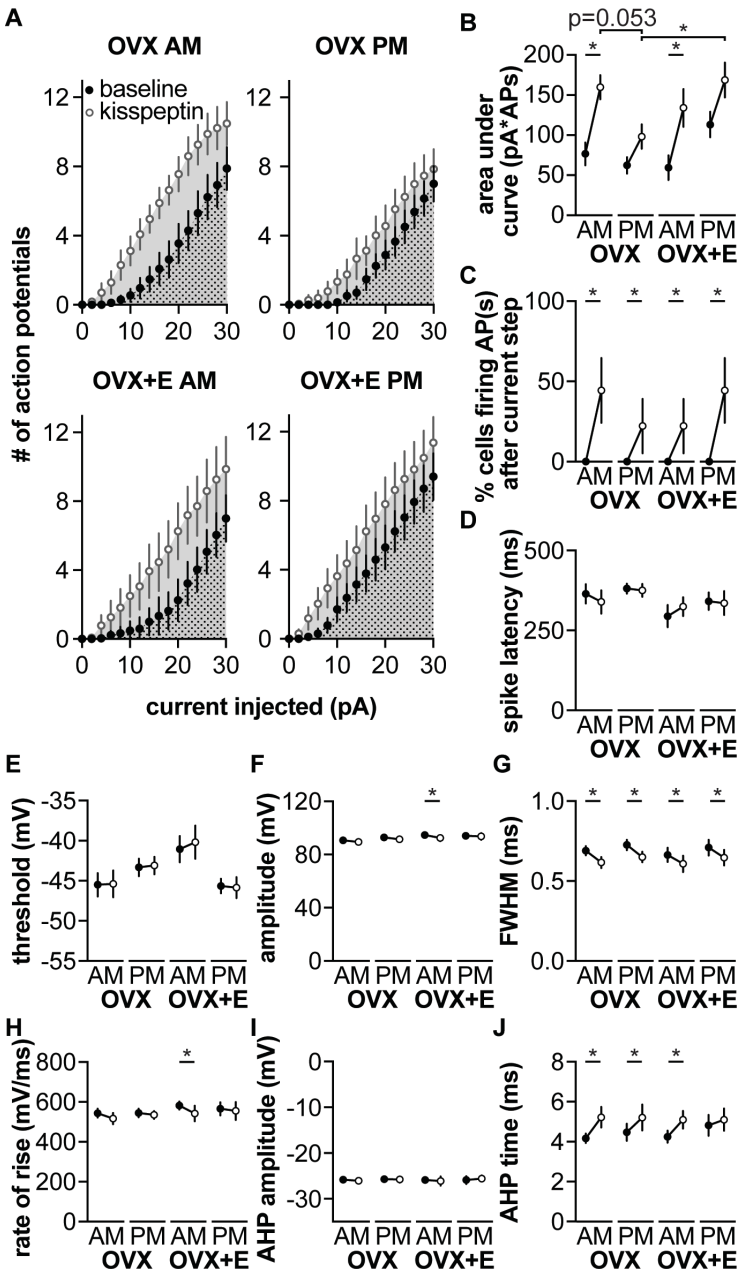

Figure 2.3. Kisspeptin increases GnRH neuron excitability in a time-of-day dependent manner.

A. Mean ± 75th percentile confidence interval for spikes elicited during 500 ms current injection (0-30 pA, 2 pA steps) before (black symbols) and during (white symbols) kisspeptin treatment. Dotted area was used to calculate area under the curve (AUC) for baseline measurements; dotted area + solid area was used to calculate AUC for kisspeptin treatment. **B-J.** Mean ± 75th percentile CI before and during kisspeptin treatment for: **B**, AUC, **C**, percent of cells firing within 1.5 seconds after termination of the current step, **D**, spike latency, **E**, threshold, **F**, action potential amplitude, **G**, FWHM, **H**, rate of rise, **I**, AHP amplitude, **J**, AHP time. When error bars are not visible, they are contained within the symbol. Lines connect means before and during kisspeptin. * $p<0.05$ baseline vs. kisspeptin three-way, repeated-measures ANOVA/Bonferroni, or Chi square (C).

Table 2.6. Three-way repeated-measures ANOVA parameters for comparison of GnRH response to current (area under the curve) and action potential characteristics before and during kisspeptin treatment among groups: cells from OVX AM, OVX PM, OVX+E AM, and OVX+E PM.

	estradiol	time-of-day	kisspeptin	kisspeptin x estradiol	kisspeptin x time-of-day	estradiol x time-of-day	kisspeptin x estradiol x time-of-day
AUC (Fig. 2.3B)	$F_{(1,1)}$=0.9	$F_{(1,1)}$=0.02	$F_{(1,1)}$=38.3***	$F_{(1,1)}$=0.08	$F_{(1,1)}$=2.7	$F_{(1,1)}$=3.9 (p=0.06)	$F_{(1,1)}$=0.5
spike latency (Fig. 2.3D)	$F_{(1,32)}$=3.4 (p=0.07)	$F_{(1,32)}$=1.5	$F_{(1,32)}$=0.02	$F_{(1,32)}$=1.1	$F_{(1,32)}$=0.1	$F_{(1,32)}$=0.003	$F_{(1,32)}$=1.1
threshold (Fig. 2.3E)	$F_{(1,32)}$=0.9	$F_{(1,32)}$=1.4	$F_{(1,32)}$=0.6	$F_{(1,32)}$=0.07	$F_{(1,32)}$=0.5	$F_{(1,32)}$=9.2**	$F_{(1,32)}$=0.8
AP amplitude (Fig. 2.3F)	$F_{(1,32)}$=3.2 (p=0.08)	$F_{(1,32)}$=0.7	$F_{(1,32)}$=12.6**	$F_{(1,32)}$<0.001	$F_{(1,32)}$=1.0	$F_{(1,32)}$=0.4	$F_{(1,32)}$=1.6
FWHM (Fig. 2.3G)	$F_{(1,32)}$=0.2	$F_{(1,32)}$=1.4	$F_{(1,32)}$=60.4***	$F_{(1,32)}$=0.8	$F_{(1,32)}$=0.05	$F_{(1,32)}$=0.01	$F_{(1,32)}$=0.02
rate of rise (Fig. 2.3H)	$F_{(1,32)}$=1.1	$F_{(1,32)}$=0.02	$F_{(1,32)}$=11.3**	$F_{(1,32)}$=0.3	$F_{(1,32)}$=3.1 (p=0.09)	$F_{(1,32)}$=0.06	$F_{(1,32)}$=0.2
AHP amplitude (Fig. 2.3I)	$F_{(1,32)}$<0.001	$F_{(1,32)}$=0.2	$F_{(1,32)}$=0.03	$F_{(1,32)}$=0.09	$F_{(1,32)}$=0.4	$F_{(1,32)}$=0.003	$F_{(1,32)}$=0.1
AHP time (Fig. 2.3J)	$F_{(1,32)}$=0.02	$F_{(1,32)}$=0.3	$F_{(1,32)}$=43.0***	$F_{(1,32)}$=2.2	$F_{(1,32)}$=4.0 (p=0.06)	$F_{(1,32)}$=0.04	$F_{(1,32)}$=0.3

*p<0.05; **p<0.01; ***p<0.001.

GnRH neuron excitability is independent of estradiol and time-of-day in kisspeptin knockout mice

Because endogenous kisspeptin release is likely to enhance GnRH neuron excitability, we hypothesized that excitability of GnRH neurons would be reduced in the absence of kisspeptin. To test this, we measured GnRH neuron response to current steps (as above) in OVX and OVX+E kisspeptin knockout mice. Because these mice are infertile and must be bred from heterozygotes, only three groups were studied (OVX PM, OVX+E AM, and OVX+E PM) as no differences were observed between cells from OVX PM and OVX AM animals in Figure 2.1 or 2.2, or in our previous work with this model (Christian et al., 2005; Christian and Moenter, 2007; Sun et al., 2010; Pielecka-Fortuna et al., 2011; Gaskins and Moenter, 2012). GnRH neuron response to current was independent of time-of-day or estradiol in cells from kisspeptin knockout mice (Figure 2.4A; OVX PM n=8, OVX+E AM n=9, and OVX+E PM n=9; one-way ANOVA/Bonferroni, $p>0.2$). To facilitate comparison of GnRH neuron excitability between knockout and control mice, GnRH neuron firing in response to current steps from Figures 2.1 and 2.4 are plotted together in Figure 2.5. GnRH neuron excitability from knockout mice is elevated relative to cells from OVX PM and OVX+E AM control mice (Figure 2.5; three-way repeated-measures ANOVA/Bonferroni, $p<0.05$), but similar to GnRH neuron excitability in OVX+E PM control mice ($p>0.1$).

No differences in action potential characteristics were observed among OVX PM, OVX+E AM, and OVX+E PM kisspeptin knockout mice (Figure 2.4, one-way ANOVA/Bonferroni for Figures 2.4B-D,G-H, $p>0.1$, and Kruskal-Wallis/Dunn for Figure 2.4F, $p>0.1$) except for FWHM, in which spike width was decreased in cells from OVX+E AM mice relative to OVX+E PM (one-way ANOVA/Bonferroni, $p=0.03$).

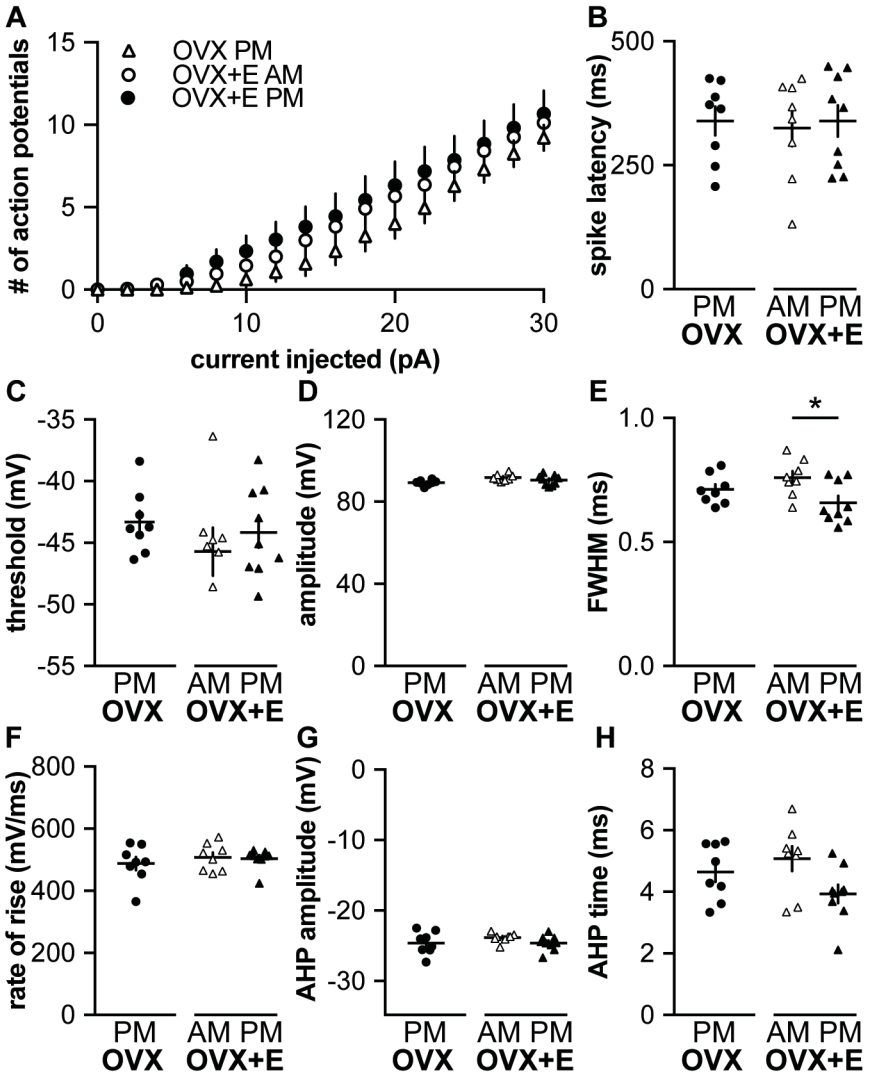

Figure 2.4. GnRH neuron excitability is independent of time-of-day and estradiol feedback in kisspeptin knockout mice.

A. Mean ± SEM number of spikes elicited during 500 ms current injection (0-30 pA, 2 pA steps). **B-H** Individual values and mean ± SEM for: **B,** latency to first spike, **C,** action potential threshold, **D,** action potential amplitude, **E**, full-width at half-maximum, **F**, action potential rate of rise, **G**, afterhyperpolarization potential (AHP) amplitude, and **H**, AHP time. *p<0.05 two-way repeated-measures ANOVA/Bonferroni test (A; group: $F_{(2,22)}$=0.9; current: $F_{(15,330)}$=128.4, p < 0.001; group x current: $F_{(30,330)}$=0.6), one-way ANOVA/Bonferroni (B, $F_{(2,22)}$=0.06; C, $F_{(2,22)}$=0.7; D, $F_{(2,22)}$=3.2, p=0.06; E, $F_{(2,22)}$=4.0, p<0.05; G, $F_{(2,22)}$=1.15; H, $F_{(2,22)}$=2.93, p=0.07) or Kruskal-Wallis/Dunn's (F, $F_{(2,22)}$=2.93, p=0.07).

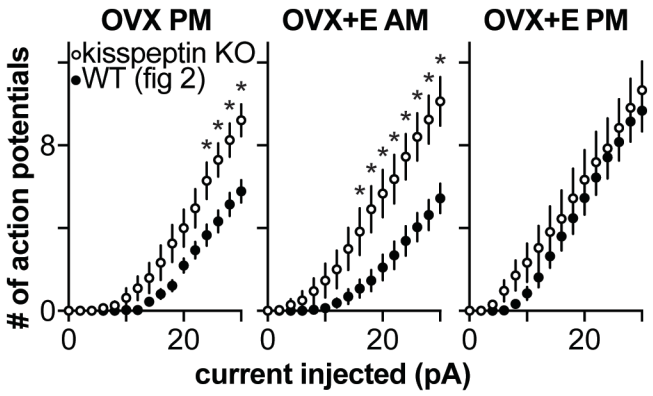

Figure 2.5. GnRH neuron excitability in kisspeptin knockout mice is similar to GnRH excitability during positive feedback in wild-type mice.
Mean ± SEM number of spikes elicited during 500 ms current injection (0-30 pA, 2 pA steps) from kisspeptin knockout mice (white circles from figure 2.4) and in control mice (black circles from figure 2.2). *p<0.05 three-way repeated-measures ANOVA/Bonferroni (group: $F_{(2,54)}$=167.2, p<0.001; kisspeptin KO: $F_{(1,54)}$=10.2, p<0.01, current: $F_{(15,810)}$=273.5, p<0.001; group x kisspeptin KO: $F_{(2,54)}$=0.4; group x current: $F_{(30,810)}$=4.1, p<0.001; kisspeptin KO x current: $F_{(15,810)}$=7.9, p<0.001; kisspeptin KO x group x current: $F_{(30,810)}$=2.2, p<0.001).

The similar firing response of GnRH neurons among negative feedback and OVX groups is effectively modeled by identifiable parameter sets with a strong inverse correlation between gA and V1/2 inactivation of I_A

The above data indicate that GnRH neurons from OVX AM, OVX PM, and OVX+E AM mice have the same action potential firing response to current injections. This was initially surprising because GnRH neurons from the two OVX groups have similar ion channel densities and properties that are different than those of cells from OVX+E AM mice (Sun et al., 2010; Pielecka-Fortuna et al., 2011). These differences led us to the original hypothesis that during negative feedback GnRH neurons exhibit decreased excitability compared to cells from OVX mice. Upon rejection of this hypothesis by the above data, our goal was to examine how individual current properties influenced excitability.

A model GnRH neuron (Moran et al., 2016) was adapted to reproduce the negative feedback state in terms of I_A, I_K, I_{HVA}, and I_{LVA} (Figure 2.6A-H), all of which have been isolated and characterized in voltage-clamp experiments (Zhang et al., 2009; Sun et al., 2010; Pielecka-Fortuna et al., 2011). These experiments demonstrated that four parameters differed in cells from OVX vs negative feedback animals: the maximum

conductances (g) of I_A, I_{LVA}, and I_{NaP} and the $V_{1/2}$ inactivation of I_A. We used MCMC to estimate the values of these four parameters that best reproduce action potential shape and excitability, permitting only these four parameters to vary. We hypothesized that more than one unimodal distribution of parameter sets would be able to reproduce excitability during negative feedback because empirical channel properties/densities varied despite the same excitability in the above data sets (OVX and negative feedback, Figure 2.2). Surprisingly, the model parameters each converged (Figure 2.7A-D) to a Gaussian, rather than a non-Gaussian or multimodal, distribution (Figure 2.7E); this model is thus "identifiable". The hypothesis that more than one distribution of parameter sets would reproduce these data was therefore rejected. Of interest, the joint probability distributions between $V_{1/2inact}$ of I_A and g_A were highly dependent on one another (Figure 2.7E); as g_A increased $V_{1/2}$ inactivation became more hyperpolarized, thus maintaining the same action potential response to current injection (Figure 2.7F-G). In contrast to $V_{1/2inact}$ of I_A and g, values for g_{HVA} and g_{NaP} were largely independent of the other parameters (Figure 2.7C). Although these parameters vary over a small range, their convergence on a Gaussian distribution indicates that there are indeed preferable parameter values to reproduce the data set; if these parameters had no influence on the solution, the distribution of possible solutions would be flat.

We repeated this experiment for two additional excitability curves from cells during negative feedback and for the mean excitability curve for negative feedback from Figure 2.2. In each case, the four parameters converged to Gaussian distributions, and the joint probabilities between $V_{1/2inact}$ of I_A and g_A strongly indicate that these parameters are highly dependent on one another (not shown).

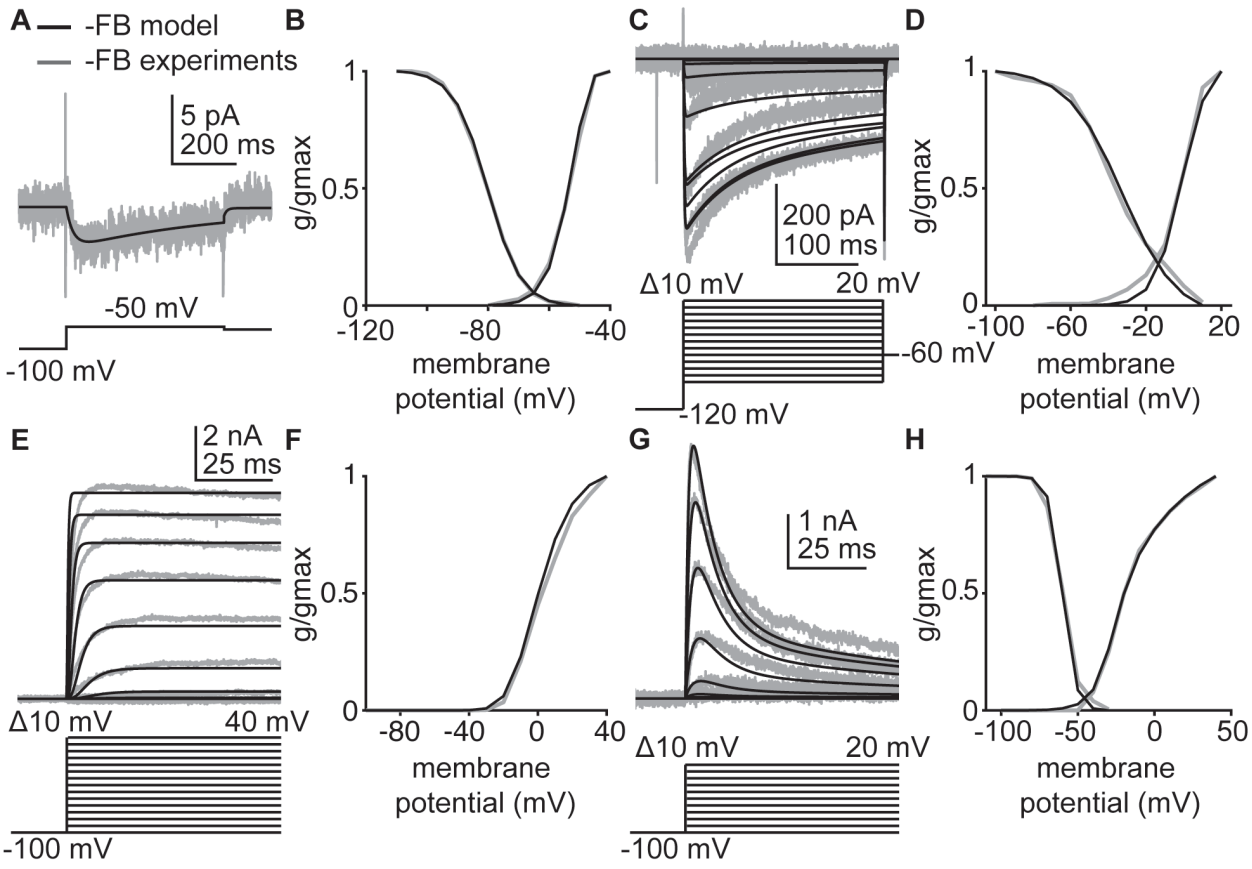

Figure 2.6. The GnRH neuron model reproduces I_A, I_K, I_{HVA}, and I_{LVA} isolated in voltage-clamp experiments performed during negative feedback.
Empirical data (grey) and model-simulated current (black) used in Hodgkin-Huxley modeling. Voltage protocols are located beneath the current responses in A,C,E, and G. Only those voltage steps used to estimate parameters for the simulated data are shown. **A.** I_{LVA} in response to a depolarizing voltage step in OVXE+ AM mice. Empirical data from (Sun et al., 2010). **B.** Simulated and empirical I_{LVA} activation and inactivation curves from OVX+E mice during negative feedback. Empirical data from (Zhang et al., 2009). **C.** Simulated and empirical I_{HVA} in response to depolarizing voltage steps (below current response) during negative feedback. Empirical data from (Sun et al., 2010). **D.** Simulated and empirical I_{HVA} activation and inactivation curves determined from voltage clamp experiments. Empirical data from (Sun et al., 2010). **E.** Simulated and empirical I_K in response to depolarizing voltage steps during negative feedback **F.** Simulated and empirical activation curves for I_K during negative feedback, determined from activation protocol in E. **G.** Simulated and empirical I_A during depolarizing voltage steps during negative feedback. **H.** Simulated and empirical activation and inactivation curves for I_A during negative feedback. Values from these fits populate Table 1, g_{vc}.

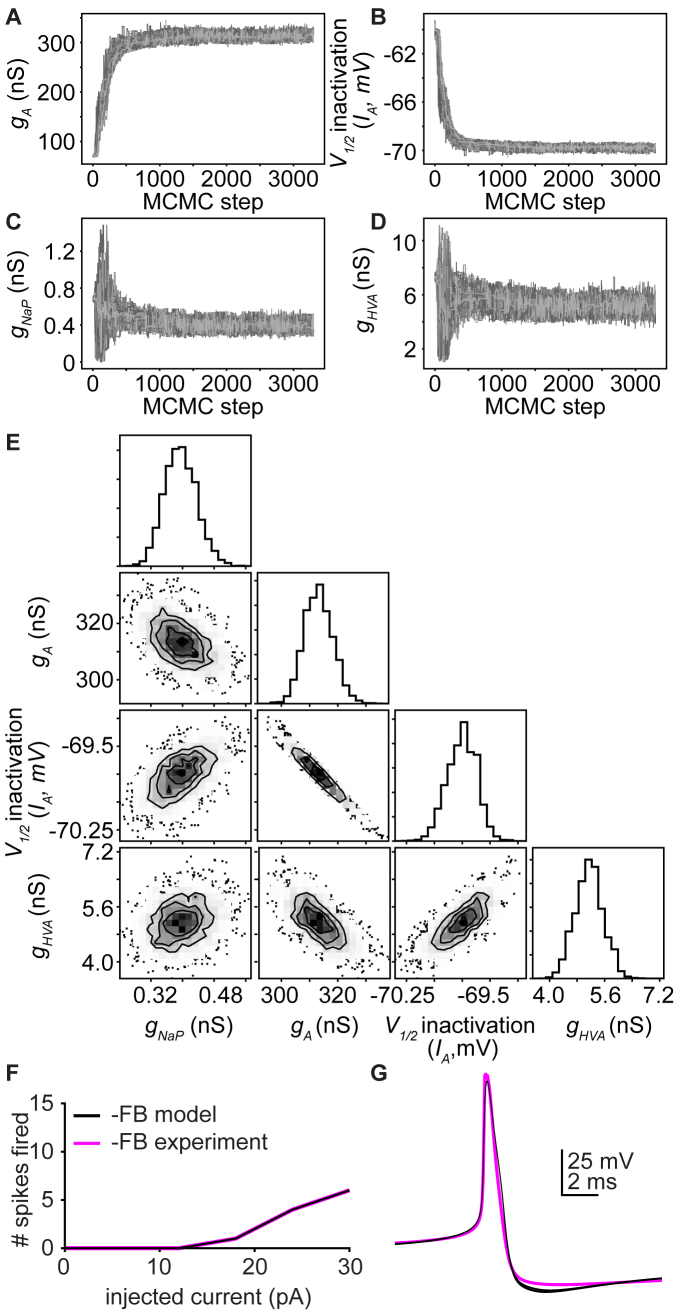

Figure 2.7. A hyperpolarizing shift in $V_{1/2}$ inactivation of I_A can oppose an increase in maximum I_A channel number to prevent changes in excitability.
A-D Convergence plots for parameters: **A,** g_A, **B,** $V_{1/2}$ inactivation of I_A, **C,** g_A, and **D,** g_{HVA}. Each line denotes the value of a single walker (of 100) over 3300 iterations. E. Far right panel in each row, individual probability distributions for the parameters g_{HVA}, $V_{1/2}$ inactivation of I_A, g_A, and g_{HVA} for the simulation in F and G. Two-dimensional probability distributions in the other panels determine if parameter values vary independently (g_{NaP} and g_{HVA}) or dependently (g_A and $V_{1/2}$ inactivation of I_A) of one another. **F.** Ten simulated (black) parameter sets selected along the interdependent distribution for gA and V1/2 inactivation, and a representative empirical GnRH neuron (magenta) responses to 500 ms current injections during negative feedback (0 – 30 pA, 6 pA steps). **G.** Ten simulated and empirical action potential waveforms during negative feedback.

The similar firing response of GnRH neurons within the positive feedback group was not effectively modeled by identifiable parameter sets

Our data demonstrate that GnRH neuron excitability was increased during positive feedback without impacting action potential shape. We used our neuron model to determine which of the steroid-dependent parameters (g_A, g_{HVA}, and I_A $V_{1/2}$ inactivation) examined above were essential for increase in excitability during positive feedback. We used the MCMC method to estimate the best parameter set(s) for reproducing positive feedback excitability without changing action potential shape. In contrast to negative feedback, the MCMC simulations did not converge to a Gaussian distribution for any parameter within the physiologic range (Figures 2.8A-E). Simulations were stopped when parameters exited their physiologic range. There were multiple combinations of g_A, g_{HVA}, and I_A $V_{1/2}$ inactivation that provided a good fit to the current-clamp data over large parameter ranges (Figure 2.8F, G). These data indicate that despite the identifiability of the model parameters for OVX+E AM and OVX groups above, this same model running under the same conditions is not identifiable.

We repeated this experiment for two additional excitability curves during positive feedback and for the mean excitability curve for positive feedback from Figure 2.2. In each case, none of the four parameters converge to Gaussian distributions within their physiologic range (not shown).

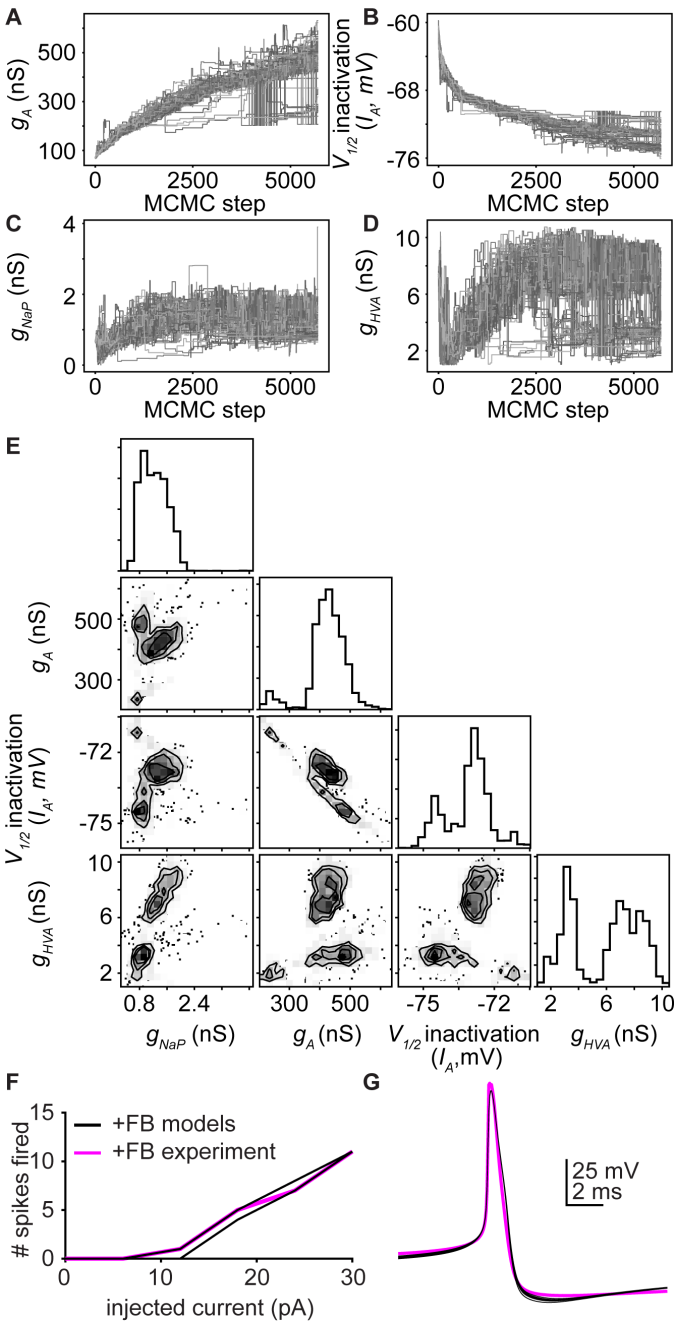

Figure 2.8. Multiple parameter sets can reproduce increased excitability during positive feedback.

A-D Convergence plots for parameters: **A,** g_A, **B**, $V_{1/2}$ inactivation of I_A, **C**, g_A, and **D**, g_{HVA}. Each line denotes the value of a single walker (of 100) over 5700 iterations. **E.** Far right panel in each row, individual probability distributions for the parameters g_{HVA}, $V_{1/2}$ inactivation of I_A, g_A, and g_{HVA} for the simulation in F and G. Two-dimensional probability distributions in the other panels determine if parameter values vary independently or dependently on one another. **F.** Ten simulated (black, randomly-selected from parameter sets in A-D) and a representative empirical GnRH neuron (magenta) response to 500 ms current step injections during positive feedback (0 – 30 pA, 6 pA steps). **G.** Ten simulated and empirical action potential waveforms during positive feedback.

Persistent sodium currents can induce spiking after termination of the current step

Kisspeptin induced firing after termination of the current step independent of time-of-day or estradiol. We were able to reproduce this effect by altering two key parameters for persistent sodium currents in the negative feedback model neuron (Figure 2.9A). It was necessary first to shift the $V_{1/2}$ activation for I_{NaP} to a more hyperpolarized potential and second, to decrease the speed at which the activation gate activated/deactivated. This led to the slow activation of I_{NaP} over the course of the current step, depolarizing the membrane potential, and culminating in a single spike (Figure 2.9B). Following the spike, I_{NaF} was inactivated, the membrane potential dropped, and I_{NaP} slowly deactivated. Spiking was also increased during the current step, from 6 to 9 action potentials fired during a +30 pA step (Figure 2.9A) suggesting kisspeptin activation of I_{NaP} may contribute to increased firing during the step as well as after.

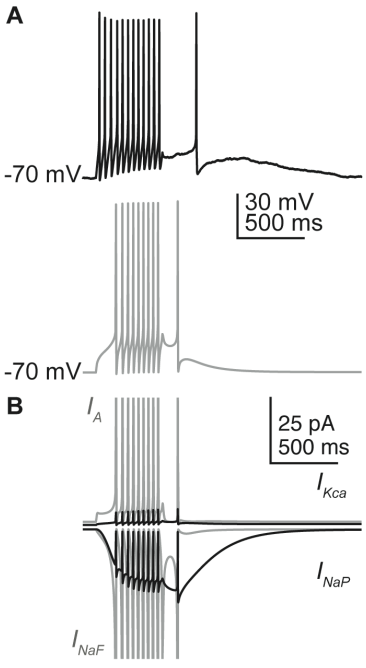

Figure 2.9. Persistent sodium currents can induce spiking after termination of a current step.

A. Spikes can be initiated after the current step in cells from an OVX+E mouse (black) and model (grey) **B.** Individual currents during model membrane response in A, I_A top grey, I_{Kca} top black, I_{NaF} bottom grey, I_{NaP} bottom black. Currents for I_{NaF} and I_A reach >1 nA during an action potential and have been truncated to more clearly observe ionic currents active after termination of the current step.

Discussion

The switch from estradiol negative to positive feedback triggers a surge of GnRH release, ultimately resulting in ovulation. GnRH release at the median eminence to control pituitary output is in part dependent on action potential firing (Glanowska and Moenter, 2015). Intrinsic conductances sculpt whether or not synaptic inputs evoke action potential firing and can also independently initiate spiking. Here we use a daily LH surge model that separates steroid and time-of-day variables contributing to estradiol feedback to show that GnRH neurons fire more action potentials during positive feedback, that the neuromodulator kisspeptin may play a role in this increase, and use a mathematical model neuron to predict that there are multiple intrinsic mechanisms that can increase excitability during positive feedback.

The increase in excitability observed in GnRH neurons during positive feedback supports and extends previous voltage-clamp experiments done in the same daily LH surge paradigm used in the present work. These studies identified multiple ionic conductances are modified by both time-of-day and estradiol. Specifically, rapidly inactivating A-type potassium currents and sustained delayed rectifier potassium currents were increased during negative feedback and decreased during positive feedback (Pielecka-Fortuna et al., 2011); high-voltage-activated calcium currents were increased during positive feedback and suppressed during negative feedback (Sun et al., 2010). In contrast, these currents did not vary in GnRH neurons from OVX mice and values were typically intermediate to those observed during estradiol negative and positive feedback. In a different estradiol feedback paradigm, low-voltage-activated calcium currents were increased during positive feedback and ATP-sensitive potassium currents were decreased during negative feedback (Zhang et al., 2007; Zhang et al., 2009). Based on these observations and the typical physiologic effects of these currents on the membrane potential, we expected decreased excitability during negative feedback and increased GnRH neuron excitability during positive feedback compared to cells from OVX mice. The latter hypothesis was supported but the former was rejected because excitability of GnRH neurons from the negative feedback animal model (OVX+E AM) was not decreased relative to that in cells from OVX mice.

Perhaps the most likely explanation for the similar excitability among these groups is that ionic conductance changes in cells from OVX+E AM mice and OVX mice have opposing effects on one another. Indeed, our model GnRH neuron predicts that the hyperpolarizing shift in I_A $V_{1/2}$ inactivation observed in OVX+E AM neurons opposes the increase in I_A current density observed at this time. Changes in other currents examined within the model were unable to compensate for the increase in I_A during negative feedback.

GnRH neuron excitability was markedly increased during estradiol positive feedback, with little effect on action potential shape or spike latency. We used the GnRH neuron model to test if any individual channel(s) could increase GnRH neuron excitability without modifying action potential shape. Interestingly, and in contrast to negative feedback and open-loop (i.e., OVX) conditions, the model did not converge on unique identifiable parameter sets within the physiologic range. This may suggest there are multiple yet to be determined mechanisms to increase GnRH neuron excitability during positive feedback; this could increase likelihood of a successful GnRH surge and thus ovulation.

Estradiol and time-of-day dependent effects on intrinsic conductances of GnRH neurons are likely transmitted through the ERα-sensitive network afferent to these cells. The neuromodulator kisspeptin is postulated to play a major role in positive feedback (Oakley et al., 2009). The present work supports and extends these findings by demonstrating that kisspeptin has both time-of-day dependent and independent effects on GnRH neurons. First, kisspeptin increased GnRH neuron excitability *during* current injection in cells recorded in the morning, but not in cells recorded in the late afternoon, regardless of estradiol status. Second, kisspeptin stimulated spiking *after* termination of the current stimulus in some cells independent of time-of-day and estradiol; no spikes were observed after stimulus termination under control conditions. The model GnRH neuron predicts that changes to the activation kinetics of persistent sodium channels may initiate spiking after termination of the current step. Of note, the model also predicts that this change in kinetics would also increase spiking during the current step; this may explain the apparent shift in the excitability curve that did not achieve significance in cells treated with kisspeptin in the PM. We postulate that *in vivo*, endogenous kisspeptin

induces two mechanistic changes with different half-lives, such that one effect (increased firing during current injection) persists into the slice preparation, whereas the other effect (increased firing after termination of current injection) does not. The lack of effect of exogenous kisspeptin on firing during the current steps in cells studied in the afternoon would thus be attributable to persistence of the effects of endogenous kisspeptin released before slice preparation on the intrinsic properties of GnRH neurons in the slice. In this regard, kisspeptin acts via mechanisms that typically have longer half-lives, such as changing gene expression (Sukhbaatar et al., 2013; Terasaka et al., 2013; Novaira et al., 2016), and mechanisms with shorter half-lives including rapid effects on ionic conductances (Zhang et al., 2008; Pielecka-Fortuna et al., 2011; Zhang et al., 2013).

Paradoxically, GnRH neuron excitability in kisspeptin knockout mice was high, similar to that during estradiol positive feedback in control mice. In contrast to controls, however, neither estradiol nor time of day altered excitability of GnRH neurons from kisspeptin knockout mice. Kisspeptin knockouts are infertile and do not have estrous cycles or exhibit estradiol positive feedback with increased LH release (Lapatto et al., 2007; Chan et al., 2009). We thus postulated GnRH neuron excitability would be low in these mice. We reject this hypothesis and offer two possible explanations. First, other mechanisms may compensate to enhance GnRH neuron excitability and release in the absence of kisspeptin. Second, GnRH neurons in kisspeptin knockout mice may fail to undergo typical maturation. In this regard, GnRH release frequency in males and firing rate in both sexes are higher before puberty than in adults (Glanowska et al., 2014; Dulka and Moenter, 2017). This typical maturational decline may be regulated by a kisspeptin-dependent circuit.

Interpretation of the present data was facilitated with mathematical modeling. A challenge for modeling biophysical systems is that a model may produce more than one set of parameters that reproduces the data, making the model “unidentifiable”. For many biological models, a single point estimate is given for each parameter, without rigorously determining if alternative values exist that also reproduce the data. A number of methods have been developed to overcome this problem. Maximum likelihood methods give a mean value and standard deviation for each parameter; large standard deviations

may hint at non-unique solutions. Markov Chain Monte Carlo methods use Bayes' theorem to determine a probability distribution for each parameter, providing not only a mean and standard deviation, but also the shape (e.g., Gaussian, bimodal, uniform) of the distribution (Siekmann et al., 2011). Using voltage-clamp and current-clamp data to constrain our model, the probability distribution for each parameter converged to a Gaussian distribution centered around a single mean value for negative feedback and open-loop conditions. A multimodal or uniform distribution would have suggested that more than one parameter set was able to reproduce the data. When we tried estimating parameters using only activation and inactivation curves, excluding voltage-clamp traces, many parameters displayed almost uniform distributions indicating these data alone were insufficient to constrain the model. It is important to point out that a non-identifiable solution can also have biological implications. For example, our positive feedback model had access to the same types of data, but did not converge within the physiologic range upon a Gaussian distribution of parameters for any of the four variables examined. Similar redundancy was reported to contribute to output among elements of the crustacean stomatogastric ganglion (Prinz et al., 2004). It remains possible that when more parameters have been empirically determined, future iterations of this model will be able to converge.

MCMC methods also determine if the predicted values of parameters are dependent or independent of one another. If two parameters are dependent, this can justify fixing one parameter and allowing the other to vary to reduce the total number of parameters in the model. Interdependence can also have a biological significance. In our negative feedback model, I_A $V_{1/2}$ inactivation became more hyperpolarized as g_A increased, suggesting that opposing changes observed in negative feedback prevent a decrease in excitability relative to that observed in the open-loop OVX condition. At present, it is not possible to manipulate individual ion channel parameters empirically; modeling and MCMC methods are thus necessary to perform these experiments.

The present studies indicate multiple parameters interact to regulate GnRH neuron excitability in an estradiol and time-of-day-dependent manner. Rigorous parameter estimation of a model neuron provided new insights into possible mechanisms underlying changes in excitability among groups. The possibility of multiple

mathematical solutions to positive feedback reminds us to keep in mind that different neurobiological mechanisms may also exist to guarantee reproductive success, including changes to intrinsic properties of GnRH neurons, fast synaptic inputs, and neuromodulators beyond kisspeptin (Gore, 2002; Christian and Moenter, 2010).

Chapter 3: Changes in GnRH Neuron Excitability and GABA PSC Frequency Drive the Increase in Firing Rate During Estradiol Positive Feedback

Abstract

The central output of gonadotropin-releasing hormone (GnRH) neurons that controls fertility is sculpted by sex-steroid feedback. A switch from estradiol negative to positive feedback initiates a surge of GnRH, culminating in ovulation. In ovariectomized mice bearing constant-release estradiol implants (OVX+E), GnRH neurons are suppressed in the morning (AM) by negative feedback and activated in the afternoon (PM) by positive feedback; no time-of-day dependent shift is observed in OVX mice. GnRH neuron intrinsic properties are shifted to favor increased firing during positive feedback, but it unclear if the observed concomitant increase in GABAergic transmission, which can excite GnRH neurons, is independently sufficient for increasing GnRH neuron firing rate during positive feedback. To test this, we used dynamic clamp to inject previously recorded trains of postsynaptic currents from the daily surge model into GnRH neurons from OVX, OVX+E AM, and OVX+E PM mice. Postsynaptic conductance trains mimicking positive feedback initiated more action potentials in cells from OVX+E PM mice than negative feedback or OVX trains. Further the positive-feedback train was most effective when applied to cells during positive feedback. These observations suggest GnRH neurons do not merely relay fast synaptic signals, but integrate and amplify these signals to increase firing during positive feedback.

Significance statement

Infertility affects 15-20% of couples; failure to ovulate is a common cause. Understanding how the brain controls ovulation is critical for new developments in both infertility treatment and contraception. Ovarian estradiol alters both the intrinsic properties of GnRH neurons and synaptic inputs to these cells coincident with production of sustained GnRH release that ultimately triggers ovulation. We

demonstrate here using dynamic clamp and mathematical modeling that estradiol-induced shifts in synaptic transmission alone can increase firing output, but that the intrinsic properties of GnRH neurons during positive feedback further poise these cells for increased response to higher frequency synaptic transmission. These data suggest that GnRH neurons integrate fast-synaptic and intrinsic changes to increase firing rates during the preovulatory GnRH surge.

Introduction

GnRH neurons form the final common pathway for central control for reproduction. GnRH initiates the release of luteinizing hormone (LH) and follicle-stimulating hormone from the pituitary. Gonadotropins activate follicle maturation and steroidogenesis in the ovary. For most of the estrous cycle, estradiol negative feedback suppresses GnRH/LH release. At the end of the follicular phase (proestrus in rodents), rising levels of estradiol switch from suppressing GnRH/LH to positive feedback action that induces a continuous surge of release that initiates an LH surge that triggers ovulation (Sarkar et al., 1976; Moenter et al., 1991).

In ovariectomized rodents implanted with estradiol capsules (OVX+E), GnRH/LH surges can be induced on a daily basis (Norman et al., 1973; Legan and Karsch, 1975; Christian et al., 2005). Release of GnRH and LH as well as GnRH firing rate are suppressed in the morning (negative feedback) and elevated in the afternoon (positive feedback) (Christian et al., 2005; Glanowska et al., 2012). No time-of-day dependent shift in GnRH neuron firing rate is observed in OVX mice not treated with estradiol. Previous work using this daily surge and other estradiol-induced surge paradigms has identified multiple estradiol and time-of-day dependent changes to GnRH neuron intrinsic properties and fast-synaptic transmission that may drive an increase in firing rate during positive feedback (Chu and Moenter, 2006; Christian and Moenter, 2007; Zhang et al., 2007; Christian et al., 2009; Zhang et al., 2009; Sun et al., 2010; Pielecka-Fortuna et al., 2011). Changes to voltage-gated sodium, potassium, and calcium channel properties culminate in an increase in GnRH neuron excitability during positive feedback and may increase both spontaneous firing and responsiveness to fast-synaptic inputs to help drive an increase in GnRH firing rate at this time (Adams et al., 2018).

In addition to these changes in intrinsic properties, GABA postsynaptic current (PSC) frequency and amplitude are suppressed during negative feedback and increased during positive feedback; activation of $GABA_A$ receptors in these cells can be excitatory (DeFazio et al., 2002; Christian and Moenter, 2007). Whether or not these changes in fast-synaptic changes are necessary or sufficient for increasing GnRH neuron firing rate during positive feedback is not known. We hypothesized that time-of-day and estradiol-dependent changes in their intrinsic properties render GnRH neurons more responsive to GABA postsynaptic currents during positive feedback compared to negative feedback and the open-loop OVX condition. To test our hypothesis, we used the daily surge paradigm to examine GnRH neuron response to trains of GABA postsynaptic conductances using dynamic clamp to introduce synaptic conductances to evoke postsynaptic potentials and measures membrane response. Trains of conductances were modeled from representative patterns from negative and positive feedback and the open-loop OVX condition.

Materials and methods

All chemicals were purchased from Sigma-Aldrich, unless noted.

Animals.

Transgenic mice expressing green fluorescent protein (GFP) under the control of the GnRH promoter (GnRH-GFP) were used (Suter et al., 2000). Mice were housed on a 14-h light:10-h dark cycle with lights off at 6 P.M. (eastern standard time). Teklad 2916 chow (Envigo) and water were available ad libitum. Adult females age 58-170 days were randomly selected from our colony. Ovariectomy was performed under isoflurane (VetOne) anesthesia. At the time of OVX, mice were randomized to either receive a Silastic (Dow Corning) capsule containing 0.625 μg 17β-estradiol suspended in sesame oil (OVX+E) or not be treated further (OVX). Bupivacaine (0.25%, APP Pharmaceuticals) was applied to surgical sites to reduce postoperative pain and distress. Electrophysiologic experiments were performed 2-3 days after surgery and estradiol status was confirmed by measurements of uterine mass of control mice (OVX, n=7, 49.1 ± 3.3 mg; OVX+E, n=12, 174.1 ± 4.8 mg; two-tailed unpaired Student's t-test,

$t_{(17)}$=18.4, p<0.001). It is important to point out that this daily surge model does not recapitulate the pattern of estradiol during the cycle. It does, however, effectively induces both negative and positive feedback on LH release *in vivo* and GnRH neuron activity in the brain slice relative to measurements in OVX mice (Christian et al., 2005). This separates two variables, time of day and circulating estradiol level, known to contribute to the generation of the LH surge in mice and other rodents and which were the targets of the present investigations. Firing rates during the daily estradiol-induced surge are not different from those during the proestrous surge of the estrous cycle (Silveira et al., 2016).

Brain Slice Preparation.

All solutions were bubbled with 95% O_2/5% CO_2 throughout the experiments and for at least 15 min before exposure to tissue. Brain slices were prepared either from 7.5-8.5 h before lights out (AM recordings) or 1-2 h before lights out (PM recordings). The brain was rapidly removed and placed in ice-cold sucrose saline solution containing the following (in mM): 250 sucrose, 3.5 KCl, 26 $NaHCO_3$, 10 D-glucose, 1.25 Na_2HPO_4, 1.2 $MgSO_4$, and 3.8 $MgCl_2$, at pH 7.6 and 345 mOsm. Coronal (300 μm) slices were cut with a VT1200S Microtome (Leica Biosystems). Slices were incubated in a 1:1 mixture of sucrose saline and artificial CSF (ACSF) containing (in mM) 135 NaCl, 3.5 KCl, 26 $NaHCO_3$, 10 D-glucose, 1.25 Na_2HPO_4, 1.2 $MgSO_4$, and 2.5 $CaCl_2$, at pH 7.4 and 305 mOsm, for 30 min at room temperature (~21 to 23°C). Slices were then transferred to 100% ACSF at room temperature for 0.5-5 h before recording.

Data Acquisition.

During recording, slices through the preoptic area and anterior hypothalamus, which contain the majority of GnRH neuron somata, were placed into a chamber continuously perfused with ACSF at a rate of 2 ml/min with oxygenated ACSF heated to 29.5-31.5°C with an inline-heating unit (Warner Instruments). GFP-positive cells were visualized with a combination of infrared differential interference contrast and fluorescence microscopy on an Olympus BX51WI microscope. Recording pipettes were pulled from borosilicate glass capillaries (1.65-mm OD x 1.12-mm ID; World Precision Instruments) using a

Flaming/Brown P-97 unit (Sutter Instrument Company). Pipettes measured 2-4.5 MΩ when filled with (in mM): 125 K gluconate, 20 KCl, 10 HEPES, 5 EGTA, 0.1 $CaCl_2$, 4 MgATP, and 0.4 NaGTP, 300 mOsm, pH 7.2 with NaOH. Pipettes were wrapped with Parafilm (Bemis) to reduce capacitive transients; remaining transients were electronically cancelled. Pipettes were placed in contact with a GFP-positive neuron using an MP-285 micromanipulator (Sutter Instrument Company). All potentials reported were corrected online for liquid junction potential of −14.2 mV (Barry, 1994). Recordings were made with an EPC-10 dual patch-clamp amplifier (HEKA Elektronik) and a Macintosh computer running Patchmaster software (HEKA Elektronik). Experiments were analyzed offline using custom software (DeFazio and Moenter, 2002; DeFazio et al., 2014) written in IgorPro (Wavemetrics).

Whole-cell patch-clamp.

After achieving a >1 GΩ seal and the whole-cell configuration, membrane potential was held at -60 mV between protocols. Series resistance (Rs), input resistance (Rin), and holding current (Ihold) were measured every 2-3 min using a 5 mV hyperpolarizing step from −60 mV (mean of 20 repeats, 20 ms duration, sampled at 100 kHz). Only recordings with a Rin of >500 MΩ, Ihold of −30 to 25 pA, stable Rs of <20 MΩ, and a stable Cm between 10 and 23 pF were used for analysis.

In current-clamp, direct current (<35 pA, -9.0±2.1 pA, n=34) was adjusted to keep cells within 3 mV of -68 mV. Membrane potential was sampled at 20 kHz and filtered at 6.7 kHz. Bridge balance (95%) was used for most cells; for a few cells, bridge balance was not used but results were similar. In all current-clamp and dynamic-clamp recordings, ACSF contained 100 μM picrotoxin, 20 μM D-APV, and 20 μM CNQX to block ionotropic GABA and glutamate receptors. To confirm estradiol and diurnal changes in GnRH neuron excitability, cells were injected with current from 0-30 pA (500 ms, 10 pA steps). Confirming previous work, GnRH neurons from OVX+E PM mice fired more spikes in response to 500 ms current steps from 20-30 pA compared to all other groups (two-way repeated-measures ANOVA/Bonferroni, $p<0.05$, data not shown)(Adams et al., 2018).

Dynamic clamp. Dynamic clamp was implemented using the freely available QuB software (MLabs edition, https://milesculabs.biology.missouri.edu/QuB.html) (Milescu et

al., 2008) running on an independent computer (Marquis C733-T with dual Intel Xeon E5-2667v2 Ivy Bridge-EP 3.3GHz, 8-core processors, 8x16Gb DDR3-1866 SDRAM, ASLabs) and data acquisition system (PCIe-6361 Multifunction DAQ card with a BNC interface, National Instruments). The digital outputs of the EPC10 were used to trigger events in the dynamic clamp system. The input to the dynamic clamp system is the membrane potential of the cell (V_m), read from the EPC10 patch-clamp amplifier in current-clamp mode; the output of the dynamic clamp is the computed command current (I_{dc}), which drives the current command input of the EPC10. This input-output cycle is repeated at ~50 kHz.

To implement the synaptic conductance model in dynamic clamp, I_{dc} was calculated from the postsynaptic conductance (g_{sim}) as a function of time after a trigger and the linear driving force: $I_{dc} = g_{sim} * (V_m - V_{rev})$, where V_{rev} is the reversal potential (E_{GABA} = -36.5mV) (DeFazio et al., 2002). The time course of each synaptic conductance was modeled using a single exponential ($g_{sim}=g_{max}(-t/\tau)$) where g_{max} is the maximum conductance and τ is the decay time constant. The decay time constant of GABAergic PSCs is relatively independent of membrane potential in the range (-60 to -75 mV) used in these studies, but is strongly dependent on the intracellular chloride concentration (Houston et al., 2009). It is thus important to use a physiologic chloride concentration to determine the endogenous conductance time course for use in dynamic clamp studies. Whole-cell voltage-clamp recordings of endogenous GABA PSCs were obtained using a physiologic 20 mM chloride pipette solution at a holding potential of -70 mV. Recordings were made in the presence of 20 μM D-APV and 20 μM CNQX to block glutamatergic transmission. The decay time constant was estimated using a single exponential fit from 90% of the peak to 10% of the peak of the averaged GABA PSC for each cell. Decay time constant was not different among groups (OVX n=6, 8.8 ± 1.2 ms, OVX+E AM n=8, 11.0 ± 2.6 ms, OVX+E PM n=5, 9.0 ± 1.5; Kruskal-Wallis/Dunn's, p=0.94). The mean±SEM was 9.8 ± 1.0 ms, thus a value of 10 ms was used in dynamic clamp experiments.

Experimental Design

We measured GnRH neuron response to conductance trains from previously recorded PSC trains (example in Figure 3.1). Representative 30 second PSC trains for each group (OVX AM, OVX+E AM, OVX+E PM) were chosen from a previously published data set containing voltage-clamp recordings of >300 cells from OVX AM, OVX PM, OVX+E AM and OVX+E PM mice. (Christian and Moenter, 2007). Because OVX AM and OVX PM trains did not differ in mean frequency, interevent interval distribution, or amplitude, these groups were combined. For each PSC train, conductance vs. time was calculated ($g=I/(V-E_{GABA})$) (OVX AM mean g_{max}=0.78±0.1 nS, OVX+E AM g_{max}=0.73±0.2, OVX+E PM g_{max}=0.9±0.2; one-way ANOVA p>0.6). Peak conductances and event times were used to construct a new conductance (PSg) train using a physiological decay time constant. Each of these three trains was injected 1-4 times into cells from OVX AM, OVX PM, OVX+E AM, and OVX+E PM animals, trains were injected in random order for each cell. Direct current (<30 pA, 1.7±2.5 pA, n=34) was adjusted to keep cells within 3 mV of -59 mV. A 30-second duration for PSg trains was chosen because it permitted data collection in response to all three train types within a 7-minute period after stabilization. Previous work in our laboratory has determined that GnRH neurons do not experience a significant decrease in excitability over this time period (Adams et al., 2018). Cells from OVX AM and PM mice did not differ in the number of action potentials fired in response to conductance trains (Mann-Whitney two-tailed U-test p>0.59), these groups were thus combined for analysis purposes.

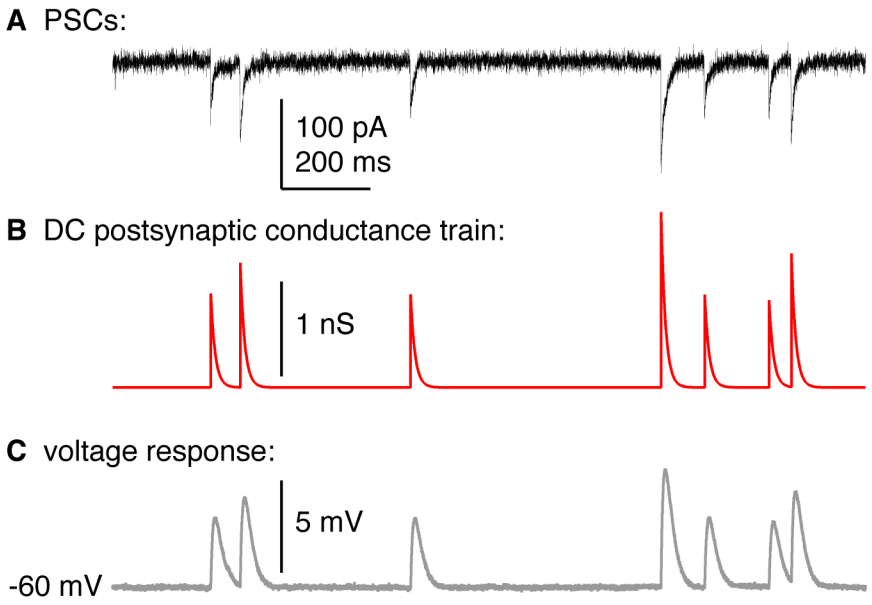

Figure 3.1. GABA postsynaptic currents in voltage-clamp were used to construct a postsynaptic conductance train for dynamic clamp studies.
A. GABA postsynaptic currents recorded at -70 mV in voltage-clamp using a high pipette chloride internal that slows decay time **B.** Simulated dynamic clamp postsynaptic conductance train constructed from the peak times and amplitudes in A, but using the decay time observed with physiological pipette chloride (10 ms) **C.** Response by an RC circuit to the postsynaptic conductance train in B.

Statistical Analyses.

Data were analyzed using Prism 7 (GraphPad) or SPSS (IBM) and are reported as the mean ± SEM unless otherwise noted. The number of cells per group is indicated by n. No more than three cells were used per animal with at least five animals tested per group. Data requiring one-way analyses were compared using one-way ANOVA with Fisher's least square difference (LSD) post hoc analysis or Kruskal–Wallis test with Dunn's post hoc analysis as dictated by data distribution. All data requiring two-way analyses were compared using two-way ANOVA with Fisher's LSD post hoc analysis. ANOVA analyses did not assume equal subgroup sizes. Fisher's LSD was selected because of the large number (18) of multiple comparisons being examined. Significance was set a $p<0.05$ but all p values <0.1 are specified. Slopes and intercepts were fit using linear regression, and ANCOVA analyses were performed to compare slopes and intercepts among groups.

Results

In the daily surge model, estradiol and time-of-day interact to alter GnRH neuron intrinsic properties, resulting in increased firing rate during positive feedback. To investigate if the concomitant changes in GABAergic transmission also increase GnRH neuron firing, we used dynamic clamp to deliver GABA PSg trains mimicking the input measured during negative feedback, positive feedback, and the open feedback loop condition into cells from OVX+E AM, OVX+E PM, and OVX mice (AM and PM combined). Figure 3.2 shows representative action potential firing from all three animal models in response to all three conductance trains. Spikes were identified as induced by a postsynaptic conductance if they occurred during the resulting postsynaptic potential and before the membrane potential returned to baseline (typically within 200 ms). In two cells from animals in positive feedback, a postsynaptic conductance initiated a burst of action potentials. These events were counted as induced events if the time interval between subsequent events was ≤ 250 ms and if a continuous increase in Vm between spikes was observed. In some cells, spontaneous spikes (that did not meet the above definition) occurred; these are marked with * in Figure 3.2. The number of spontaneous action potentials was not different between post-synaptic conductance trains or among groups (OVX+E PM: 3.2±0.8 spikes, OVX+E AM: 0.3±0.2 spikes, OVX 2.4±0.6 spikes; two-way repeated-measures ANOVA, $p>0.1$). Data quantifying response to trains (Figure 3.3) include only spikes that were induced by a postsynaptic conductance.

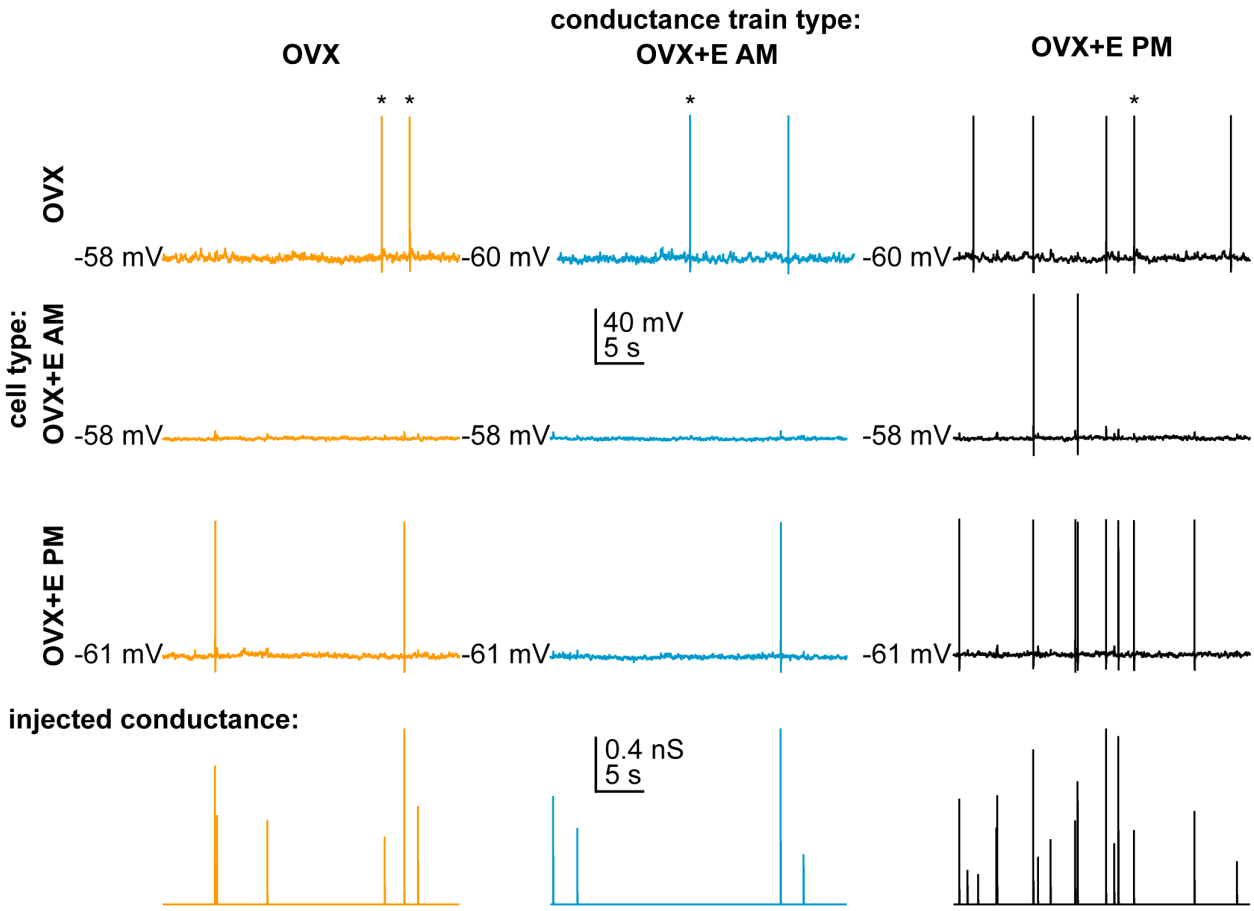

Figure 3.2. Representative recordings of cells from OVX (top), OVX+E AM (middle), and OVX+E PM (bottom) animals in response to conductance trains from OVX (orange), OVX+E AM (blue), and OVX+E PM (black).
* denotes spontaneous action potentials that were not induced by a postsynaptic conductance.

The positive feedback conductance train induced more action potentials in cells from all three animal models than the negative feedback or open-loop OVX conductance trains (Figure 3.3, two-way repeated-measures ANOVA/Fisher's LSD, $p<0.05$). This analysis also showed that in addition to conductance train type, animal model influenced the GnRH response. Specifically, positive feedback trains initiated more induced action potentials in cells during positive feedback (OVX+E PM) than in cells during negative feedback (OVX+E AM) or cells from OVX mice. These changes were not attributable to differences in either input resistance or capacitance among groups, but a difference in holding current approached significance (Table 3.1). There was no difference in number of action potentials induced by PSg trains from negative feedback vs the open-loop

condition among any of the groups, despite a difference in frequency and amplitude of GABA transmission between these states (Christian and Moenter, 2007).

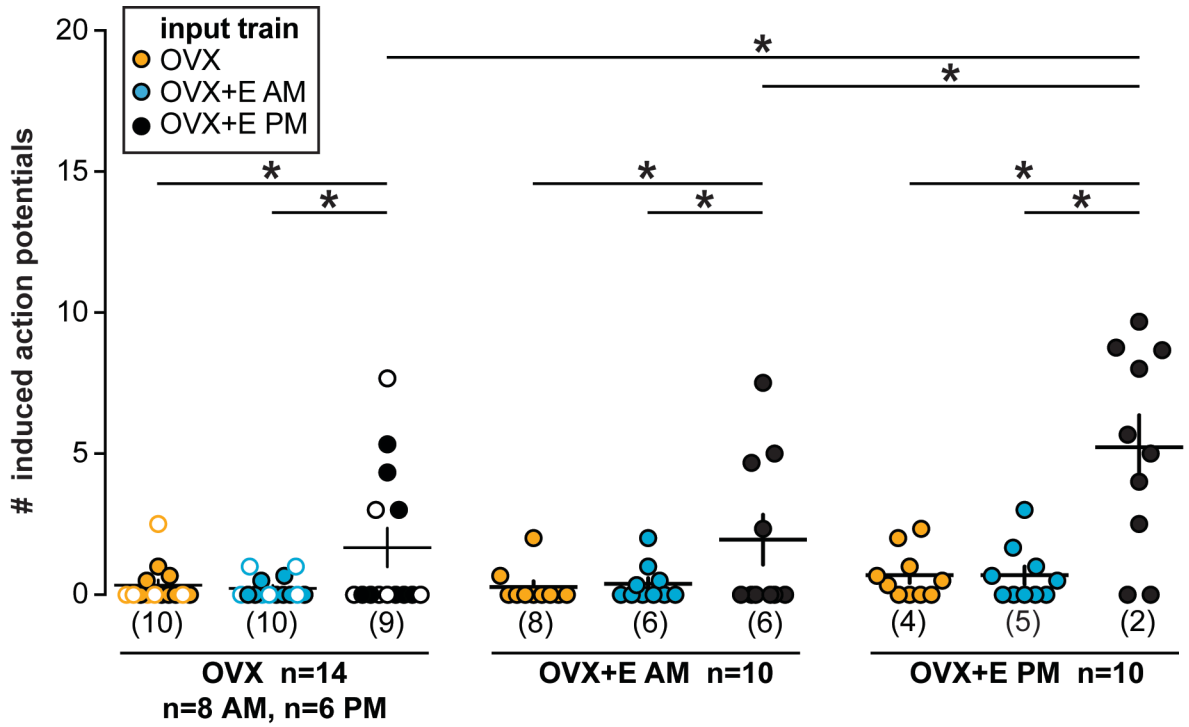

Figure 3.3. Positive feedback conductance trains are most effective at initiating spikes, but animal model of recorded cell also affects response.
Individual values and mean ± SEM spikes induced during individual postsynaptic conductances in each train in all three cell types. In the OVX group, open circles denote cells recorded in the PM and closed circles denote cells recorded in the AM. Numbers in parentheses along x axis indicate number of cells not firing any spikes. *p<0.05 two-way repeated-measures ANOVA/Fisher's LSD test (cell type: $F_{(2,31)}=3.8$ p=0.03, train: $F_{(2,62)}=33.4$ p<0.001, interaction: $F_{(4,62)}=5.3$ p=0.001)

Table 3.1. Whole-cell recording properties for Figures 3.2-4

Mean±SEM of GnRH whole-cell passive properties from Figures 3.2-4			
	OVX	*OVX+E AM*	*OVX+E PM*
Input resistance (MΩ)	951±60	819±68	1040±96
Capacitance (pF)	16.9±0.9	15.4±1.0	14.9±0.8
Series resistance(MΩ)	11.6±0.9	11.4±0.8	11.6±0.8
Holding current (pA)	0.7±4.1	6.1±3.8	-8.3±4.5
One-way ANOVA for comparison of GnRH passive properties among groups: cells from diestrous and proestrous mice (Figures 3.2-4)			
	group		
Input resistance (MΩ)	$F_{(2,31)}$=2.1		
Capacitance (pF)	KW statistic = 2.3		
Series resistance (MΩ)	KW statistic = 0.6		
Holding current (pA)	KW statistic = 4.8 (p=0.09)		

To assess if amplitude of the dynamic-clamp induced postsynaptic potentials and/or time between these events affected the probability of inducing an action potential, postsynaptic conductances from all trains were combined and sorted according to their peak conductance and interevent interval. Increased peak conductance was correlated with increased probability of initiating an action potential in cells from all three animal models (Figure 3.4A-B, linear regression, $p<0.001$) and the slopes of the linear regressions differed among these, being greatest in OVX+E PM cells and lowest in OVX+E AM cells ($p<0.001$). In contrast, the likelihood of initiating a spike was independent of interevent interval (Figure 3.4C-D, linear regression/ANCOVA, $p>0.1$). The slopes of the linear regressions of interevent interval did not differ among cells from different animal models, but the overall elevations (intercepts) did (OVX+E PM = 0.27±0.05, OVX+E AM = 0.076±0.02, OVX = 0.072±0.02) reflecting the increased response to postsynaptic conductance trains during positive feedback relative to all other cell types ($p<0.001$).

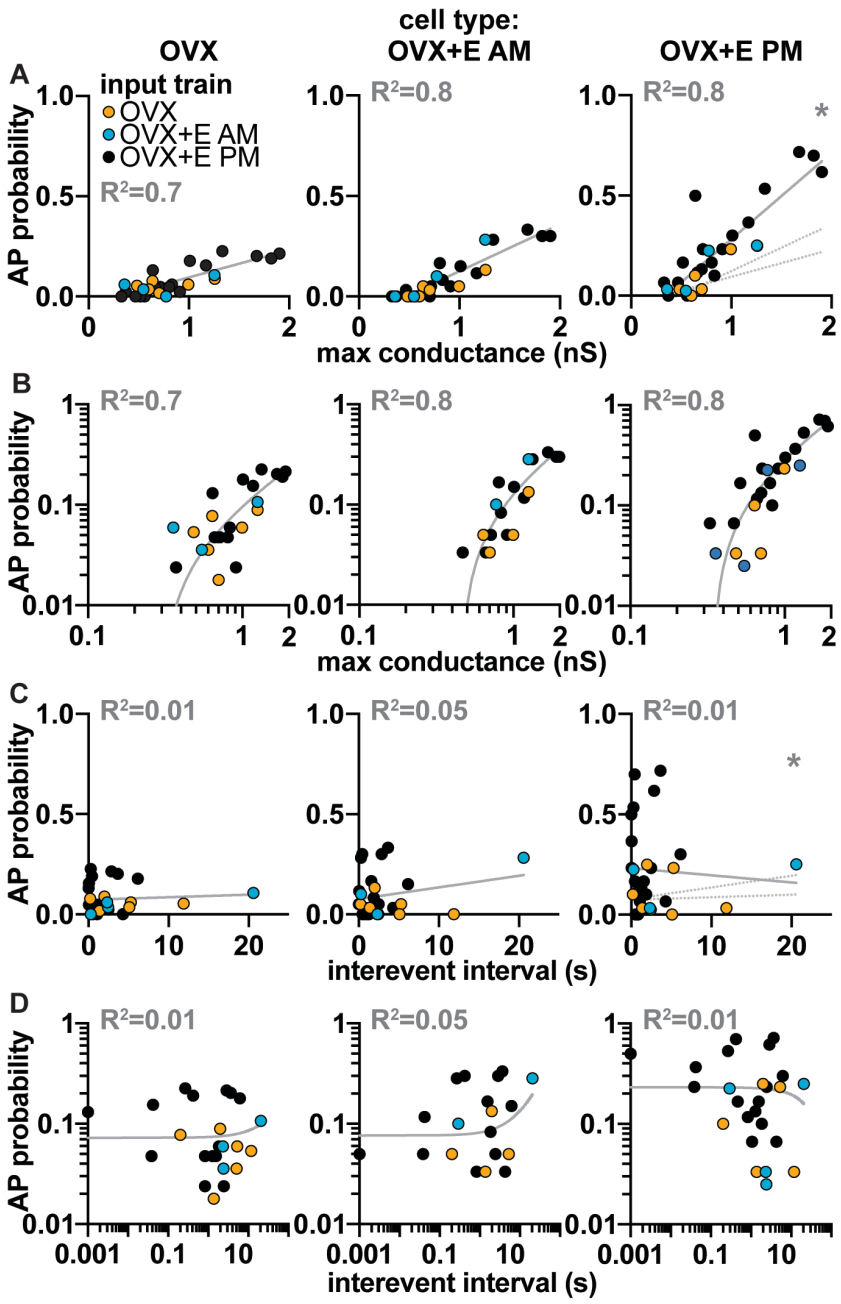

Figure 3.4. Increasing maximum peak conductance increases the probability of initiating an action potential.
Mean likelihood of initiating an action potential for individual conductances from OVX (orange), OVX+E AM (blue), and OVX+E PM (black) postsynaptic conductance trains in cells from OVX (left column), OVX+E AM (middle column), and OVX+E PM (right column) mice, considering: conductance amplitude (**A** linear scale, **B** log-log scale) or time since previous event (**C** linear scale, **D** log-log scale). Grey lines in left and middle columns are a linear fit to the data (R-squared is listed above each fit); and the three individual fits (from OVX, OVX+E AM, and OVX+E PM cells) are shown in the right-most column. *p<0.05 ANCOVA (A, slope: $F_{(2,78)}$=22.4; B, slope: $F_{(2,78)}$=0.5, intercept: $F_{(2,80)}$=8.4).

Discussion

For the majority of the mammalian reproductive cycle, GnRH is released in a pulsatile manner and estradiol feedback suppresses GnRH and LH release. A switch from estradiol negative to positive feedback at the end of the follicular phase initiates a surge of continuous GnRH release culminating in ovulation (Sarkar et al., 1976; Moenter et al., 1991). Here we show that during positive feedback, GnRH neurons integrate concomitant changes in fast-synaptic transmission and intrinsic properties to increase firing rate.

The present observations support and extend previous research demonstrating that GABAergic drive to GnRH neurons is correlated with an increased firing rate. In the daily surge model, GABA postsynaptic current (PSC) frequency and amplitude are suppressed during negative feedback and increased during positive feedback relative to values observed in cells from OVX mice (Christian and Moenter, 2007). The data demonstrate that GABAergic transmission mimicking positive feedback is more effective at driving firing of GnRH neurons from all animal models compared to trains mimicking negative feedback or the open-loop condition. This suggests that increasing levels of GABAergic inputs contribute to the increased action potential firing during positive feedback. The intrinsic changes in GnRH neurons during positive feedback are also playing a role in firing output as the efficacy of the GABA conductance trains was modulated by the feedback state of the cell it was applied to. Specifically, the response to the positive feedback train was augmented in cells recorded during positive feedback, suggesting the intrinsic changes that occur in GnRH neurons during positive feedback poise the cell to respond to increased transmission to further increase firing rate. Furthermore, positive feedback cells were the only cell type to initiate burst firing in response to a postsynaptic conductance. Burst firing has been linked to hormone release in other hypothalamic populations (Dutton and Dyball, 1979; Cazalis et al., 1985). These data support previous work in the daily surge model that showed GnRH neuron responsiveness (excitability) to 500 ms steps of current is increased during positive feedback compared to all other cell types and extend that work to show that shifts in intrinsic properties of GnRH neurons during positive feedback are sufficiently

robust to modulate the response to these short duration, lower amplitude physiologic inputs.

Previous work established that although GnRH neuron excitability does not differ between OVX and negative feedback groups due to opposing changes in the properties of A-type potassium currents. These opposing changes may account for the similar response to positive feedback, negative feedback, and OVX trains in cells from OVX and negative feedback mice. However, GABA PSC frequency and amplitude and GnRH neuron firing rate in OVX animals are intermediate to GnRH neurons from OVX+E AM and OVX+E PM cells (Christian et al., 2005; Christian and Moenter, 2007). It was thus surprising that no difference in firing response was observed between OVX and negative feedback conductance trains. It is possible that 30-second patterns are not sufficient for observing a difference in firing rate between these two groups, considering that most extracellular recordings determining firing rate were averaged over 30 minutes to 1 hour. Alternatively, changes in the whole-cell configuration in which many second messenger systems are dialyzed may account for the differences observed between whole-cell recordings and the extracellular configuration.

In many neurons, postsynaptic potentials decay to baseline in a matter of milliseconds (<100 ms) and tens to hundreds of coordinated PSPs are necessary to initiate an action potential. Some neurons in the hypothalamus appear unique in that their membrane potentials decay more slowly, permitting fast-synaptic inputs to summate over prolonged timescales (Branco et al., 2016). Specifically, in AGRP, POMC and PVH neurons, activation of a voltage-gated sodium current slows postsynaptic potential decay times and consequently, relatively few successive postsynaptic potentials can depolarize the membrane until threshold is reached and a spike is initiated. Given these observations, we postulated that decreasing time between successive postsynaptic conductances would increase spiking. We rejected this hypothesis as interevent interval did not influence the probability of initiating a spike. In contrast, peak conductance amplitude was highly correlated with action potential firing. Because the median peak conductances between the three train types did not differ, increasing the total number of postsynaptic conductances inevitably increases the number of postsynaptic conductances ≥1nS within the 30s train; this likely drives the increase in firing in

response to this conductance train. These data suggest that postsynaptic conductance amplitudes and GnRH neuron responsiveness appear to be more important than coordinated or successive GABA release from GnRH afferents. The present studies were done in brain slices but it is tempting to speculate that shifts in conductance via the $GABA_A$ receptor also modulate GnRH neuron *in vivo*. Numerous substances interact with this receptor in an allosteric manner to increase total conductance including the neurosteroid allopregnenolone and benzodiazepines (Defazio and Hablitz, 1998; Sullivan and Moenter, 2003). *In vivo* studies which preserve synaptic connections may also reveal shorter intervals that are more effective in initiating action potentials.

GnRH neurons typically do not express detectable estrogen receptor α (ERα), needed for both negative and positive feedback, thus estrogen-receptive afferents likely convey estradiol feedback signals (Hrabovszky et al., 2000; Hrabovszky et al., 2001; Couse et al., 2003; Wintermantel et al., 2006; Christian et al., 2008). One putative site for the relay of positive feedback is the anteroventral periventricular (AVPV) nucleus. AVPV neurons express kisspeptin, GABA, and glutamate and the majority express ERα (Smith et al., 2005; Smith et al., 2006). The neuromodulator kisspeptin acts directly by modulating multiple ionic currents in GnRH neurons, suppressing A-type and calcium-activated potassium currents and activating a non-selective cation current, effects that enhance GnRH neuron excitability and stimulate action potential firing (Pielecka-Fortuna et al., 2008; Zhang et al., 2008; Pielecka-Fortuna et al., 2011; Zhang et al., 2013; Adams et al., 2018). AVPV kisspeptin expression is increased on the afternoon of proestrus, and AVPV kisspeptin neurons fire higher frequency action potentials and more bursts at this time (Zhang et al., 2015; Wang et al., 2016). We postulate that kisspeptin release during positive feedback enhances GnRH neuron responsiveness to the concurrent increase in GABAergic fast-synaptic inputs. Of note, glutamatergic transmission to GnRH neurons is very low frequency, with no AMPA or NMDA-mediated currents detected in about one-third of cells and a typical frequency under 0.3 Hz (Christian et al., 2009; Liu et al., 2017). These low frequencies make comparisons difficult among animal models and suggest that the minor differences detected are unlikely to further influence firing despite a more depolarized reversal potential (Christian et al., 2009). AVPV kisspeptin neurons may also have a dual role in driving

the increased GnRH firing rate as kisspeptin as also acts indirectly via unspecified afferents to increase GABA PSC frequency and amplitude and glutamate EPSC frequency (Pielecka-Fortuna et al., 2008).

Multiple factors can influence the switch from negative to positive feedback. In addition to time-of-day and estradiol dependent signals, other internal and environmental cues may play a role. It remains unclear if each of these signals are necessary for initiating the GnRH surge, or if they act as redundant mechanisms for ensuring ovulation. The present studies suggest that GnRH neurons do not merely relay upstream signals, but act to integrate a multitude of signals to modulate firing rate and to initiate GnRH release.

Chapter 4: Changes in GABAergic Transmission to and Intrinsic Excitability of Gonadotropin-Releasing Hormone (GnRH) Neuron During the Estrous Cycle in Mice.

Abstract

GnRH neurons form the final common central output pathway regulating fertility. These cells are regulated by sex steroid feedback. A switch in estradiol feedback action from negative to positive feedback initiates a surge of GnRH release, ultimately triggering ovulation. Underlying mechanisms have been studied in ovariectomized, estradiol-treated (OVX+E) mice that exhibit GnRH surges on a daily basis; GnRH neurons are suppressed in the AM and activated in the PM. During the estrous cycle, however, changes between estradiol negative and positive feedback occur with cycle stage, with most of the cycle being controlled by negative feedback and positive feedback occurring in the PM of proestrus. To test the hypotheses that synaptic and intrinsic properties of GnRH neurons are regulated by cycle stage, we performed whole-cell patch-clamp studies in the PM of GnRH neurons in brain slices from female mice in diestrus (negative feedback) or proestrus (positive feedback). GABAergic transmission, which can excite these cells, was higher frequency in cells from proestrous vs diestrous mice; this increase was activity independent. Similarly, excitability, measured as action potential response to current injection, was greater in cells from proestrous mice. These changes were similar to those in the daily surge model. This suggests commonality in mechanisms when the switch between these feedback modes is observed at the same time of day in a cycle-dependent manner, and when the switch is triggered by a daily shift in response to estradiol.

Significance statement

Infertility affects 15-20% of couples; failure to ovulate is a common cause. Understanding how the brain controls ovulation is critical for new developments in both

infertility treatment and contraception. GnRH neurons are the final common pathway for central neural control of fertility. We studied how stage of the reproductive cycle regulates synaptic transmission to GnRH neurons and excitability of these cells. Both GABAergic transmission and excitability are down-regulated on diestrus, characterized by negative feedback by gonadal steroids, vs proestrus, when positive feedback and ovulation occur.

Introduction

GnRH neurons form the final pathway for neural control of reproduction. GnRH triggers the release of pituitary hormones, luteinizing hormone (LH) and follicle-stimulating hormone, which promote sex steroid production and gametogenesis (Schally et al., 1971b). For most of the reproductive cycle, the steroid estradiol suppresses GnRH/LH release (negative feedback). However, at the end of the follicular phase (proestrus in rodents), rising levels of estradiol switch from suppressing GnRH/LH release to inducing a surge of GnRH/LH release (positive feedback), triggering ovulation.

In rodents, ovulation is tightly coupled to time-of-day, and the GnRH/LH surges begin 1-2 hours before lights out in nocturnal species (Everett and Sawyer, 1950; Sarkar et al., 1976). To study the switch from negative to positive feedback, mice, rats and hamsters, can be induced to have daily LH surges at the same time in the late afternoon by ovariectomy combined with constant estradiol replacement (OVX+E) at high physiologic levels (Norman et al., 1973; Legan and Karsch, 1975; Christian et al., 2005). In OVX+E mice, LH release is suppressed in the morning (AM) and increased in the afternoon (PM) relative to ovariectomized mice that do not receive estradiol (OVX). This pattern persists in brain slices with GnRH firing rates and release suppressed in the AM relative to the PM in OVX+E mice (Christian et al., 2005; Glanowska et al., 2012). Using this daily surge model, changes in multiple intrinsic and fast-synaptic properties have been correlated with the switch from negative to positive feedback (Chu and Moenter, 2006; Christian and Moenter, 2007; Christian et al., 2009; Sun et al., 2010; Pielecka-Fortuna et al., 2011; Adams et al., 2018).

Because estradiol implants achieve near constant levels of steroid, this paradigm permits independent study of two variables, estradiol (OVX vs OVX+E) and time-of-day

(AM vs PM), as well as their interaction, revealing that the interaction induces the switch from negative to positive feedback. Constant estradiol, even at physiologic levels, is not, however, characteristic of female reproductive cycles. Surge-induction paradigms that attempt to emulate cyclic changes use a constant level of estradiol to mimic negative feedback for several days followed by an additional estrogen injection (OVX+E+E) to mimic the proestrous estradiol rise (Bronson and Vom Saal, 1979; Bronson, 1981). Both regimens induce LH surges (Dror et al., 2013), but the switch between negative and positive feedback relies on time of day in the OVX+E daily surge model, vs increased estradiol levels in the OVX+E+E model. An interesting biological question is whether or not the underlying neurobiological mechanisms are the same.

In this regard, the increase in GABAergic transmission, which can excite GnRH neurons, between negative and positive feedback that is observed in the OVX+E daily surge model does not appear to extend to the OVX+E+E surge model (Christian and Moenter, 2007; Christian et al., 2009; Liu et al., 2017). This discrepancy may point to interesting differences in diurnal inputs and estradiol feedback between the two models, and it also highlights that how the pattern of GABAergic transmission and other properties of GnRH neurons have not been studied during stages of the estrous cycle that exhibit these feedback modes. We examined the rates of GABAergic fast synaptic transmission, the primary fast synaptic input to GnRH neurons, as well as GnRH neuron excitability, measured as action potential firing rate in response to current injection, and action potential properties on diestrus vs proestrus. Diestrus is a relatively low estradiol state characterized by pulsatile LH release typical of the operation of this neuroendocrine system under homeostatic negative feedback; proestrus is the day of positive feedback (Czieselsky et al., 2016). We hypothesize that during the estrous cycle, the switch from diestrus to proestrus induces similar change in the intrinsic properties and fast-synaptic inputs GnRH neurons to those observed in the daily surge model.

Materials and methods

All chemicals were purchased from Sigma-Aldrich, unless noted.

Animals.

Transgenic mice expressing green fluorescent protein (GFP) under the control of the GnRH promoter (GnRH-GFP) were used (Suter et al., 2000). Mice were housed on a 14-h light:10-h dark cycle with lights off at 6 P.M. (eastern standard time). Teklad 2916 chow (Envigo) and water were available ad libitum. Estrous cycles of adult females aged 60-128 days were monitored by vaginal cytology to determine estrous cycle stage; mice were studied on diestrus or proestrus. Uterine mass was measured at the time of brain slice preparation to confirm cycle stage as it is directly proportional to circulating estradiol levels (Shim et al., 2000). Uterine mass was within the published range for diestrus (n=10, 47.3 ± 2.7 mg) and proestrus (n=9, 121.5 ± 2.7 mg)(Silveira et al., 2016), with mass being greater on proestrus (unpaired two-tailed Student's t-test, $p<0.0001$).

Brain Slice Preparation.

All solutions were bubbled with 95% O_2/5% CO_2 throughout the experiments and for at least 15 min before exposure to tissue. Brain slices were prepared 1.5-2.5 h before lights out. The brain was rapidly removed and placed in ice-cold sucrose saline solution containing the following (in mM): 250 sucrose, 3.5 KCl, 26 $NaHCO_3$, 10 D-glucose, 1.25 Na_2HPO_4, 1.2 $MgSO_4$, and 3.8 $MgCl_2$, at pH 7.6 and 345 mOsm. Coronal (300 µm) slices were cut with a VT1200S Microtome (Leica Biosystems). Slices were incubated in a 1:1 mixture of sucrose saline and artificial CSF (ACSF) containing (in mM) 135 NaCl, 3.5 KCl, 26 $NaHCO_3$, 10 D-glucose, 1.25 Na_2HPO_4, 1.2 $MgSO_4$, and 2.5 $CaCl_2$, at pH 7.4 and 305 mOsm, for 30 min at room temperature (~21 to 23°C). Slices were then transferred to 100% ACSF at room temperature for 0.5-5 h before recording.

Data Acquisition.

During recording, slices containing the preoptic area and anterior hypothalamus, which contain the majority of GnRH neuron somata, were placed into a chamber continuously

perfused with ACSF at a rate of 2 ml/min with oxygenated ACSF heated to 29.5-31.5°C with an inline-heating unit (Warner Instruments). GFP-positive cells were visualized with a combination of infrared differential interference contrast and fluorescence microscopy on an Olympus BX51WI microscope. Borosilicate glass capillaries (1.65-mm OD x 1.12-mm ID; World Precision Instruments, Inc.) were pulled by using a Flaming/Brown P-97 unit (Sutter Instrument Company) to make recording pipettes. Pipettes measured 2-4.5 MΩ when filled with (in mM): 125 K gluconate, 20 KCl, 10 HEPES, 5 EGTA, 0.1 CaCl2, 4 MgATP, and 0.4 NaGTP, 300 mOsm, pH 7.2 with NaOH for current-clamp recordings or when filled with (in mM): 140 KCl, 10 HEPES, 5 EGTA, 0.1 CaCl2, 4 MgATP, and 0.4 NaGTP, 300 mOsm, pH 7.2 with NaOH for recording GABAergic PSCs. Pipettes were wrapped with Parafilm (Bemis) to reduce capacitive transients; remaining transients were electronically cancelled. Pipettes were placed in contact with a GFP-positive neuron using an MP-285 micromanipulator (Sutter Instrument Company). All potentials reported were corrected online for liquid junction potential of −14.2 mV (Barry, 1994). Recordings were made with an EPC-10 dual patch-clamp amplifier (HEKA Elektronik) and a Macintosh computer running Patchmaster software (HEKA Elektronik). Experiments were analyzed offline using custom software (DeFazio and Moenter, 2002; DeFazio et al., 2014) written in IgorPro (Wavemetrics).

Experimental Design

Whole-cell patch-clamp.

After achieving a >1 GΩ seal and the whole-cell configuration, membrane potential was held at -60 mV between protocols. Series resistance (Rs), input resistance (Rin), and holding current (Ihold) were measured every 2-3 min using a 5 mV hyperpolarizing step from −60 mV (mean of 20 repeats, 20 ms duration, sampled at 100 kHz and filtered at 10 kHz). Only recordings with a Rin of >500 MΩ, Ihold of −50 to 20 pA, stable Rs of <20 MΩ, and a stable Cm between 8.5 and 23 pF were used for analysis.

Spontaneous GABAergic postsynaptic currents (sPSCs) were measured in voltage-clamp at a holding potential of -70 mV. Current was sampled at 10 kHz and filtered at 10 kHz. Pipettes were filled with a solution containing (in mM): KCl 140 HEPES 10, EGTA 5, CaCl2 0.01, mM MgATP 4 and mM NaGTP 0,4, pH 7.2, 310 mOsm/L. ACSF

contained 20 μM D-APV, and 20 μM CNQX to block ionotropic glutamate receptors. At least two 120 second recordings were made for each cell. To measure activity-independent miniature PSCs (mPSCs), two to three 120 seconds recordings were made before and during bath application of 1 μM tetrodotoxin (TTX) in a separate set of cells.

GnRH neuron excitability was assessed in current-clamp recordings. Direct current (15 to -55 pA, -14.1±3.8 pA, n=19) was adjusted to keep cells within 2 mV of -69 mV. Membrane potential was sampled at 20 kHz and filtered at 7.3 kHz. Bridge balance (95%) was used for most cells; for a few cells in both groups, bridge balance was not used but results were similar. ACSF contained 100 μM picrotoxin, 20 μM D-APV, and 20 μM CNQX to block ionotropic GABA and glutamate receptors. Cells were injected with current from 0-30 pA (500 ms, 2 pA steps). This protocol was repeated two to three times per cell and the number of action potentials at each step was averaged. The first spike fired was used to determine the following action potential characteristics: latency from start of the current injection to first spike, firing threshold (first derivative of the voltage trace > 1 mV/s), peak amplitude relative to threshold, full width at half-maximum (FWHM), rate-of-rise, and time and amplitude of after-hyperpolarization potential (AHP, the amplitude and time, relative to action potential initiation, of local minimum after the spike peak).

Statistical Analyses.

Data were analyzed using Prism 7 (GraphPad) or SPSS (IBM) and are reported as the mean ± SEM. The number of cells per group is indicated by n. No more than two cells were used per animal with at least four animals tested per group. Data requiring analyses between two groups (e.g., diestrus vs. proestrus) were compared using unpaired two-tailed Student's t-test or Mann-Whitney U test as dictated by data distribution, which was determined using a Shapiro-Wilk test for normality. Distributions were compared using the Kolmogrov-Smirnov test. All data requiring two-way analyses were compared using two-way ANOVA with Bonferroni post hoc tests; this test is considered sufficiently robust for non-normally as well as normally distributed data (Underwood, 1996). ANOVA analyses did not assume equal subgroup sizes. Significance was set a $p<0.05$ but all p values <0.1 are specified.

Results

GABAergic transmission to GnRH neurons is increased during proestrus.

In the daily surge model, GABAergic transmission is decreased during negative feedback and increased during positive feedback relative to OVX controls (Christian and Moenter, 2007). To examine if GABA transmission to GnRH neurons in modulated between the phases of the estrous cycle during which physiologic negative and positive feedback are observed, spontaneous GABAergic postsynaptic currents (sPSCs) were recorded near the time of lights out from GnRH neurons in brain slices obtained from diestrous (negative feedback) or proestrous (positive feedback) mice. Representative recordings are shown in Figure 4.1A. Frequency of spontaneous GABAergic PSCs (sPSCs) was increased during proestrus relative to diestrus (Figure 4.1B, diestrus n = 12, proestrus n = 16, Mann-Whitney U test, $p=0.029$). Similarly, the sPSC interevent interval distribution was shifted towards shorter intervals on proestrus (Figure 4.1C, Kolmogrov-Smirnov test, $p<0.0001$). No difference was observed in mean sPSC amplitude (Figure 4.1E, unpaired two-tailed Student's t-test, $p>0.5$), however, their probability distributions differed with proestrus having events distributed over a wider range of amplitudes (Figure 4.1F, Kolmogrov-Smirnov test, $p<0.0001$). No difference was observed in decay time between 90% and 10% of the maximum current amplitude (Figure 4.1G, unpaired two-tailed Student's t-test, $p>0.4$). Input resistance, holding current, and capacitance were not different between groups (Table 4.1).

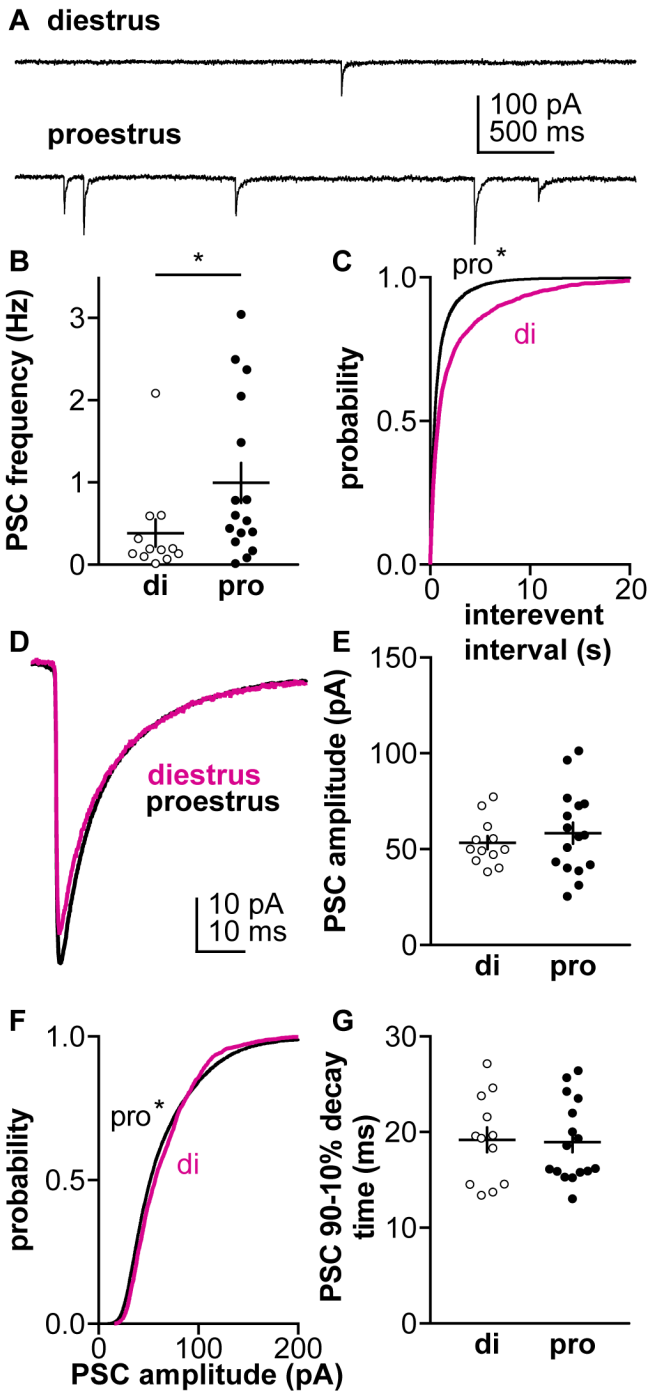

Figure 4.1. GABAergic sPSC frequency is increased on proestrus vs diestrus.
A. Representative sPSC recording from a neuron in each group. **B.** Individual values and mean ± SEM of spontaneous GABAergic PSC frequency. **C.** Cumulative probability distribution of interevent interval for each group. **D.** Average of all sPSC from all cells in each group. **E.** Individual values and mean ± SEM of sPSC amplitude. **F.** Cumulative probability distribution of sPSC amplitude. **G.** Individual values and mean ± SEM of time decay time between 90% and 10% of the maximum current amplitude. *p<0.05 Mann-Whitney U test (**B**, U=49), Kolmogorov-Smirnov test (**C**, D=0.2; **F**, D=0.07) or unpaired two-tailed Student's t-test (**D**, $t_{(26)}$=0.7; E, $t_{(26)}$=0.1).

Table 4.1. Whole-cell recording properties for Figures 4.1-3

Mean±SEM of GnRH whole-cell passive properties from Figure 4.1			
	diestrus	*proestrus*	
Input resistance (MΩ)	916±40	1034±63	
Capacitance (pF)	14.5±0.6	14.5±0.7	
Series resistance(MΩ)	13.3±0.6	14.6±0.7	
Holding current (pA)	-13.6±3.8	-17±2.8	
Student's t-test parameters for comparison of GnRH passive properties among groups: cells from diestrous and proestrous mice (Figure 4.1)			
	group		
Input resistance (MΩ)	$t_{(26)}$=1.5		
Capacitance (pF)	U=92		
Series resistance (MΩ)	$t_{(26)}$=1.4		
Holding current (pA)	U=71		
Mean±SEM of GnRH whole-cell passive properties from Figure 4.2			
	diestrus	*proestrus*	
Input resistance (MΩ) before TTX during TTX	 1053±88 846±83	 1113±145 775±91	
Capacitance (pF) before TTX during TTX	 15.8±0.8 15.0±0.8	 13.2±0.9 13.8±1.0	
Series resistance(MΩ) before TTX during TTX	 12.1±0.9 13.3±1.5	 12.3±0.6 14.7±0.8	
Holding current (pA) before TTX during TTX	 -16.4±3.5 -25.1±6.3	 -19.4±2.6 -28.5±3.8	
Two-way repeated measures ANOVA for comparison of GnRH passive properties among groups: cells from diestrous and proestrous mice (Figure 4.2)			
	group	*TTX*	*group x TTX*
Input resistance (MΩ)	$F_{(1,9)}$=0.001	$F_{(1,9)}$=36.0***	$F_{(1,9)}$=2.1
Capacitance (pF)	$F_{(1,9)}$=2.5	$F_{(1,9)}$=0.1	$F_{(1,9)}$=6.9*
Series resistance (MΩ)	$F_{(1,9)}$=0.4	$F_{(1,9)}$=6.0*	$F_{(1,9)}$=0.7
Holding current (pA)	$F_{(1,9)}$=0.3	$F_{(1,9)}$=14.1**	$F_{(1,9)}$=0.01
Mean±SEM of GnRH whole-cell passive properties from Figure 4.3			
	diestrus	*proestrus*	
Input resistance (MΩ)	1125±150	1361±144	
Capacitance (pF)	13.7±0.7	12.5±0.8	
Series resistance(MΩ)	13.5±0.9	13.5±1.4	
Holding current (pA)	-0.8±5.2	-10±4.4	
Student's t-test parameters for comparison of GnRH passive properties among groups: cells from diestrous and proestrous mice (Figure 4.3)			
	group		
Input resistance (MΩ)	$t_{(16)}$=1.1		
Capacitance (pF)	$t_{(16)}$=1.2		
Series resistance (MΩ)	$t_{(16)}$=0.02		
Holding current (pA)	U=19 (p=0.06)		

*p<0.05; **p<0.01; ***p<0.001. U=Mann-Whitney U test statistic

GABAergic transmission is activity independent

Increased GABAergic PSC frequency during proestrus may be due to an increase in presynaptic activity and/or synaptic connectivity to GnRH neurons. To differentiate between these mechanisms, PSC frequency and amplitude were recorded before and during treatment with the voltage-gated sodium channel blocker tetrodotoxin (TTX). TTX isolates activity-dependent neurotransmission, which is proportionate to the number of functional synaptic connections (Auger and Marty, 2000; Kaeser and Regehr, 2014). PSC frequency (Figure 4.2B), amplitude (Figure 4.2D), and decay time (Figure 4.2E) were not altered during TTX treatment.

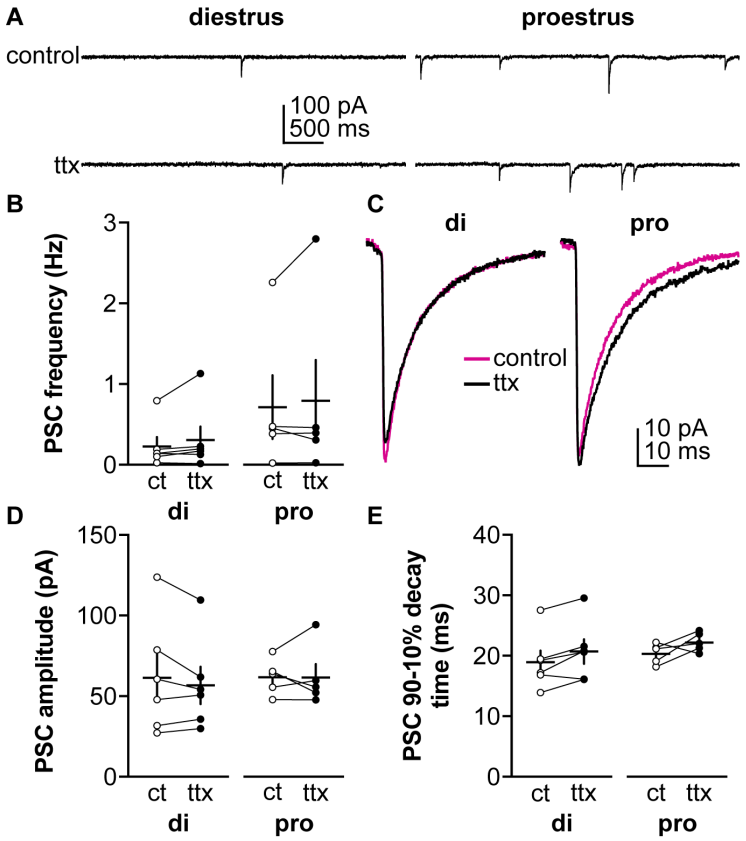

Figure 4.2. TTX does not affect GABAergic PSC frequency or amplitude in diestrous and proestrous mice.
A. Representative recordings from a representative neuron in each group before (control or ct, top) and during (bottom) TTX treatment. **B.** Individual values and mean ± SEM of GABAergic PSC frequency. **C.** Average of all PSC traces for control or ttx periods from all cells in each group. **D-E** Individual values and mean ± SEM for: **D,** PSC amplitude, **E,** decay time between 90% and 10% of the maximum current amplitude. No statistical differences were detected using two-way repeated-measures ANOVA/Bonferroni test (B, cycle stage: $F_{(1,9)}$=1.3; TTX: $F_{(1,9)}$=1.6; cycle stage x TTX: $F_{(1,9)}$=0.0; D, cycle stage: $F_{(1,9)}$=0.3; TTX: $F_{(1,9)}$=0.6; cycle stage x TTX: $F_{(1,9)}$=0.5; E, cycle stage: $F_{(1,9)}$=0.5; TTX: $F_{(1,9)}$=6.4 (p=0.01); cycle stage x TTX: $F_{(1,9)}$=0.9)

GnRH neuron excitability is increased during positive feedback.

In the daily surge model, estradiol and time-of-day interact to alter GnRH intrinsic properties, resulting in increased excitability during positive feedback (Adams et al., 2018). To investigate if GnRH neuron excitability is also modulated during the estrous cycle, we measured GnRH neuron response to depolarizing steady-state current injections (0-30 pA, 2 pA steps, 500ms). Figure 4.3A shows representative response to +12 and +24 pA injections. The minimum current required to initiate spikes was lower during proestrus than diestrus (diestrus n = 9, proestrus n = 9, unpaired two-tailed Student's t-test, $p<0.05$). Once firing was initiated, GnRH neurons from proestrous mice fired more spikes at each current step from 18-30 pA than cells from diestrous mice (Figure 4.3B, two-way repeated-measures ANOVA/Bonferroni, $p<0.05$). These changes were not attributable to differences in either input resistance or capacitance between groups (Table 4.1). The holding current in voltage-clamp, however, approached the level set for significance (Mann-Whitney U test, $p=0.06$). This may reflect the increased excitability of these cells.

In addition to action potential firing, the properties of these events were analyzed as a function of cycle stage. A number of properties approached but did not achieve significance, between the cycle stages examined, including time to first spike (spike latency, Figure 4.3D, unpaired two-tailed Student's t-test, $p=0.06$), action potential threshold (Figure 4.3E, unpaired two-tailed Student's t-test, $p=0.07$), and the full-width at half-maximum (Figure 4.3G, unpaired two-tailed Student's t-test, $p=0.06$). Afterhyperpolarization time was reduced during proestrus (Figure 3J, unpaired two-tailed Student's t-test, $p<0.05$). No cycle-dependent changes were observed in spike amplitude (Figure 4.3F, Mann-Whitney U test, $p>0.5$), rate-of-rise (Figure 4.3H, Mann-Whitney U test, $p>0.25$), or AHP amplitude (Figure 4.3I, Mann-Whitney U test, $p>0.5$).

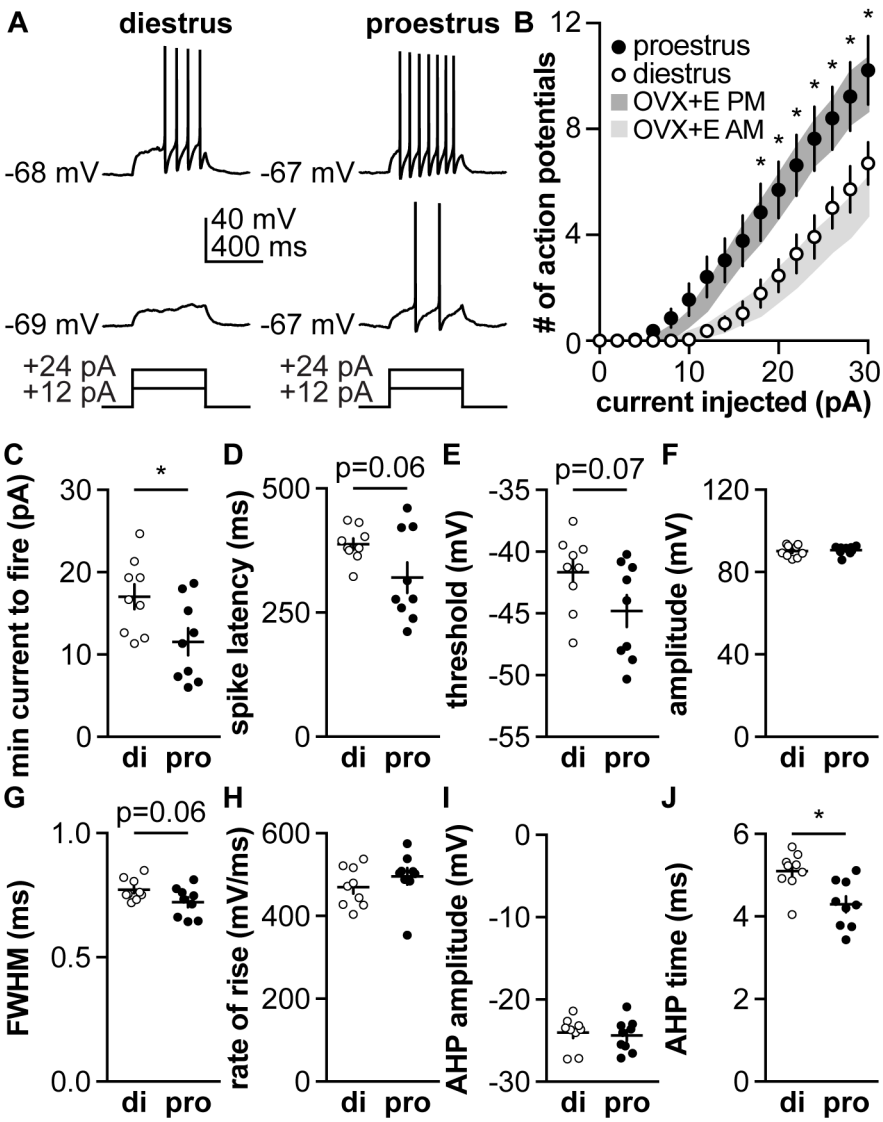

Figure 4.3. GnRH neuron excitability is increased on proestrus vs diestrus.
A. Representative traces from a neuron in each group during 500 ms current injections of 12 and 24 pA (current injection protocol below). **B.** Mean ± SEM spikes elicited for each current injection step during diestrus and proestrus. Grey shading, shows the range of values within the SEM from (Adams et al., 2018) from mice prepared in the daily surge model; light grey OVX+E AM (negative feedback), dark grey OVX+E PM (positive feedback). **C-H** Individual values and mean ± SEM for: **C,** minimum current to initiate spiking, **D,** latency to first spike, **E,** action potential threshold, **F,** action potential amplitude, **G**, full-width at half-maximum, **H**, action potential rate of rise, **I**, afterhyperpolarization potential (AHP) amplitude, and **J**, AHP time. *p<0.05 two-way repeated-measures ANOVA/Bonferroni test (B, cycle stage: $F_{(1,16)}$=6.7, current: $F_{(15,240)}$=83.7, interaction: $F_{(15,240)}$=5.0), two-tailed unpaired Student's t-test (C, $t_{(16)}$=2.5; D, $t_{(16)}$=2.1; E, $t_{(16)}$=1.9; G, $t_{(16)}$=2.0; J, $t_{(16)}$=3.3), or Mann-Whitney U test (F, U=39; H, U=28; I, U=37).

Discussion

The female reproductive cycle is characterized by one of the rare examples of positive feedback in physiology, specifically the induction of a surge mode of GnRH and LH release at the end of the follicular phase (proestrus in rodents). This is largely attributed to exposure to high sustained levels of estradiol from the dominant follicle (Docke and Dorner, 1965). Here we show that GABAergic transmission to GnRH neurons and their excitability are both increased during proestrus (positive feedback) relative to diestrus (negative feedback).

The present observations support and extend work in an OVX+E mouse model in which the switch from estradiol negative to positive feedback occurs on a daily basis. The levels of estradiol achieved in the daily surge model are in the physiologic range, but are persistently, rather than cyclically, elevated. Given the estradiol level is similar during negative and positive feedback, it is not an estradiol rise that triggers the change between states, which is different from the cycle in which sustained exposure to elevated estradiol is viewed as the trigger for the transition. The question is thus raised of whether or not underlying mechanistic differences observed between feedback states in the daily surge model are the same as those between feedback states during the cycle. The similarity in GnRH neuron excitability and GABA transmission observed in the present work in cycling mice to published observations in the OVX+E daily surge model indicates at least some of the neurobiological mechanisms underlying the feedback switch are the same between these models. Given these similarities, it is not surprising that the GnRH neuron firing rate has also been shown to be similar during positive feedback whether induced by OVX+E or occurring on the afternoon of proestrus (Silveira et al., 2016),.

In addition to the pattern of estradiol being different, other ovarian hormones are also missing in the OVX+E daily surge model. Estradiol has long been identified as the primary steroid underlying the induction of positive feedback (Docke and Dorner, 1965), but a role for progesterone has also been postulated. This is based in part on its ability to amplify the LH surge in rats and mice (Bronson and Vom Saal, 1979). More recent studies have identified both central changes induced by progesterone and potential ligand-independent actions of the progesterone receptor as important for the LH surge

(Chappell et al., 1999; Chappell and Levine, 2000; Micevych and Sinchak, 2011). In women, progesterone and 17α-hydroxyprogesterone levels rise during the preovulatory period (Baird and Fraser, 1974). The amplitude of the proestrous LH surge in mice is greater than the estradiol-induced surge, attributable at least in part to augmented pituitary response to GnRH on proestrus (Silveira et al., 2016). Recent work in women demonstrates progesterone administration during the late follicular phase augments LH pulse amplitude (likely response to endogenous GnRH) but does not alter pulse frequency, which would require a central action (Hutchens et al., 2016). Longer-term constant progesterone treatment reduces GABAergic transmission to GnRH neurons and decreases the amplitude of voltage-gated calcium conductances, both of which would tend to reduce output from these neurons (Sullivan and Moenter, 2005; Sun and Moenter, 2010). Together these observations may indicate some boosting effects of progestins on LH surge amplitude occur downstream of the GnRH network.

Consistent with this postulate, the present observations of GnRH neuron excitability, which reflects largely intrinsic properties, reveal strikingly similar to observations in the daily surge model (Adams et al., 2018). While the rate of GABAergic transmission followed the same shift of low frequency during negative feedback and high frequency during positive feedback and the same activity independence, mean frequency values may be slightly higher during both negative and positive feedback during the cycle. This may indicate an influence of progesterone or other ovarian factors on synaptic inputs or via glial elements. GABAergic neurons in the preoptic area and hypothalamus have been shown to express progesterone receptors, thus effects of progesterone could be directly upon this cell type (Leranth et al., 1991). It is also important to point out that in the acute brain slice preparation, some connections between GnRH and their afferents are severed. If progesterone affected inputs arising outside the slice, this would be difficult to detect with this approach.

The existence of a daily central signal for ovulation such as implied in the daily surge model was identified in the middle of the last century in studies that demonstrated that barbiturate anesthesia during a critical period on proestrus blocked ovulation for 24 hours in rats (Everett and Sawyer, 1950). Ovulation can occur on a daily basis during

the breeding season in many fish and bird species (Krishnan et al., 1993; Karigo et al., 2012). Daily ovulation *per se* has not been observed in placental mammals but in some mammals, ovulation occurs at a particular time of day. This is especially observed in rodents, in which the LH surge occurs at the start of the active period in both nocturnal and diurnal species (Sarkar et al., 1976; Mahoney et al., 2004). Similarly, LH surges in women occur more often during late sleep/early wake hours (Cahill et al., 1998; Kerdelhue et al., 2002), and shiftwork, which can disrupt the circadian clock, is linked to menstrual cycle irregularities and increased time to pregnancy (Bisanti et al., 1996; Labyak et al., 2002; Boden and Kennaway, 2006).

The lack of observation of daily ovulation in mammals may be attributed in part to the time needed for a follicle to mature to the point that it can produce sufficient estradiol to trigger positive feedback. Of interest in this regard, *tau* mutant hamsters, in which the free-running period is ~20h vs just under 24h in the wild type, exhibit estrous cycles lasting five circadian days, or about 100 hours. This is similar in duration to the typical four-day (96 hour) estrous cycle in wild type golden hamsters (Refinetti and Menaker, 1992). Daily LH surges are induced during subjective afternoon in OVX+E tau hamsters, and the period consecutive LH surges was shorter than in wild type hamsters (Lucas et al., 1999). These observations are consistent with the postulate that follicle maturation and subsequent estradiol production are limiting and that the reproductive cycle does not result from a mere counting of circadian days. Thus provision of a constant high physiologic estradiol level would circumvent this limitation, allowing surges to occur on a daily basis as observed.

The concept that estradiol regulates synaptic properties of GnRH neurons to bring about the switch from negative to positive feedback were not supported in recent work using another LH-surge induction model in which OVX mice are treated with basal estradiol replacement then an additional estrogen injection to mimic the proestrous estradiol rise (Bronson and Vom Saal, 1979; Bronson, 1981). No differences were observed in sPSC or mPSC frequency between negative feedback (OVX+basal E, slices made 4.5-5 hours before lights out, recordings made 1-3.5 hours before lights off) and positive feedback (OVX+basal E+E injection, slices made 1.5-2 hours before lights out, recordings 1 hour before to 1.5 hours after lights out) (Liu et al., 2017). Despite this

difference, both models reliably produce an LH surge. This could indicate that changes in GABAergic PSC frequency may not be necessary for initiating positive feedback. In this regard, knockout of estradiol receptor alpha from GABAergic neurons eliminates estradiol positive feedback (Cheong et al., 2015). Of note, this would remove ERα from a large percentage of kisspeptin neurons in the AVPV that utilize GABA as a co-transmitter; the lack of a surge may reflect reduced activation of these neurons (Cravo et al., 2011; Frazao et al., 2013). Another possibility is that elements of the daily surge persist in the OVX+basal estradiol model used for negative feedback in those studies. If time of day interacts with estradiol to generate the changes observed in synaptic transmission to GnRH neurons, it is possible that the switch to positive feedback levels of transmission had already occurred based on basal estradiol alone. Of note, the frequency of synaptic transmission in that study is higher in all groups that we have observed either in daily surge or cycling mice.

The LH surge is important for ovulation, reproduction and the continuation of species. The present studies add to a literature that indicates multiple factors can influence the switch from negative to positive feedback. These mechanistic studies in both daily surge and cycling models reveal strikingly similar changes in intrinsic excitability and GABAergic transmission. Feedback stage-dependent shifts in both GnRH neuron intrinsic excitability and fast-synaptic inputs likely contribute to the increase in firing rate and GnRH release during positive feedback.

Chapter 5: Conclusion

GnRH neurons form the final pathway for neural control of reproduction. For the majority of the reproductive cycle, the sex steroid estradiol suppresses pulsatile GnRH/LH release (negative feedback). However, at the end of the follicular phase, rising levels of estradiol switch from suppressing GnRH/LH to inducing a surge of GnRH/LH release (positive feedback), triggering ovulation.

Previous studies using the daily surge model have elucidated multiple GnRH neuron intrinsic and fast-synaptic changes during the switch from negative to positive feedback (Chu and Moenter, 2006; Christian and Moenter, 2007; Zhang et al., 2007; Christian et al., 2009; Zhang et al., 2009; Sun et al., 2010; Pielecka-Fortuna et al., 2011). Prior to this work, it was unclear which if any of these changes were necessary for initiating the switch to positive feedback. In the present work, we used electrophysiological recordings and mathematical modeling to demonstrate three key findings. In chapter 2, we demonstrate that changes to GnRH neuron ionic conductances render GnRH neurons more excitable during positive feedback relative to OVX controls, but changes to ionic conductances between the open loop condition and negative feedback have no net effect on GnRH neuron excitability. A novel mathematical technique predicted that multiple combinations of changes to GnRH intrinsic conductances can produce the firing response in positive feedback, and changes to two interdependent parameters accounted for similar neural responses during negative feedback and in OVX mice. In chapter 3, we injected positive feedback, negative feedback, and OVX post-synaptic conductance trains to demonstrate that increasing GABAergic drive increases GnRH neuron firing rate in OVX, OVX+E AM, and OVX+E PM cells and GnRH neurons are more responsive to post-synaptic conductances during positive feedback relative to all other groups. In chapter 4, we demonstrate that changes to GnRH neuron intrinsic properties and fast-synaptic inputs during estrous cycle are strikingly similar to those

observed between negative and positive feedback in the daily surge model. GABA inputs and GnRH neuron excitability are both increased during positive feedback (proestrus) relative to negative feedback (diestrus). In this chapter I will expand upon each of these points and conclude with a working model for increasing GnRH neuron firing rate to initiate the switch from negative to positive feedback.

GnRH neuron excitability is regulated by estradiol feedback

Estradiol and time-of-day signals modify of a number of GnRH neuron ion channel properties in the daily surge model (Chu and Moenter, 2006; Zhang et al., 2007; Zhang et al., 2009; Sun et al., 2010; Pielecka-Fortuna et al., 2011). In chapter 2, we hypothesized that these changes would make GnRH neurons more excitable during positive feedback and less excitable during negative feedback. Our hypothesis was only partially supported. GnRH neurons fired more action potentials in response to 500 ms steps of current relative to all other groups (OVX AM, OVX PM, and OVX+E AM). However, GnRH neuron excitability did not differ between negative feedback and OVX controls. We extended our work to the estrous cycle by demonstrating similar changes in GnRH neuron excitability between proestrous and diestrous mice in Chapter 4. GnRH neuron excitability was increased during proestrus relative to diestrus and similar to GnRH neuron input-output levels observed in OVX+E PM mice. GnRH neuron excitability in diestrous mice was comparable to input-output curves from OVX/negative feedback mice. These data suggest that the neurobiological mechanisms underlying changes in excitability during the estrous cycle are recapitulated by estradiol feedback in OVX+E mice. It is also possible that despite having similar levels of excitability, their ion channel distributions may differ due to the presence of additional sex steroids during the estrous cycle. For example, the ovarian sex steroid progesterone suppresses activation of voltage-gated calcium channels. An interesting course of future investigation would be to characterize individual ionic conductances in diestrus and proestrus mice and compare them to changes observed in daily surge model.

To test the individual and combinatorial contributions of ionic conductances in determining GnRH neuron excitability, we adapted a mathematical model of a GnRH neuron developed by Anmar Khadra and Arthur Sherman (LeBeau et al., 2000; Van

Goor et al., 2000; Moran et al., 2016). We used a Markov Chain Monte Carlo parameter estimation method, which estimates probability distributions for each parameter (rather than a single point estimate) and covariances between parameters (Foreman-Mackey et al., 2013). Because GnRH neuron excitability does not differ between negative feedback and OVX controls, despite their different ion channel properties (i.e., g_A, $V_{1/2inact}$ of I_A, g_{NaP}, g_{HVA}), we expected that more than one unimodal distribution of parameter sets would be able to reproduce excitability during negative feedback. This hypothesis was rejected when the MCMC method converged to a single unimodal ("identifiable") distribution of parameter sets. However, the parameter distributions of $V_{1/2inact}$ and g_A were highly-dependent on one another. As g_A decreased, $V_{1/2inact}$ shifted to more depolarized potentials to maintain the same response to current injection. This is the same shift we observe experimentally between OVX and negative feedback groups, suggesting that these two parameters counteract one another *in vivo* to maintain homeostasis in the face of a changing steroid milieu. Presently, it is not possible to shift the electrophysiologic properties of individual channels to test the model predictions directly. Dynamic clamp studies to inject potassium conductances that have opposing changes in $V_{1/2inact}$ and g_A to determine their effects on GnRH neuron excitability may help to resolve this question.

To study how the above changes to potassium currents contribute to action potential firing, we measured potassium currents during an action potential shaped waveform in voltage-clamp (action potential clamp). To isolate potassium currents in action-potential clamp in cells from OVX+E AM (n=3), OVX+E PM (n=2), and OVX mice (OVX PM n=4, OVX AM n=1), we blocked voltage-gated Na^+ and Ca^+ channels with tetrodotoxin and $CdCl_2$, respectively. Differences in current amplitude before and during the action potential were recorded. Prior to action potential initiation, potassium currents were increased during negative feedback relative to positive feedback and potassium currents from OVX cells were intermediate to the two (Figure 5.1A). Although the differences in current density are small (~0.4 pA/pF or 6 pA in a typical 15 pF cell), GnRH neuron input resistance is relatively high (R_{in}~1 GΩ) and Ohm's law ($V=IR$) predicts that this change can amount to a difference of 6 mV in current-clamp and likely sufficient to reduce spike initiation during negative feedback. Potassium currents

peaked, as expected, during the repolarization phase of the action potential (Figure 5.1B). Peak potassium currents were greatest during negative feedback, decreased during positive feedback, and were smallest in cells from OVX mice. Potassium currents returned to baseline fastest during positive feedback and were slowest to return to baseline in OVX cells (Figure 5.1B). These data suggest that potassium currents before and during an AP are decreased during positive feedback relative negative feedback; these changes would be expected to increase excitability during positive feedback. Meanwhile, potassium currents in OVX cells were smaller before and during the AP, but slower to return to baseline relative to OVX+E AM cells. The first change would be expected to increase action potential firing in OVX cells, and the latter change would be expected to decrease it. These conflicting results may be attributable the counteracting changes to g_A and $V_{1/2inact}$ that occur between these two cell types, and to prevent a change an excitability between cells from OVX and OVX+E AM mice.

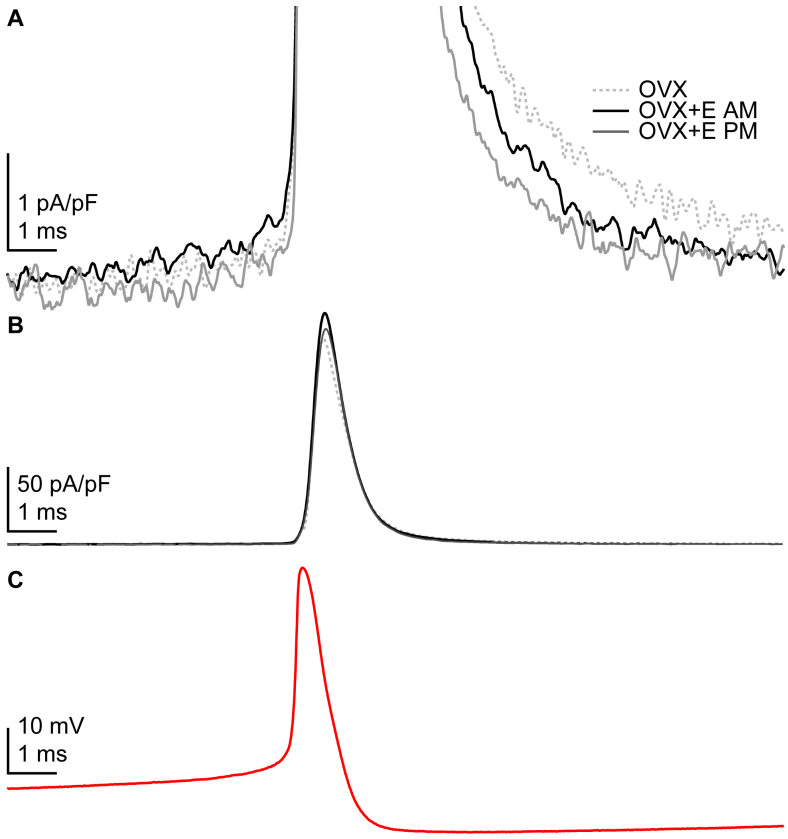

Figure 5.1. Time-of-day and estradiol alter potassium current density (A-B) during an action potential waveform (C).

We also used the MCMC method to estimate the best parameter set(s) for reproducing GnRH neuron response during positive feedback. To our surprise, the MCMC simulations did not converge to a unimodal distribution of parameters as it did in the negative feedback model. There were multiple combinations of parameters, over a wide physiological range, that provided equally good fits to the current-clamp data. This suggests that there are multiple, redundant mechanisms for increasing GnRH excitability during positive feedback, potentially to ensure ovulation. It is unclear if these redundant mechanisms are targeted to every cell, or if they are directed at separate cells. To answer this question, future studies could measure correlations in the densities of ion channels in individual cells across the GnRH neuron population (O'Leary et al., 2013).

MCMC methods surpass other parameter estimation methods because they provide a probability distribution for each parameter and co-variances between parameters. As a consequence, our MCMC simulations made it possible to dissect the individual and combined roles of ionic currents in determining GnRH neuron excitability; experiments which cannot be performed empirically. However, every mathematical model is limited by the data that it has access to and including additional data (and future experiments) may provide information that constrains the positive feedback model to a unimodal distribution of parameter sets. To test this, we re-estimated our parameter set for the positive feedback model to include a fifth estradiol and time-of-day dependent parameter, the maximum conductance for I_K, but this did not change the result. Future iterations of the model could include estradiol-dependent changes to low-voltage activated calcium and fast transient sodium currents that have been observed in other feedback paradigms (Zhang et al., 2009; Wang et al., 2010).

Kisspeptin increases GnRH neuron excitability

Because GnRH neurons do not express the estrogen receptor required for feedback, estradiol-dependent changes to GnRH neuron intrinsic properties and excitability are likely mediated via estrogen-sensitive afferents. The majority of anteroventral periventricular (AVPV) kisspeptin neurons express estrogen receptor alpha and may convey estradiol signals to GnRH neurons during positive feedback (Smith et al., 2005;

Smith et al., 2006). Kisspeptin directly inhibits GnRH neuron voltage-gated A-type, inwardly rectifying and calcium-gated potassium channels and activates cationic store-operated TRPC channels to ultimately stimulate action potential firing (Pielecka-Fortuna et al., 2008; Zhang et al., 2008; Pielecka-Fortuna et al., 2011; Zhang et al., 2013). In chapter 2, we demonstrated that kisspeptin increases GnRH neuron excitability and is required for increased excitability during positive feedback.

During the current injection, kisspeptin increased GnRH neuron firing in OVX and OVX+E AM animals but had no effect in cells from OVX+E PM and OVX PM animals. Kisspeptin had a second, time-of-day independent effect; at termination the current step, kisspeptin initiated action potential firing in all four groups. We postulate that these two effects are mediated by separate mechanisms with different half-lives. The first effect (increasing firing during current injection) may be attributable to a change in gene expression that persists into the brain slice preparation. Kisspeptin is capable of inducing changes in gene expression in both GT1-7 cells and in GnRH neurons situated in cultured embryonic brain slices (Sukhbaatar et al., 2013; Terasaka et al., 2013; Novaira et al., 2016; Soga et al., 2016). In our experiments, the presence of endogenous kisspeptin in the afternoon may prevent a response to exogenous kisspeptin in OVX+E PM and OVX PM animals and may drive the increase in excitability during positive feedback in our control experiments. A daily PM signal may arise from the AVPV as there are late afternoon increases in cAMP levels in this region on all cycle days in rats (Chappell et al., 2000).

The second effect (increased firing after termination of current injection) may be attributable to a short-lived (e.g. post-translational) modification that does not persist into brain slices but can be induced by exogenous kisspeptin. Our model GnRH neuron predicted that changes to I_{NaP} (but not I_{KCa} or I_h) can initiate firing at the termination of the current step. To induce spiking, it was necessary first to shift the $V_{1/2}$ activation for I_{NaP} to a more hyperpolarized potential and to decrease the speed at which the activation gate activated/deactivated. To test the model's prediction, voltage-clamp experiments to isolated and characterize I_{NaP} could be performed before and during kisspeptin treatment. Inhibition of I_{KCa} was not sufficient to initiate action potentials after the current step in our model. Kisspeptin inhibits calcium-activated potassium channels

via a protein kinase pathway to reduce the magnitude of the hyperpolarization potential (I_{AHP}) that follows an AP (Zhang et al., 2013). Although our model predicts that inhibiting I_{KCa} cannot initiating spiking alone, reduction in the I_{AHP} may act to enhance the effects of I_{NaP} on the membrane potential after termination of the current step. One caveat to our studies is that the GnRH model neuron did not include and thus could not test for effects of store-operated TRPC channels, which typically carry inward current (at potentials hyperpolarized relative to 0 mV) and are activated upon depletion of calcium stores (e.g., after AP firing) in the endoplasmic reticulum (Zhang et al., 2008). Kisspeptin activates TRPC channels via a protein kinase pathway and provides an additional testable mechanism for firing after termination of the current step.

We expected that GnRH neuron excitability would be decreased in the absence of kisspeptin. Kisspeptin knockout mice are infertile, do not exhibit regular estrous cycles, and have a delay in vaginal opening (Seminara et al., 2003; Lapatto et al., 2007; Chan et al., 2009). Remarkably, GnRH neurons excitability in kisspeptin knock-out mice was comparable to estradiol positive feedback in control mice. In contrast to controls, GnRH neuron excitability did not change with time-of-day or estradiol. In the absence of kisspeptin, other mechanisms may compensate to increase GnRH neuron excitability and maintain homeostasis. Supporting this argument, about half of kisspeptin knockout mice have gonadal weights comparable to wild-type females and exhibit persistent vaginal cornification typical of estrus (Lapatto et al., 2007). Given time, the majority of mutant mice eventually enter estrus and spontaneously transition from estrus to diestrus and back (in the absence of ovulation)(Chan et al., 2009). Collectively, these data suggest that sufficient GnRH activity and/or LH release develops to induce significant changes in uterine weight and vaginal cytology. Alternatively, changes in uterine weight and vaginal cytology could be due to homeostatic mechanisms at the level of the pituitary. In this case, GnRH neuron excitability may be heightened because kisspeptin knockout mice do not progress normally through puberty, GnRH neurons may fail to undergo the typical decline in activity that accompanies maturation (Dulka and Moenter, 2017). There are at least two approaches to separate these mechanisms. First, an inducible kisspeptin knockout could be developed. If excitability is increased in the inducible knock-out, this would point to a homeostatic mechanism. Second, changes to

GnRH neuron excitability during development in kisspeptin knock-out and wild-type mice could be compared. If we observe an increase in excitability during development that drops during adulthood in wildtype but not in kisspeptin knockout mice, this would suggest a developmental mechanism.

A number of intrinsic changes may drive the increase in excitability in kisspeptin knockout mice. Such mechanisms may include changes to potassium currents, which are critical determinants of GnRH neuron excitability and have been implicated in maintaining homeostasis in other cell types (Desai et al., 1999; DeFazio and Moenter, 2002). Preliminary data in male and female mice lacking the kisspeptin gene suggest that A-type potassium currents have hyperpolarized steady-state inactivation curves relative to most other groups (data not shown). These changes would be expected to enhance GnRH neuron excitability, and may be one mechanism for maintaining activity in the absence of kisspeptin.

GABAergic inputs are increased during positive feedback in the estrous cycle

In the daily surge model, estradiol levels are persistently elevated in the physiological range and the switch from negative to positive feedback is initiated by diurnal cues. This is in contrast to the estrous cycle, when rising levels of estradiol from the dominant follicle induce a surge of GnRH. Thus, the question is raised whether similar neurobiological mechanisms underpin estradiol-induced (daily LH surges) and preovulatory GnRH/LH surges. In chapter 4, we demonstrated GnRH neuron excitability is shifted during proestrus relative to diestrus, similar to shifts observed in the daily surge model. Because GABA PSC frequency are increased during positive feedback (OVX+E PM) and decreased during negative feedback (OVX+E AM) relative to OVX animals, we also expected to observe differences in GABAergic inputs between negative and positive feedback during the cycle (Christian and Moenter, 2007). Our hypothesis was supported when we demonstrated an increase GABA PSC frequency in GnRH neurons from proestrous mice compared to diestrous mice.

One obvious caveat to our studies is that they are performed using a brain slice preparation, which inevitability severs synaptic connections between GnRH neurons and their afferents. Thus, the majority of spontaneous PSCs appear to be activity

independent and will largely depend on the number of presynaptic terminals present in the slice. This permits us to probe the relative connectivity in coronal brain slices between physiological states, but may not reflect action potential dependent firing that occurs in the intact brain where synaptic connections are preserved. Future investigations to study GABA PSC frequency in alternative brain slices orientations or *in vivo* would help to resolve this issue.

GnRH neurons integrate fast-synaptic and intrinsic changes to increase firing rate during positive feedback

Because GABA PSC amplitude and frequency and GnRH neuron excitability are modulated by estradiol feedback, we hypothesized that both an increase in GnRH neuron responsiveness and fast-synaptic input was necessary for reproducing positive feedback firing rates. To test this, we measured GnRH neuron membrane response to negative feedback, positive feedback, and OVX postsynaptic conductance trains in cells from OVX, OVX+E AM, and OVX+E PM mice. In every cell type, the GABAergic conductance train mimicking positive feedback was more effective at inducing action potential firing compared to trains mimicking the negative feedback and OVX condition. GnRH responsiveness was also affected by the feedback state of the cell. Specifically, the positive feedback train induced nearly twice the number of action potentials in positive feedback cells compared to the two other cell types. This finding supports our finding in chapters 2 and 4 that GnRH neuron excitability to a 500 ms current step is increased during positive feedback and suggest that GnRH neurons integrate fast-synaptic and intrinsic changes to enhance firing rate during positive feedback. Whether both changes are required for the switch from negative to positive feedback, or if they are redundant mechanisms each capable of initiating an GnRH surge, remains unclear.

Multiple studies have attempted to investigate if increasing GABAergic drive is sufficient for initiating LH surges *in vivo*. ERα knock-out in GABAergic neurons blocked positive feedback and the LH surge in mice (Cheong et al., 2015). In a second study, optical activation of GABAergic neurons in the AVPV initiated LH surges (Kalil et al., 2016). However, AVPV GABAergic neurons co-express kisspeptin, and both experiments are likely affecting both kisspeptin and GABA release. Thus, we can only conclude that one

or both are essential for initiating the LH surge, but their relative importance continues to be elusive.

Unified model for the regulation of GnRH neuron activity in the switch from negative to positive feedback

Ovulation is required for the continuation of a species and thus it is likely that multiple redundant mechanisms exist to guarantee reproductive success. In the preceding chapters, I have demonstrated that changes to GnRH neuron excitability and fast-synaptic inputs are both regulated across multiple feedback paradigms, including the naturally occurring estrous cycle. Furthermore, our dynamic clamp experiments suggest that GnRH neurons integrate these changes to enhance activity during the preovulatory surge. Based on these studies, I propose a working model of the mechanisms by which estradiol feedback switches from suppressing GnRH neuron activity to inducing it.

During negative feedback (diestrus and OVX+E AM mice), GABA release onto GnRH neurons is relatively low and provides few stimulatory inputs. Glutmatergic input is also decreased in OVX+E AM mice and we hypothesize it to decrease in diestrous animals as well. Concurrently, changes to I_{NaP}, I_A, I_K, and I_{HVA} render GnRH neuron less responsive to the low levels of fast-synaptic input. Together, these changes interact to decrease GnRH neuron firing rate and release at this time (Christian et al., 2005; Glanowska et al., 2012; Silveira et al., 2016). In OVX mice, GABA and glutamate PSC frequency are increased relative to OVX+E AM mice. However, opposing changes in $V_{1/2inact}$ and I_A prevent a change in excitability between the negative feedback and open-loop condition and may explain the moderate increase in firing rates observed the open-loop condition (Christian et al., 2005). During positive feedback (proestrous and OVX+E PM mice), GABAergic drive is increased relative to negative feedback and OVX mice. Furthermore, the model predicts that multiple, redundant changes to I_{NaP}, I_A, I_K, and I_{HVA} lead to the observed increase in GnRH neuron response to postsynaptic inputs. Some of these changes to intrinsic conductances may be driven by kisspeptin release at this time. We propose that these intrinsic and fast-synaptic changes interact to drive amplified GnRH neuron activity and release during positive feedback (Christian et al., 2005; Glanowska et al., 2012; Silveira et al., 2016).

This work provides substantial evidence that both intrinsic and fast-synaptic changes to GnRH neurons are important for increasing GnRH neuron activity during the preovulatory surge. A number of important questions remain to be investigated. Are both fast-synaptic and intrinsic changes required for initiating a robust GnRH surge? Even if both are required for a robust GnRH surge, is one or the other capable of initiating sufficient GnRH release for triggering an LH surge and ovulation? Do these redundant changes occur in the same cells, or if they are directed at separate cells? Future studies are essential for enhancing our understanding of the neurobiological mechanisms underpinning reproduction.

Bibliography

Abe H, Oka Y (1999) Characterization of K+ currents underlying pacemaker potentials of fish gonadotropin-releasing hormone cells. J Neurophysiol 81:643-653.

Abramowitz M, Stegun IA (1964) Handbook of mathematical functions with formulas, graphs, and mathematical tables. Washington: U.S. Govt. Print. Off.

Adams C, Stroberg W, DeFazio RA, Schnell S, Moenter SM (2018) Gonadotropin-Releasing Hormone (GnRH) Neuron Excitability Is Regulated by Estradiol Feedback and Kisspeptin. J Neurosci 38:1249-1263.

Adams TE, Norman RL, Spies HG (1981) Gonadotropin-releasing hormone receptor binding and pituitary responsiveness in estradiol-primed monkeys. Science 213:1388-1390.

Arias P, Jarry H, Leonhardt S, Moguilevsky JA, Wuttke W (1993) Estradiol modulates the LH release response to N-methyl-D-aspartate in adult female rats: studies on hypothalamic luteinizing hormone-releasing hormone and neurotransmitter release. Neuroendocrinology 57:710-715.

Atkinson LE, Bhattacharya AN, Monroe SE, Dierschke DJ, Knobil E (1970) Effects of gonadectomy on plasma LH concentration in the rhesus monkey. Endocrinology 87:847-849.

Auger C, Marty A (2000) Quantal currents at single-site central synapses. J Physiol 526 Pt 1:3-11.

Backstrom CT, McNeilly AS, Leask RM, Baird DT (1982) Pulsatile secretion of LH, FSH, prolactin, oestradiol and progesterone during the human menstrual cycle. Clinical endocrinology 17:29-42.

Bailey JD, Centers A, Jennes L (2006) Expression of AMPA receptor subunits (GluR1-GluR4) in gonadotrophin-releasing hormone neurones of young and middle-aged persistently oestrous rats during the steroid-induced luteinising hormone surge. J Neuroendocrinol 18:1-12.

Baird DT, Fraser IS (1974) Blood production and ovarian secretion rates of estradiol-17 beta and estrone in women throughout the menstrual cycle. J Clin Endocrinol Metab 38:1009-1017.

Barry PH (1994) JPCalc, a software package for calculating liquid junction potential corrections in patch-clamp, intracellular, epithelial and bilayer measurements and for correcting junction potential measurements. J Neurosci Methods 51:107-116.

Bauer HG (1954) Endocrine and other clinical manifestations of hypothalamic disease; a survey of 60 cases, with autopsies. J Clin Endocrinol Metab 14:13-31.

Belchetz PE, Plant TM, Nakai Y, Keogh EJ, Knobil E (1978) Hypophysial responses to continuous and intermittent delivery of hypopthalamic gonadotropin-releasing hormone. Science 202:631-633.

Bennett GW, Edwardson JA, Holland D, Jeffcoate SL, White N (1975) Release of immunoreactive luteinising hormone-releasing hormone and thyrotrophin-releasing hormone from hypothalamus. Nature 257:323-325.

Bicknell RJ, Leng G (1981) Relative efficiency of neural firing patterns for vasopressin release in vitro. Neuroendocrinology 33:295-299.

Bisanti L, Olsen J, Basso O, Thonneau P, Karmaus W (1996) Shift work and subfecundity: a European multicenter study. European Study Group on Infertility and Subfecundity. J Occup Environ Med 38:352-358.

Blaustein JD, Wade GN (1978) Progestin binding by brain and pituitary cell nuclei and female rat sexual behavior. Brain Res 140:360-367.

Boden MJ, Kennaway DJ (2006) Circadian rhythms and reproduction. Reproduction 132:379-392.

Boukhliq R, Goodman RL, Berriman SJ, Adrian B, Lehman MN (1999) A subset of gonadotropin-releasing hormone neurons in the ovine medial basal hypothalamus is activated during increased pulsatile luteinizing hormone secretion. Endocrinology 140:5929-5936.

Branco T, Tozer A, Magnus CJ, Sugino K, Tanaka S, Lee AK, Wood JN, Sternson SM (2016) Near-Perfect Synaptic Integration by Nav1.7 in Hypothalamic Neurons Regulates Body Weight. Cell 165:1749-1761.

Brann DW, Mahesh VB (1991) Endogenous excitatory amino acid involvement in the preovulatory and steroid-induced surge of gonadotropins in the female rat. Endocrinology 128:1541-1547.

Brann DW, Mahesh VB (1992) Excitatory amino acid regulation of gonadotropin secretion: modulation by steroid hormones. J Steroid Biochem Mol Biol 41:847-850.

Bronson FH (1981) The regulation of luteinizing hormone secretion by estrogen: relationships among negative feedback, surge potential, and male stimulation in juvenile, peripubertal, and adult female mice. Endocrinology 108:506-516.

Bronson FH, Vom Saal FS (1979) Control of the Preovulatory Release of Luteinizing Hormone By Steroids in the Mouse*. Endocrinology 104:1247-1255.

Brown-Grant K, Raisman G (1977) Abnormalities in reproductive function associated with the destruction of the suprachiasmatic nuclei in female rats. Proc R Soc Lond B Biol Sci 198:279-296.

Cahill DJ, Wardle PG, Harlow CR, Hull MG (1998) Onset of the preovulatory luteinizing hormone surge: diurnal timing and critical follicular prerequisites. Fertil Steril 70:56-59.

Cazalis M, Dayanithi G, Nordmann JJ (1985) The role of patterned burst and interburst interval on the excitation-coupling mechanism in the isolated rat neural lobe. J Physiol 369:45-60.

Chan YM, Broder-Fingert S, Wong KM, Seminara SB (2009) Kisspeptin/Gpr54-independent gonadotrophin-releasing hormone activity in Kiss1 and Gpr54 mutant mice. J Neuroendocrinol 21:1015-1023.

Chappell PE, Levine JE (2000) Stimulation of gonadotropin-releasing hormone surges by estrogen. I. Role of hypothalamic progesterone receptors. Endocrinology 141:1477-1485.

Chappell PE, Lee J, Levine JE (2000) Stimulation of gonadotropin-releasing hormone surges by estrogen. II. Role of cyclic adenosine 3'5'-monophosphate. Endocrinology 141:1486-1492.

Chappell PE, Schneider JS, Kim P, Xu M, Lydon JP, O'Malley BW, Levine JE (1999) Absence of gonadotropin surges and gonadotropin-releasing hormone self-priming in ovariectomized (OVX), estrogen (E2)-treated, progesterone receptor knockout (PRKO) mice. Endocrinology 140:3653-3658.

Chen P, Moenter SM (2009) GABAergic transmission to gonadotropin-releasing hormone (GnRH) neurons is regulated by GnRH in a concentration-dependent manner engaging multiple signaling pathways. J Neurosci 29:9809-9818.

Chen X, Sneyd J (2015) A Computational Model of the Dendron of the GnRH Neuron. Bull Math Biol 77:904-926.

Chen X, Iremonger K, Herbison A, Kirk V, Sneyd J (2013) Regulation of electrical bursting in a spatiotemporal model of a GnRH neuron. Bull Math Biol 75:1941-1960.

Cheong RY, Czieselsky K, Porteous R, Herbison AE (2015) Expression of ESR1 in Glutamatergic and GABAergic Neurons Is Essential for Normal Puberty Onset, Estrogen Feedback, and Fertility in Female Mice. J Neurosci 35:14533-14543.

Christian CA, Moenter SM (2007) Estradiol induces diurnal shifts in GABA transmission to gonadotropin-releasing hormone neurons to provide a neural signal for ovulation. J Neurosci 27:1913-1921.

Christian CA, Moenter SM (2008) Critical roles for fast synaptic transmission in mediating estradiol negative and positive feedback in the neural control of ovulation. Endocrinology 149:5500-5508.

Christian CA, Moenter SM (2010) The neurobiology of preovulatory and estradiol-induced gonadotropin-releasing hormone surges. Endocr Rev 31:544-577.

Christian CA, Mobley JL, Moenter SM (2005) Diurnal and estradiol-dependent changes in gonadotropin-releasing hormone neuron firing activity. Proc Natl Acad Sci U S A 102:15682-15687.

Christian CA, Pielecka-Fortuna J, Moenter SM (2009) Estradiol suppresses glutamatergic transmission to gonadotropin-releasing hormone neurons in a model of negative feedback in mice. Biol Reprod 80:1128-1135.

Christian CA, Glidewell-Kenney C, Jameson JL, Moenter SM (2008) Classical estrogen receptor alpha signaling mediates negative and positive feedback on gonadotropin-releasing hormone neuron firing. Endocrinology 149:5328-5334.

Chu Z, Moenter SM (2006) Physiologic regulation of a tetrodotoxin-sensitive sodium influx that mediates a slow afterdepolarization potential in gonadotropin-releasing hormone neurons: possible implications for the central regulation of fertility. J Neurosci 26:11961-11973.

Chu Z, Andrade J, Shupnik MA, Moenter SM (2009) Differential regulation of gonadotropin-releasing hormone neuron activity and membrane properties by acutely applied estradiol: dependence on dose and estrogen receptor subtype. J Neurosci 29:5616-5627.

Clarke IJ, Cummins JT (1982) The temporal relationship between gonadotropin releasing hormone (GnRH) and luteinizing hormone (LH) secretion in ovariectomized ewes. Endocrinology 111:1737-1739.

Clarke IJ, Cummins JT (1984) Direct pituitary effects of estrogen and progesterone on gonadotropin secretion in the ovariectomized ewe. Neuroendocrinology 39:267-274.

Clarke IJ, Cummins JT, Crowder ME, Nett TM (1988) Pituitary receptors for gonadotropin-releasing hormone in relation to changes in pituitary and plasma gonadotropins in ovariectomized hypothalamo/pituitary-disconnected ewes. II. A marked rise in receptor number during the acute feedback effects of estradiol. Biol Reprod 39:349-354.

Clarke IJ, Cummins JT, Crowder ME, Nett TM (1989) Long-term negative feedback effects of oestrogen and progesterone on the pituitary gland of the long-term ovariectomized ewe. The Journal of endocrinology 120:207-214.

Clarkson J, Herbison AE (2006) Postnatal development of kisspeptin neurons in mouse hypothalamus; sexual dimorphism and projections to gonadotropin-releasing hormone neurons. Endocrinology 147:5817-5825.

Clarkson J, d'Anglemont de Tassigny X, Moreno AS, Colledge WH, Herbison AE (2008) Kisspeptin-GPR54 signaling is essential for preovulatory gonadotropin-releasing hormone neuron activation and the luteinizing hormone surge. J Neurosci 28:8691-8697.

Couse JF, Yates MM, Walker VR, Korach KS (2003) Characterization of the hypothalamic-pituitary-gonadal axis in estrogen receptor (ER) Null mice reveals hypergonadism and endocrine sex reversal in females lacking ERalpha but not ERbeta. Mol Endocrinol 17:1039-1053.

Cravo RM, Margatho LO, Osborne-Lawrence S, Donato J, Jr., Atkin S, Bookout AL, Rovinsky S, Frazao R, Lee CE, Gautron L, Zigman JM, Elias CF (2011) Characterization of Kiss1 neurons using transgenic mouse models. Neuroscience 173:37-56.

Critchlow V (1958) Ovulation induced by hypothalamic stimulation in the anesthetized rat. Am J Physiol 195:171-174.

Csercsik D, Farkas I, Szederkenyi G, Hrabovszky E, Liposits Z, Hangos KM (2010) Hodgkin-Huxley type modelling and parameter estimation of GnRH neurons. Biosystems 100:198-207.

Czieselsky K, Prescott M, Porteous R, Campos P, Clarkson J, Steyn FJ, Campbell RE, Herbison AE (2016) Pulse and Surge Profiles of Luteinizing Hormone Secretion in the Mouse. Endocrinology 157:4794-4802.

De La Iglesia HO, Blaustein JD, Bittman EL (1999) Oestrogen receptor-alpha-immunoreactive neurones project to the suprachiasmatic nucleus of the female Syrian hamster. J Neuroendocrinol 11:481-490.

de Roux N, Genin E, Carel JC, Matsuda F, Chaussain JL, Milgrom E (2003) Hypogonadotropic hypogonadism due to loss of function of the KiSS1-derived peptide receptor GPR54. Proc Natl Acad Sci U S A 100:10972-10976.

DeFazio RA, Moenter SM (2002) Estradiol feedback alters potassium currents and firing properties of gonadotropin-releasing hormone neurons. Mol Endocrinol 16:2255-2265.

DeFazio RA, Elias CF, Moenter SM (2014) GABAergic transmission to kisspeptin neurons is differentially regulated by time of day and estradiol in female mice. J Neurosci 34:16296-16308.

DeFazio RA, Heger S, Ojeda SR, Moenter SM (2002) Activation of A-type gamma-aminobutyric acid receptors excites gonadotropin-releasing hormone neurons. Mol Endocrinol 16:2872-2891.

Defazio T, Hablitz JJ (1998) Zinc and zolpidem modulate mIPSCs in rat neocortical pyramidal neurons. J Neurophysiol 80:1670-1677.

Desai NS, Rutherford LC, Turrigiano GG (1999) Plasticity in the intrinsic excitability of cortical pyramidal neurons. Nat Neurosci 2:515-520.

Dierschke DJ, Bhattacharya AN, Atkinson LE, Knobil E (1970) Circhoral oscillations of plasma LH levels in the ovariectomized rhesus monkey. Endocrinology 87:850-853.

Docke F, Dorner G (1965) The mechanism of the induction of ovulation by oestrogens. The Journal of endocrinology 33:491-499.

Dror T, Franks J, Kauffman AS (2013) Analysis of multiple positive feedback paradigms demonstrates a complete absence of LH surges and GnRH activation in mice lacking kisspeptin signaling. Biol Reprod 88:146.

Dulka EA, Moenter SM (2017) Prepubertal development of gonadotropin-releasing hormone (GnRH) neuron activity is altered by sex, age and prenatal androgen exposure. Endocrinology.

Dungan HM, Gottsch ML, Zeng H, Gragerov A, Bergmann JE, Vassilatis DK, Clifton DK, Steiner RA (2007) The role of kisspeptin-GPR54 signaling in the tonic regulation and surge release of gonadotropin-releasing hormone/luteinizing hormone. J Neurosci 27:12088-12095.

Dutton A, Dyball RE (1979) Phasic firing enhances vasopressin release from the rat neurohypophysis. J Physiol 290:433-440.

Ellis GB, Desjardins C, Fraser HM (1983) Control of pulsatile LH release in male rats. Neuroendocrinology 37:177-183.

Estienne MJ, Schillo KK, Hileman SM, Green MA, Hayes SH (1990) Effect of N-methyl-d,l-aspartate on luteinizing hormone secretion in ovariectomized ewes in the absence and presence of estradiol. Biol Reprod 42:126-130.

Evans HM, Long JA (1921a) The effect of the anterior lobe of the hypophysis administered intraperitoneally upon growth and maturity and oestrous cycles of the rat. The Anatomical Record 21:62-63.

Evans HM, Long JA (1921b) The effect of feeding the anterior lobe of the hypophysis on the oestrous cycle of the rat. The Anatomical Record 21:62.

Evans HM, Long JA (1922) Characteristic Effects upon Growth, Oestrus and Ovulation Induced by the Intraperitoneal Administration of Fresh Anterior Hypophyseal Substance. Proc Natl Acad Sci U S A 8:38-39.

Evans NP, Dahl GE, Glover BH, Karsch FJ (1994) Central regulation of pulsatile gonadotropin-releasing hormone (GnRH) secretion by estradiol during the period leading up to the preovulatory GnRH surge in the ewe. Endocrinology 134:1806-1811.

Everett JW (2006) Pituitary and Hypothalamus: Perspectives and Overview. In: Knobil and Neill's Physiology of Reproduction, Third Edition (Neill JD, ed), pp 1289-1307.

Everett JW, Sawyer CH (1950) A 24-hour periodicity in the "LH-release apparatus" of female rats, disclosed by barbiturate sedation. Endocrinology 47:198-218.

Eyigor O, Jennes L (1996) Identification of glutamate receptor subtype mRNAs in gonadotropin-releasing hormone neurons in rat brain. Endocrine 4:133-139.

Filicori M, Santoro N, Merriam GR, Crowley WF, Jr. (1986) Characterization of the physiological pattern of episodic gonadotropin secretion throughout the human menstrual cycle. J Clin Endocrinol Metab 62:1136-1144.

Fletcher PA, Li YX (2009) An integrated model of electrical spiking, bursting, and calcium oscillations in GnRH neurons. Biophys J 96:4514-4524.

Foreman-Mackey D, Hogg DW, Lang D, Goodman J (2013) emcee: The MCMC Hammer. Publications of the Astronomical Society of the Pacific 125:306-312.

Frazao R, Cravo RM, Donato J, Jr., Ratra DV, Clegg DJ, Elmquist JK, Zigman JM, Williams KW, Elias CF (2013) Shift in Kiss1 cell activity requires estrogen receptor alpha. J Neurosci 33:2807-2820.

Fricker D, Verheugen JA, Miles R (1999) Cell-attached measurements of the firing threshold of rat hippocampal neurones. J Physiol 517 (Pt 3):791-804.

Gaskins GT, Moenter SM (2012) Orexin a suppresses gonadotropin-releasing hormone (GnRH) neuron activity in the mouse. Endocrinology 153:3850-3860.

Glanowska KM, Moenter SM (2015) Differential regulation of GnRH secretion in the preoptic area (POA) and the median eminence (ME) in male mice. Endocrinology 156:231-241.

Glanowska KM, Venton BJ, Moenter SM (2012) Fast scan cyclic voltammetry as a novel method for detection of real-time gonadotropin-releasing hormone release in mouse brain slices. J Neurosci 32:14664-14669.

Glanowska KM, Burger LL, Moenter SM (2014) Development of gonadotropin-releasing hormone secretion and pituitary response. J Neurosci 34:15060-15069.

Gomez-Ospina N, Tsuruta F, Barreto-Chang O, Hu L, Dolmetsch R (2006) The C terminus of the L-type voltage-gated calcium channel Ca(V)1.2 encodes a transcription factor. Cell 127:591-606.

Goodman J, Weare J (2010) Ensemble Samplers with Affine Invariance. Communications in Applied Mathematics and Computational Science 5:65-80.

Goodman RL, Karsch FJ (1980) Pulsatile secretion of luteinizing hormone: differential suppression by ovarian steroids. Endocrinology 107:1286-1290.

Goodman RL, Bittman EL, Foster DL, Karsch FJ (1981) The endocrine basis of the synergistic suppression of luteinizing hormone by estradiol and progesterone. Endocrinology 109:1414-1417.

Gore A (2002) GnRH: The Master Molecule of Reproduction, 1 Edition. Boston, MA: Springer.

Gottsch ML, Cunningham MJ, Smith JT, Popa SM, Acohido BV, Crowley WF, Seminara S, Clifton DK, Steiner RA (2004) A role for kisspeptins in the regulation of gonadotropin secretion in the mouse. Endocrinology 145:4073-4077.

Green JD, Harris GW (1949) Observation of the hypophysioportal vessels of the living rat. J Physiol 108:359-361.

Greep RO (1936) Functional pituitary grafts in rats. Proc Soc Exp Biol Med 34:754-755.

Haighton J, Garthshore M (1797) An Experimental Inquiry concerning Animal Impregnation. By John Haighton, M. D. Communicated by Maxwell Garthshore, M. D. F. R. S. Philosophical Transactions of the Royal Society of London 87:159-196.

Han SK, Abraham IM, Herbison AE (2002) Effect of GABA on GnRH neurons switches from depolarization to hyperpolarization at puberty in the female mouse. Endocrinology 143:1459-1466.

Han SK, Todman MG, Herbison AE (2004) Endogenous GABA release inhibits the firing of adult gonadotropin-releasing hormone neurons. Endocrinology 145:495-499.

Han SK, Gottsch ML, Lee KJ, Popa SM, Smith JT, Jakawich SK, Clifton DK, Steiner RA, Herbison AE (2005) Activation of gonadotropin-releasing hormone neurons by kisspeptin as a neuroendocrine switch for the onset of puberty. J Neurosci 25:11349-11356.

Harris GW (1937) The Induction of Ovulation in the Rabbit, by Electrical Stimulation of the Hypothalamo-hypophysial Mechanism. Proc R Soc Lond B Biol Sci 122:374-394.

Harris GW, Jacobsohn D (1952) Functional grafts of the anterior pituitary gland. Proc R Soc Lond B Biol Sci 139:263-276.

Herbison AE, Skynner MJ, Sim JA (2001) Erratum: Lack of detection of estrogen receptor-alpha transcripts in mouse gonadotropin releasing-hormone neurons. . Endocrinology 142:493.

Hille B (2001) Ion channels of excitable membranes, 3rd Edition. Sunderland, Mass.: Sinauer.

Hoffman GE, Finch CE (1986) LHRH neurons in the female C57BL/6J mouse brain during reproductive aging: no loss up to middle age. Neurobiol Aging 7:45-48.

Hohlweg W, Chamorro A (1937) Über die luteinisierende Wirkung des Follikelhormons durch Beinflussung der endogenen Hypophysenvorderlappensekretion. Klin Wochenschr 16:196-197.

Houston CM, Bright DP, Sivilotti LG, Beato M, Smart TG (2009) Intracellular chloride ions regulate the time course of GABA-mediated inhibitory synaptic transmission. J Neurosci 29:10416-10423.

Hrabovszky E, Shughrue PJ, Merchenthaler I, Hajszan T, Carpenter CD, Liposits Z, Petersen SL (2000) Detection of estrogen receptor-beta messenger ribonucleic acid and 125I-estrogen binding sites in luteinizing hormone-releasing hormone neurons of the rat brain. Endocrinology 141:3506-3509.

Hrabovszky E, Steinhauser A, Barabas K, Shughrue PJ, Petersen SL, Merchenthaler I, Liposits Z (2001) Estrogen receptor-beta immunoreactivity in luteinizing hormone-releasing hormone neurons of the rat brain. Endocrinology 142:3261-3264.

Hrabovszky E, Molnar CS, Nagy R, Vida B, Borsay BA, Racz K, Herczeg L, Watanabe M, Kallo I, Liposits Z (2012) Glutamatergic and GABAergic innervation of human gonadotropin-releasing hormone-I neurons. Endocrinology 153:2766-2776.

Hutchens EG, Ramsey KA, Howard LC, Abshire MY, Patrie JT, McCartney CR (2016) Progesterone has rapid positive feedback actions on LH release but fails to reduce LH pulse frequency within 12 h in estradiol-pretreated women. Physiol Rep 4.

Irvine CH, Alexander SL (1994) The dynamics of gonadotrophin-releasing hormone, LH and FSH secretion during the spontaneous ovulatory surge of the mare as revealed by intensive sampling of pituitary venous blood. The Journal of endocrinology 140:283-295.

Jarry H, Hirsch B, Leonhardt S, Wuttke W (1992) Amino acid neurotransmitter release in the preoptic area of rats during the positive feedback actions of estradiol on LH release. Neuroendocrinology 56:133-140.

Jarry H, Leonhardt S, Schwarze T, Wuttke W (1995) Preoptic rather than mediobasal hypothalamic amino acid neurotransmitter release regulates GnRH secretion during the estrogen-induced LH surge in the ovariectomized rat. Neuroendocrinology 62:479-486.

Johnstone RH, Bardenet R, Gavaghan DJ, Polonchuk L, Davies MR, Mirams GR (2016a) Hierarchical Bayesian modelling of variability and uncertainty in synthetic action potential traces. In: Computing in Cardiology, pp 1089-1092.

Johnstone RH, Chang ETY, Bardenet R, de Boer TP, Gavaghan DJ, Pathmanathan P, Clayton RH, Mirams GR (2016b) Uncertainty and variability in models of the cardiac action potential: Can we build trustworthy models? Journal of Molecular and Cellular Cardiology 96:49-62.

Kaeser PS, Regehr WG (2014) Molecular mechanisms for synchronous, asynchronous, and spontaneous neurotransmitter release. Annu Rev Physiol 76:333-363.

Kaila K (1994) Ionic basis of GABAA receptor channel function in the nervous system. Prog Neurobiol 42:489-537.

Kaila K, Voipio J (1987) Postsynaptic fall in intracellular pH induced by GABA-activated bicarbonate conductance. Nature 330:163-165.

Kalil B, Mcclennan T, Piet R, Herbison A (2016) Role of rostral periventricular area of the third ventricle (RP3V) GABAergic neurons in generating the preovulatory luteinizing hormone surge in female mouse. In: Society for Neuroscience. San Diego, CA: Neuroscience Meeting Planner. Online.

Karigo T, Kanda S, Takahashi A, Abe H, Okubo K, Oka Y (2012) Time-of-day-dependent changes in GnRH1 neuronal activities and gonadotropin mRNA expression in a daily spawning fish, medaka. Endocrinology 153:3394-3404.

Kerdelhue B, Brown S, Lenoir V, Queenan JT, Jr., Jones GS, Scholler R, Jones HW, Jr. (2002) Timing of initiation of the preovulatory luteinizing hormone surge and its relationship with the circadian cortisol rhythm in the human. Neuroendocrinology 75:158-163.

Khadra A, Li YX (2006) A model for the pulsatile secretion of gonadotropin-releasing hormone from synchronized hypothalamic neurons. Biophys J 91:74-83.

Kiss J, Kocsis K, Csaki A, Halasz B (2003) Evidence for vesicular glutamate transporter synapses onto gonadotropin-releasing hormone and other neurons in the rat medial preoptic area. Eur J Neurosci 18:3267-3278.

Knobil E, Plant TM, Wildt L, Belchetz PE, Marshall G (1980) Control of the rhesus monkey menstrual cycle: permissive role of hypothalamic gonadotropin-releasing hormone. Science 207:1371-1373.

Krishnan KA, Proudman JA, Bolt DJ, Bahr JM (1993) Development of an homologous radioimmunoassay for chicken follicle-stimulating hormone and measurement of plasma FSH during the ovulatory cycle. Comp Biochem Physiol Comp Physiol 105:729-734.

Krupa M, Vidal A, Clement F (2013) A network model of the periodic synchronization process in the dynamics of calcium concentration in GnRH neurons. J Math Neurosci 3:4.

Kuehl-Kovarik MC, Pouliot WA, Halterman GL, Handa RJ, Dudek FE, Partin KM (2002) Episodic bursting activity and response to excitatory amino acids in acutely dissociated gonadotropin-releasing hormone neurons genetically targeted with green fluorescent protein. J Neurosci 22:2313-2322.

Labyak S, Lava S, Turek F, Zee P (2002) Effects of shiftwork on sleep and menstrual function in nurses. Health Care Women Int 23:703-714.

Lapatto R, Pallais JC, Zhang D, Chan YM, Mahan A, Cerrato F, Le WW, Hoffman GE, Seminara SB (2007) Kiss1-/- mice exhibit more variable hypogonadism than Gpr54-/- mice. Endocrinology 148:4927-4936.

LeBeau AP, Van Goor F, Stojilkovic SS, Sherman A (2000) Modeling of membrane excitability in gonadotropin-releasing hormone-secreting hypothalamic neurons regulated by Ca2+-mobilizing and adenylyl cyclase-coupled receptors. J Neurosci 20:9290-9297.

Lee JH, Miele ME, Hicks DJ, Phillips KK, Trent JM, Weissman BE, Welch DR (1996) KiSS-1, a novel human malignant melanoma metastasis-suppressor gene. J Natl Cancer Inst 88:1731-1737.

Lee K, Duan W, Sneyd J, Herbison AE (2010a) Two slow calcium-activated afterhyperpolarization currents control burst firing dynamics in gonadotropin-releasing hormone neurons. J Neurosci 30:6214-6224.

Lee K, Porteous R, Campbell RE, Luscher B, Herbison AE (2010b) Knockdown of GABA(A) receptor signaling in GnRH neurons has minimal effects upon fertility. Endocrinology 151:4428-4436.

Legan SJ, Karsch FJ (1975) A daily signal for the LH surge in the rat. Endocrinology 96:57-62.

Leranth C, Shanabrough M, Naftolin F (1991) Estrogen induces ultrastructural changes in progesterone receptor-containing GABA neurons of the primate hypothalamus. Neuroendocrinology 54:571-579.

Levine JE, Pau K-YF, Ramirez VD, Jackson GL (1982) Simultaneous Measurement of Luteinizing Hormone-Releasing Hormone and Luteinizing Hormone Release in Unanesthetized, Ovariectomized Sheep. Endocrinology 111:1449-1455.

Levine JE, Norman RL, Gliessman PM, Oyama TT, Bangsberg DR, Spies HG (1985) In vivo gonadotropin-releasing hormone release and serum luteinizing hormone measurements in ovariectomized, estrogen-treated rhesus macaques. Endocrinology 117:711-721.

Li YX, Khadra A (2008) Robust synchrony and rhythmogenesis in endocrine neurons via autocrine regulations in vitro and in vivo. Bull Math Biol 70:2103-2125.

Lincoln GA, Fraser HM (1979) Blockade of episodic secretion of luteinizing hormone in the ram by the administration of antibodies to luteinizing hormone releasing hormone. Biol Reprod 21:1239-1245.

Liu X, Porteous R, Herbison AE (2017) Dynamics of GnRH Neuron Ionotropic GABA and Glutamate Synaptic Receptors Are Unchanged during Estrogen Positive and Negative Feedback in Female Mice. eNeuro 4.

Lopez FJ, Donoso AO, Negro-Vilar A (1990) Endogenous excitatory amino acid neurotransmission regulates the estradiol-induced LH surge in ovariectomized rats. Endocrinology 126:1771-1773.

Lucas RJ, Stirland JA, Darrow JM, Menaker M, Loudon AS (1999) Free running circadian rhythms of melatonin, luteinizing hormone, and cortisol in Syrian hamsters bearing the circadian tau mutation. Endocrinology 140:758-764.

Luderer U, Strobl FJ, Levine JE, Schwartz NB (1993) Differential gonadotropin responses to N-methyl-D,L-aspartate in metestrous, proestrous, and ovariectomized rats. Biol Reprod 48:857-866.

Mackay L, Zemkova H, Stojilkovic SS, Sherman A, Khadra A (2017) Deciphering the regulation of P2X4 receptor channel gating by ivermectin using Markov models. PLOS Computational Biology 13:e1005643.

MacLusky NJ, McEwen BS (1978) Oestrogen modulates progestin receptor concentrations in some rat brain regions but not in others. Nature 274:276-278.

Mahoney MM, Sisk C, Ross HE, Smale L (2004) Circadian regulation of gonadotropin-releasing hormone neurons and the preovulatory surge in luteinizing hormone in the diurnal rodent, Arvicanthis niloticus, and in a nocturnal rodent, Rattus norvegicus. Biol Reprod 70:1049-1054.

Marshall FHA, Verney EB (1936) The occurrence of ovulation and pseudo-pregnancy in the rabbit as a result of central nervous stimulation. J Physiol 86:327-336.321.

Martin K, Santoro N, Hall J, Filicori M, Wierman M, Crowley WF, Jr. (1990) Clinical review 15: Management of ovulatory disorders with pulsatile gonadotropin-releasing hormone. J Clin Endocrinol Metab 71:1081A-1081G.

Matsuo H, Baba Y, Nair RM, Arimura A, Schally AV (1971) Structure of the porcine LH- and FSH-releasing hormone. I. The proposed amino acid sequence. Biochem Biophys Res Commun 43:1334-1339.

Merel J, Shababo B, Naka A, Adesnik H, Paninski L (2016) Bayesian methods for event analysis of intracellular currents. J Neurosci Methods 269:21-32.

Messager S, Chatzidaki EE, Ma D, Hendrick AG, Zahn D, Dixon J, Thresher RR, Malinge I, Lomet D, Carlton MB, Colledge WH, Caraty A, Aparicio SA (2005) Kisspeptin directly stimulates gonadotropin-releasing hormone release via G protein-coupled receptor 54. Proc Natl Acad Sci U S A 102:1761-1766.

Micevych P, Sinchak K (2011) The Neurosteroid Progesterone Underlies Estrogen Positive Feedback of the LH Surge. Front Endocrinol (Lausanne) 2:90.

Midgley AR, Jr. (1966) Radioimmunoassay: a method for human chorionic gonadotropin and human luteinizing hormone. Endocrinology 79:10-18.

Milescu LS, Yamanishi T, Ptak K, Mogri MZ, Smith JC (2008) Real-time kinetic modeling of voltage-gated ion channels using dynamic clamp. Biophysical journal 95:66-87.

Moenter SM, Caraty A, Karsch FJ (1990) The estradiol-induced surge of gonadotropin-releasing hormone in the ewe. Endocrinology 127:1375-1384.

Moenter SM, Caraty A, Locatelli A, Karsch FJ (1991) Pattern of gonadotropin-releasing hormone (GnRH) secretion leading up to ovulation in the ewe: existence of a preovulatory GnRH surge. Endocrinology 129:1175-1182.

Monroe SE, Atkinson LE, Knobil E (1970a) Patterns of circulating luteinizing hormone and their relation to plasma progesterone levels during the menstrual cycle of the Rhesus monkey. Endocrinology 87:453-455.

Monroe SE, Peckham WD, Neill JD, Knobil E (1970b) A radioimmunoassay for rhesus monkey luteinizing hormone (RhLH). Endocrinology 86:1012-1018.

Moore RY, Speh JC (1993) GABA is the principal neurotransmitter of the circadian system. Neurosci Lett 150:112-116.

Moran S, Moenter SM, Khadra A (2016) A unified model for two modes of bursting in GnRH neurons. J Comput Neurosci 40:297-315.

Naor Z, Clayton RN, Catt KJ (1980) Characterization of gonadotropin-releasing hormone receptors in cultured rat pituitary cells. Endocrinology 107:1144-1152.

Neill JD, Patton JM, Dailey RA, Tsou RC, Tindall GT (1977) Luteinizing Hormone Releasing Hormone (LHRH) in Pituitary Stalk Blood of Rhesus Monkeys: Relationship to Level of LH Release. Endocrinology 101:430-434.

Norman RL, Blake CA, Sawyer CH (1973) Estrogen-dependent 24-hour periodicity in pituitary LH release in the female hamster. Endocrinology 93:965-970.

Novaira HJ, Sonko ML, Radovick S (2016) Kisspeptin Induces Dynamic Chromatin Modifications to Control GnRH Gene Expression. Mol Neurobiol 53:3315-3325.

O'Leary T, Williams AH, Caplan JS, Marder E (2013) Correlations in ion channel expression emerge from homeostatic tuning rules. Proc Natl Acad Sci U S A 110:E2645-2654.

Oakley AE, Clifton DK, Steiner RA (2009) Kisspeptin signaling in the brain. Endocr Rev 30:713-743.

Ohtaki T et al. (2001) Metastasis suppressor gene KiSS-1 encodes peptide ligand of a G-protein-coupled receptor. Nature 411:613-617.

Ottem EN, Godwin JG, Petersen SL (2002) Glutamatergic signaling through the N-methyl-D-aspartate receptor directly activates medial subpopulations of luteinizing hormone-releasing hormone (LHRH) neurons, but does not appear to mediate the effects of estradiol on LHRH gene expression. Endocrinology 143:4837-4845.

Ottem EN, Godwin JG, Krishnan S, Petersen SL (2004) Dual-phenotype GABA/glutamate neurons in adult preoptic area: sexual dimorphism and function. J Neurosci 24:8097-8105.

Pau KY, Berria M, Hess DL, Spies HG (1993) Preovulatory gonadotropin-releasing hormone surge in ovarian-intact rhesus macaques. Endocrinology 133:1650-1656.

Pelletier G, Labrie F, Puviani R, Arimura A, Schally AV (1974) Immunohistochemical localization of luteinizing hormone-releasing hormone in the rat median eminence. Endocrinology 95:314-317.

Pielecka-Fortuna J, Moenter SM (2010) Kisspeptin increases gamma-aminobutyric acidergic and glutamatergic transmission directly to gonadotropin-releasing hormone neurons in an estradiol-dependent manner. Endocrinology 151:291-300.

Pielecka-Fortuna J, Chu Z, Moenter SM (2008) Kisspeptin acts directly and indirectly to increase gonadotropin-releasing hormone neuron activity and its effects are modulated by estradiol. Endocrinology 149:1979-1986.

Pielecka-Fortuna J, DeFazio RA, Moenter SM (2011) Voltage-gated potassium currents are targets of diurnal changes in estradiol feedback regulation and kisspeptin action on gonadotropin-releasing hormone neurons in mice. Biol Reprod 85:987-995.

Ping L, Mahesh VB, Wiedmeier VT, Brann DW (1994) Release of glutamate and aspartate from the preoptic area during the progesterone-induced LH surge: in vivo microdialysis studies. Neuroendocrinology 59:318-324.

Ping L, Mahesh VB, Bhat GK, Brann DW (1997) Regulation of gonadotropin-releasing hormone and luteinizing hormone secretion by AMPA receptors. Evidence for a physiological role of AMPA receptors in the steroid-induced luteinizing hormone surge. Neuroendocrinology 66:246-253.

Pompolo S, Pereira A, Scott CJ, Fujiyma F, Clarke IJ (2003) Evidence for estrogenic regulation of gonadotropin-releasing hormone neurons by glutamatergic neurons in the ewe brain: An immunohistochemical study using an antibody against vesicular glutamate transporter-2. J Comp Neurol 465:136-144.

Popa G, Fielding U (1930) A Portal Circulation from the Pituitary to the Hypothalamic Region. J Anat 65:88-91.

Prinz AA, Bucher D, Marder E (2004) Similar network activity from disparate circuit parameters. Nat Neurosci 7:1345-1352.

Refinetti R, Menaker M (1992) Evidence for separate control of estrous and circadian periodicity in the golden hamster. Behav Neural Biol 58:27-36.

Reid CA, Bekkers JM, Clements JD (2003) Presynaptic Ca2+ channels: a functional patchwork. Trends Neurosci 26:683-687.

Reyes A, Xia LN, Ferin M (1991) Modulation of the effects of N-methyl-D,L-aspartate on luteinizing hormone by the ovarian steroids in the adult rhesus monkey. Neuroendocrinology 54:405-411.

Roberts CB, Best JA, Suter KJ (2006) Dendritic processing of excitatory synaptic input in hypothalamic gonadotropin releasing-hormone neurons. Endocrinology 147:1545-1555.

Roberts CB, O'Boyle MP, Suter KJ (2009) Dendrites determine the contribution of after depolarization potentials (ADPs) to generation of repetitive action potentials in hypothalamic gonadotropin releasing-hormone (GnRH) neurons. J Comput Neurosci 26:39-53.

Roberts CB, Campbell RE, Herbison AE, Suter KJ (2008) Dendritic action potential initiation in hypothalamic gonadotropin-releasing hormone neurons. Endocrinology 149:3355-3360.

Rosales R, Stark JA, Fitzgerald WJ, Hladky SB (2001) Bayesian restoration of ion channel records using hidden Markov models. Biophys J 80:1088-1103.

Rossmanith WG, Liu CH, Laughlin GA, Mortola JF, Suh BY, Yen SS (1990) Relative changes in LH pulsatility during the menstrual cycle: using data from hypogonadal women as a reference point. Clinical endocrinology 32:647-660.

Sarkar DK, Chiappa SA, Fink G, Sherwood NM (1976) Gonadotropin-releasing hormone surge in pro-oestrous rats. Nature 264:461-463.

Schally AV, Nair RMG, Redding TW, Arimura A (1971a) Isolation of the Luteinizing Hormone and Follicle-stimulating Hormone-releasing Hormone from Porcine Hypothalami. Journal of Biological Chemistry 246:7230-7236.

Schally AV, Arimura A, Kastin AJ, Matsuo H, Baba Y, Redding TW, Nair RM, Debeljuk L, White WF (1971b) Gonadotropin-releasing hormone: one polypeptide regulates secretion of luteinizing and follicle-stimulating hormones. Science 173:1036-1038.

Seminara SB, Messager S, Chatzidaki EE, Thresher RR, Acierno JS, Jr., Shagoury JK, Bo-Abbas Y, Kuohung W, Schwinof KM, Hendrick AG, Zahn D, Dixon J, Kaiser UB, Slaugenhaupt SA, Gusella JF, O'Rahilly S, Carlton MB, Crowley WF, Jr., Aparicio SA, Colledge WH (2003) The GPR54 gene as a regulator of puberty. N Engl J Med 349:1614-1627.

Shim WS, Conaway M, Masamura S, Yue W, Wang JP, Kmar R, Santen RJ (2000) Estradiol hypersensitivity and mitogen-activated protein kinase expression in

long-term estrogen deprived human breast cancer cells in vivo. Endocrinology 141:396-405.

Shupnik MA, Rosenzweig BA (1991) Identification of an estrogen-responsive element in the rat LH beta gene. DNA-estrogen receptor interactions and functional analysis. J Biol Chem 266:17084-17091.

Shupnik MA, Gharib SD, Chin WW (1988) Estrogen suppresses rat gonadotropin gene transcription in vivo. Endocrinology 122:1842-1846.

Siekmann I, Sneyd J, Crampin EJ (2012) MCMC can detect nonidentifiable models. Biophys J 103:2275-2286.

Siekmann I, Wagner LE, 2nd, Yule D, Fox C, Bryant D, Crampin EJ, Sneyd J (2011) MCMC estimation of Markov models for ion channels. Biophys J 100:1919-1929.

Silveira M, Burger LL, DeFazio RA, Wagenmaker ER, Moenter SM (2016) GnRH neuron activity and pituitary response in estradiol-induced vs proestrous luteinizing hormone surges in female mice. Endocrinology:en20161771.

Sim JA, Skynner MJ, Herbison AE (2001) Heterogeneity in the basic membrane properties of postnatal gonadotropin-releasing hormone neurons in the mouse. J Neurosci 21:1067-1075.

Simms BA, Zamponi GW (2014) Neuronal voltage-gated calcium channels: structure, function, and dysfunction. Neuron 82:24-45.

Skinner DC, Evans NP, Delaleu B, Goodman RL, Bouchard P, Caraty A (1998) The negative feedback actions of progesterone on gonadotropin-releasing hormone secretion are transduced by the classical progesterone receptor. Proc Natl Acad Sci U S A 95:10978-10983.

Skynner MJ, Sim JA, Herbison AE (1999) Detection of estrogen receptor alpha and beta messenger ribonucleic acids in adult gonadotropin-releasing hormone neurons. Endocrinology 140:5195-5201.

Smith JT, Cunningham MJ, Rissman EF, Clifton DK, Steiner RA (2005) Regulation of Kiss1 gene expression in the brain of the female mouse. Endocrinology 146:3686-3692.

Smith JT, Popa SM, Clifton DK, Hoffman GE, Steiner RA (2006) Kiss1 neurons in the forebrain as central processors for generating the preovulatory luteinizing hormone surge. J Neurosci 26:6687-6694.

Smith PE (1926) Ablation and transplantation of the hypophyses in the rat. The Anatomical Record 32:221.

Soga T, Lim WL, Khoo AS, Parhar IS (2016) Kisspeptin Activates Ankrd 26 Gene Expression in Migrating Embryonic GnRH Neurons. Front Endocrinol (Lausanne) 7:15.

Spergel DJ, Kruth U, Hanley DF, Sprengel R, Seeburg PH (1999) GABA- and glutamate-activated channels in green fluorescent protein-tagged gonadotropin-releasing hormone neurons in transgenic mice. J Neurosci 19:2037-2050.

Sukhbaatar U, Kanasaki H, Mijiddorj T, Oride A, Miyazaki K (2013) Kisspeptin induces expression of gonadotropin-releasing hormone receptor in GnRH-producing GT1-7 cells overexpressing G protein-coupled receptor 54. Gen Comp Endocrinol 194:94-101.

Sullivan SD, Moenter SM (2003) Neurosteroids alter gamma-aminobutyric acid postsynaptic currents in gonadotropin-releasing hormone neurons: a possible mechanism for direct steroidal control. Endocrinology 144:4366-4375.

Sullivan SD, Moenter SM (2005) GABAergic integration of progesterone and androgen feedback to gonadotropin-releasing hormone neurons. Biol Reprod 72:33-41.

Sun J, Moenter SM (2010) Progesterone treatment inhibits and dihydrotestosterone (DHT) treatment potentiates voltage-gated calcium currents in gonadotropin-releasing hormone (GnRH) neurons. Endocrinology 151:5349-5358.

Sun J, Chu Z, Moenter SM (2010) Diurnal in vivo and rapid in vitro effects of estradiol on voltage-gated calcium channels in gonadotropin-releasing hormone neurons. J Neurosci 30:3912-3923.

Suter KJ (2004) Control of firing by small (S)-alpha-amino-3-hydroxy-5-methyl-isoxazolepropionic acid-like inputs in hypothalamic gonadotropin releasing-hormone (GnRH) neurons. Neuroscience 128:443-450.

Suter KJ, Song WJ, Sampson TL, Wuarin JP, Saunders JT, Dudek FE, Moenter SM (2000) Genetic targeting of green fluorescent protein to gonadotropin-releasing hormone neurons: characterization of whole-cell electrophysiological properties and morphology. Endocrinology 141:412-419.

Terasaka T, Otsuka F, Tsukamoto N, Nakamura E, Inagaki K, Toma K, Ogura-Ochi K, Glidewell-Kenney C, Lawson MA, Makino H (2013) Mutual interaction of kisspeptin, estrogen and bone morphogenetic protein-4 activity in GnRH regulation by GT1-7 cells. Mol Cell Endocrinol 381:8-15.

Todman MG, Han SK, Herbison AE (2005) Profiling neurotransmitter receptor expression in mouse gonadotropin-releasing hormone neurons using green fluorescent protein-promoter transgenics and microarrays. Neuroscience 132:703-712.

Underwood AJ (1996) Experiments in Ecology: Their Logical Design and Interpretation Using Analysis of Variance: Cambridge University Press.

Urbanski HF, Garyfallou VT, Kohama SG, Hess DL (1997) Alpha-adrenergic receptor antagonism and N-methyl-D-aspartate (NMDA) induced luteinizing hormone release in female rhesus macaques. Brain Res 744:96-104.

Van der Beek EM, Horvath TL, Wiegant VM, Van den Hurk R, Buijs RM (1997) Evidence for a direct neuronal pathway from the suprachiasmatic nucleus to the gonadotropin-releasing hormone system: combined tracing and light and electron microscopic immunocytochemical studies. J Comp Neurol 384:569-579.

Van Goor F, LeBeau AP, Krsmanovic LZ, Sherman A, Catt KJ, Stojilkovic SS (2000) Amplitude-dependent spike-broadening and enhanced Ca(2+) signaling in GnRH-secreting neurons. Biophys J 79:1310-1323.

Verheugen JA, Fricker D, Miles R (1999) Noninvasive measurements of the membrane potential and GABAergic action in hippocampal interneurons. J Neurosci 19:2546-2555.

Vida B, Hrabovszky E, Kalamatianos T, Coen CW, Liposits Z, Kallo I (2008) Oestrogen receptor alpha and beta immunoreactive cells in the suprachiasmatic nucleus of mice: distribution, sex differences and regulation by gonadal hormones. J Neuroendocrinol 20:1270-1277.

Vida B, Deli L, Hrabovszky E, Kalamatianos T, Caraty A, Coen CW, Liposits Z, Kallo I (2010) Evidence for suprachiasmatic vasopressin neurones innervating kisspeptin neurones in the rostral periventricular area of the mouse brain: regulation by oestrogen. J Neuroendocrinol 22:1032-1039.

Wakerley JB, Lincoln DW (1973) The milk-ejection reflex of the rat: a 20- to 40-fold acceleration in the firing of paraventricular neurones during oxytocin release. The Journal of endocrinology 57:477-493.

Wang L, DeFazio RA, Moenter SM (2016) Excitability and Burst Generation of AVPV Kisspeptin Neurons Are Regulated by the Estrous Cycle Via Multiple Conductances Modulated by Estradiol Action. eNeuro 3.

Wang Y, Garro M, Kuehl-Kovarik MC (2010) Estradiol attenuates multiple tetrodotoxin-sensitive sodium currents in isolated gonadotropin-releasing hormone neurons. Brain Res 1345:137-145.

Watson RE, Jr., Langub MC, Jr., Engle MG, Maley BE (1995) Estrogen-receptive neurons in the anteroventral periventricular nucleus are synaptic targets of the suprachiasmatic nucleus and peri-suprachiasmatic region. Brain Res 689:254-264.

Wen S, Gotze IN, Mai O, Schauer C, Leinders-Zufall T, Boehm U (2011) Genetic identification of GnRH receptor neurons: a new model for studying neural circuits underlying reproductive physiology in the mouse brain. Endocrinology 152:1515-1526.

Westenbroek RE, Hell JW, Warner C, Dubel SJ, Snutch TP, Catterall WA (1992) Biochemical properties and subcellular distribution of an N-type calcium channel alpha 1 subunit. Neuron 9:1099-1115.

Wildt L, Hausler A, Marshall G, Hutchison JS, Plant TM, Belchetz PE, Knobil E (1981) Frequency and amplitude of gonadotropin-releasing hormone stimulation and gonadotropin secretion in the rhesus monkey. Endocrinology 109:376-385.

Wilson RC, Kesner JS, Kaufman JM, Uemura T, Akema T, Knobil E (1984) Central electrophysiologic correlates of pulsatile luteinizing hormone secretion in the rhesus monkey. Neuroendocrinology 39:256-260.

Wintermantel TM, Campbell RE, Porteous R, Bock D, Grone HJ, Todman MG, Korach KS, Greiner E, Perez CA, Schutz G, Herbison AE (2006) Definition of estrogen receptor pathway critical for estrogen positive feedback to gonadotropin-releasing hormone neurons and fertility. Neuron 52:271-280.

Wislocki GB, King LS (1936) The permeability of the hypophysis and hypothalamus to vital dyes, with a study of the hypophyseal vascular supply. American Journal of Anatomy 58:421-472.

Wray S, Hoffman G (1986) Postnatal morphological changes in rat LHRH neurons correlated with sexual maturation. Neuroendocrinology 43:93-97.

Wray S, Grant P, Gainer H (1989) Evidence that cells expressing luteinizing hormone-releasing hormone mRNA in the mouse are derived from progenitor cells in the olfactory placode. Proc Natl Acad Sci U S A 86:8132-8136.

Wu TJ, Gibson MJ, Rogers MC, Silverman AJ (1997) New observations on the development of the gonadotropin-releasing hormone system in the mouse. J Neurobiol 33:983-998.

Xia L, Van Vugt D, Alston EJ, Luckhaus J, Ferin M (1992) A surge of gonadotropin-releasing hormone accompanies the estradiol-induced gonadotropin surge in the rhesus monkey. Endocrinology 131:2812-2820.

Yip SH, Boehm U, Herbison AE, Campbell RE (2015) Conditional Viral Tract Tracing Delineates the Projections of the Distinct Kisspeptin Neuron Populations to

Gonadotropin-Releasing Hormone (GnRH) Neurons in the Mouse. Endocrinology 156:2582-2594.

Zhang C, Ronnekleiv OK, Kelly MJ (2013) Kisspeptin inhibits a slow afterhyperpolarization current via protein kinase C and reduces spike frequency adaptation in GnRH neurons. Am J Physiol Endocrinol Metab 304:E1237-1244.

Zhang C, Roepke TA, Kelly MJ, Ronnekleiv OK (2008) Kisspeptin depolarizes gonadotropin-releasing hormone neurons through activation of TRPC-like cationic channels. J Neurosci 28:4423-4434.

Zhang C, Bosch MA, Levine JE, Ronnekleiv OK, Kelly MJ (2007) Gonadotropin-releasing hormone neurons express K(ATP) channels that are regulated by estrogen and responsive to glucose and metabolic inhibition. J Neurosci 27:10153-10164.

Zhang C, Bosch MA, Rick EA, Kelly MJ, Ronnekleiv OK (2009) 17Beta-estradiol regulation of T-type calcium channels in gonadotropin-releasing hormone neurons. J Neurosci 29:10552-10562.

Zhang C, Bosch MA, Qiu J, Ronnekleiv OK, Kelly MJ (2015) 17beta-Estradiol increases persistent Na(+) current and excitability of AVPV/PeN Kiss1 neurons in female mice. Mol Endocrinol 29:518-527.